POLITECNICO DI TORINO

Master Degree Course in Biomedical Engineering

Master Degree Thesis

Automated Distance Evaluation for Pulse Wave Velocity Estimation.

Supervisors:

Prof. Danilo Demarchi
Ing. Davide Lena
Ing. Irene Buraioli

Candidate:

Valerio Russo

December 2018

Summary

Chapter 1 Introduction

The study of arterial tree stiffness, assessed through the Pulse wave velocity (PWV) measurement addressing the carotidal and femoral sites, is now a widely accepted approach in cardiovascular risk stratification. The increase in PWV is an independent risk factor compared to all other commonly used factors (age, smoking, obesity). At present, the limiting factor for the inclusion of this parameter in clinical practice is the cost of the equipment and the difficulty of use.

In practice, the measurement of PWV is obtained by determining the time interval used by the pulse wave to propagate from the carotid artery down to the femoral artery, this time known as Pulse Transit Time (PTT). Therefore, by dividing the distance between the two acquisition sites by the PTT, the wave propagation speed is obtained. But the need to carry out a sort of "aerial projection" away from the patient's body for distance estimation, to avoid considering any physical forms, certainly does not increase the accuracy of the measurement.

The proposed innovation lies in integrating the Pulse Wave Velocity evaluation system with other types of sensors that allow automatic detection of the distance between the carotid-femoral sites, considerably reducing the uncertainty of the measurement and thus increasing the accuracy and the performances of the whole system.

The purpose of this thesis work was to design a low-cost system able to extract distance for PWV with a simple measurement procedure. To do this, a device able to emit and acquire a signal is considered. Specifically, a MEMS microphones together with miniaturized loudspeakers or micro-actuators are employed to exploit the propagation delay of the acoustic wave.
The miniaturized speaker and the MEMS microphone will be directly placed on the sensor probes employed for PWV acquisition.

When requested, the speaker will emit a sound signal at a specific frequency and the microphone, located on the other sensor, will record this signal. If the system is properly synchronized and evaluating the sound propagation delay, the distance between the two sensors can be obtained.
For the emission and acquisition of the sound wave a proper conditioning circuit has been designed. After the analog conditioning circuits, a microcontroller based system acquires and converts the signals. Then, by means of a USB interface data are transferred to a laptop and finally processed by a Time of Flight (TOF) extraction algorithms. From the acquired signals, several algorithms have been considered, developed and compared.
In detail, this thesis work is organized as follow:

• Chapter 2: ***Background***
In the first part of the work, a review of the state of the art covering the addressed theme will be exposed. Especially, all the topics involved in this project realization will be treated: the human body physiology, sound's physic, and the electronic components specifications. A general description of the cardiovascular system, Pulse Wave Velocity distance measurement techniques and their related features are provided.

• Chapter 3: ***Signals Acquisition***
This chapter details the conditioning circuits implemented to emit a sound wave by a sound speaker and to detect it by a MEMS microphone. These circuits comprise analog filters introduced to extract only the useful signal components. Moreover, they include amplification stages able to correctly feed the Analog to Digital Converter (ADC) maximizing its input dynamic range. And finally, a description of the speaker driving circuit is given.

• Chapter 4: ***Algorithms AM Implementation***
This section covers all the algorithms implemented for the amplitude modulated (AM) signal in order to evaluate the sound time of flight (TOF). This is the focal and essential step in the sensors distance estimation procedure. Specifically, four different algorithms have been employed: distance of peaks, simple threshold, double threshold parable fit, and an iterative method.

• Chapter 5: ***Algorithm FSK Implementation***
This chapter describes the algorithm implementation based on Frequency shift keying (FSK) in order to estimate the sound time of arrival (TOA). It is an essential step in distance estimation.

• Chapter 6: ***Results Discussion***
In this section, all obtained results are shown and discussed. The algorithm that best approached the distance estimation is evaluated. Lastly, the best AM and FSK methods will be compared.

• Chapter 7: ***Conclusions and future developments***
In the last chapter, some conclusions are summarized, and the possible future development briefly discussed.

Chapter 2 Background

2.1 Cardiovascular system physiology

The heart is an organ essential for the life of human body: it works like a mechanical pump that pushes blood into the circulatory system (***Figure 2.1-2***). The ensemble of heart and vascular structure forms the cardiovascular system; its principle scopes are the nutrients transfer and the pickup of waste products to and from tissues.

The human heart is placed in the middle of the body, between the lungs, above the diaphragm, behind and slightly to the left of centre breastbone.
Multiple layers constitute walls of the cardiac muscle: the outside thin layer is the pericardium; the middle layer is myocardium and the inside sheet is called endocardium. Concerning the external coating, pericardium, it is formed by two strata; the first and external, linking the heart to bounder tissues, has a structural function, whereas the internal part, called serous pericardium, adheres to the myocardium. The fluid layer allows heartbeat and the consequent pericardium deformation.

The heart is firstly divided into two regions by a wall, called septum. Moreover, the right and left sides are again subdivided into other two parts by valves. In this way, the organ has a total of four chambers, named by their position: the uppers are atria and the lowers ventricles. The two types of chambers have a different function; the atria receive entering blood flow, instead, the ventricles, that are more muscular, push blood out of the heart into the body.

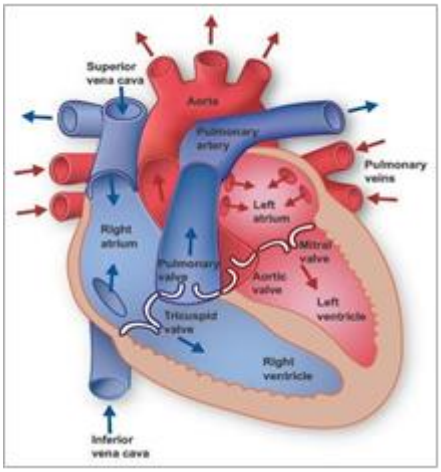

Figure 2.1 Human heart

The organization of the cardiac organ can be considered as divided into two districts: the deoxygenated blood, arriving from vena cava, flows in the right side, while, the oxygenated blood, coming from pulmonary vein, streams to the heart's left side.

There are four valves in heart and they can be of two types: atrium-ventricular and semilunar, depending on their positions. All these work by giving a mechanical response to gradient pressure: each valve gets opened when the pressure in the upper chamber is higher than the one in the lower cavity.
The two atrium-ventricular valves, located between atrium and ventricle, are called tricuspid (right side) and mitral (left side); instead, the semilunar valves are a link between ventricular and aorta or pulmonary artery and their names are pulmonary (right side) and aortic (left side).
The stimulation with electrical impulses of myocardium causes the contraction. These electrical impulses are generated in the sinoatrial node (SA), which is sited at the upper side of right atrium and works as "natural pacemaker".

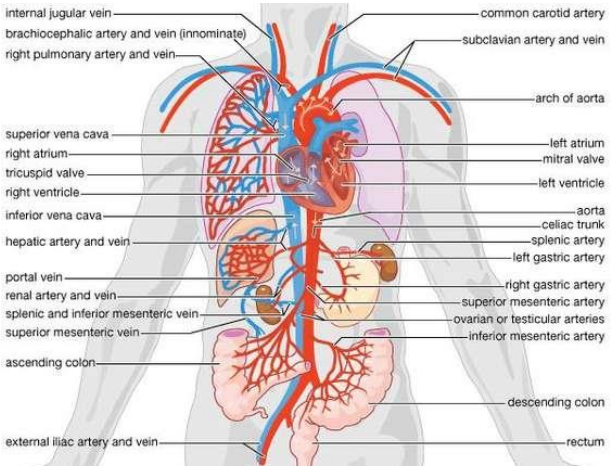

Figure 2.2 Circulatory system [1].

The alternation between relax and contraction of myocardium's muscular cells provides the pumping action of heart, the relaxation phase is called diastole and contraction phase is called systole. The heartbeat rate follows SA activation, that is controlled by autonomous and central nervous system. The whole cardiac cycle can be seen as a sequence formed by four periods, as shown in *Figure 2.3*:

1. Isovolumic relaxation ventricular: When ventricles are relaxed and their pressure decreases, blood flow streams back to semilunar valves and influences their closure. In the same time atriums are filling.
2. Inflow ventricular filling: Atriums and ventricles are relaxed, the atrium-ventricular valves are open for pressure gradient, so the blood flow fills the ventricular chambers.
3. Atrial systole: Contraction of atriums pushes the last part of blood to ventricles.
4. Ventricular isovolumic contraction: It is the first step of ventricular contraction and causes the tapering of AV valves, but it does not produce a massive pressure to open semilunar valves.

Left ventricle contraction mostly increases the pressure, and this gives energy to the blood flow. Thanks to this, blood can proceed through the circulatory system, which is composed of veins, arteries, and capillaries; then, finally, it comes back to the right atrium. At capillaries level, the blood, arrived from arteries, provides oxygen and nutrients to tissues. Meanwhile, tissues release waste product, like carbon dioxide, into vessels and the blood de-oxygenated can come back in heart to repeat the cycle [3].

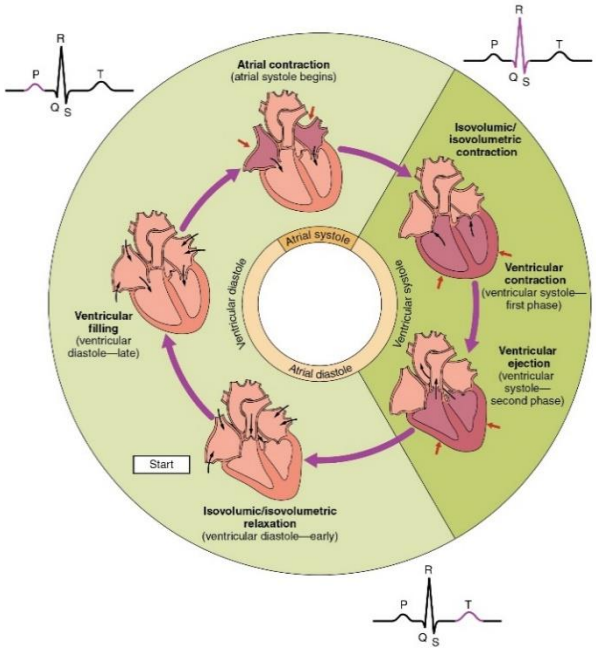

Figure 2.3 Cardiac cycle.

2.2 PULSE WAVE VELOCITY(PWV)

Considering the intricacy of the cardiovascular system, to investigate its properties and to understand health condition of patients, numerous signals as electro cardiac signal, heart sound and parameters like Pulse wave velocity (PWV) could be analysed.

For this purpose, the PWV is an important cardiovascular parameter, that gives information about the danger of the illness, the efficiency of a pharmacological plane and vascular adaptation.

PWV is the velocity at which blood pulse propagates through the arteries in the circulatory system. This parameter is correlated with the mechanical properties of the vessels: higher is the value of PWV, more the artery walls are stiff and few expandable. For example, a variation of stiffness increases the diseases outbreaks.

The clinical approach for non-invasive measurement of Pulse wave velocity is to take the signal pulse in two different arterial points. This let to measure the time employed by the pulse to propagate from one to the other (PTT, pulse propagation time). These sites are taken in correspondence with the carotid arteria, a proximal point that is supposed to be near heart, and with brachial or femoral artery, a distal point situated in a peripheral site.

Several types of waveforms could be used to estimate PWV: Doppler, distension wave, pressure wave. Moreover, usually, ECG is used as reference signal, to consider the initial time of the pulse propagation. There is also another signal, the photoplethysmogram (PPG), that is used more for consumer application. [5]
Finally, PWV is obtained with the following equation:

$$\mathrm{PWV} = \frac{\mathrm{distance}}{\mathrm{pulsedistal(time)} - \mathrm{pulseproximal\ (time)}} = \frac{\mathrm{distance}}{\mathrm{PTT}} \quad (2.1)$$

In this formula, PTT is the pulse transit time and the “distance” is the waves’ spatial pathway of the artery.
A representation of PWV estimation is depicted in ***Figure2.4***.

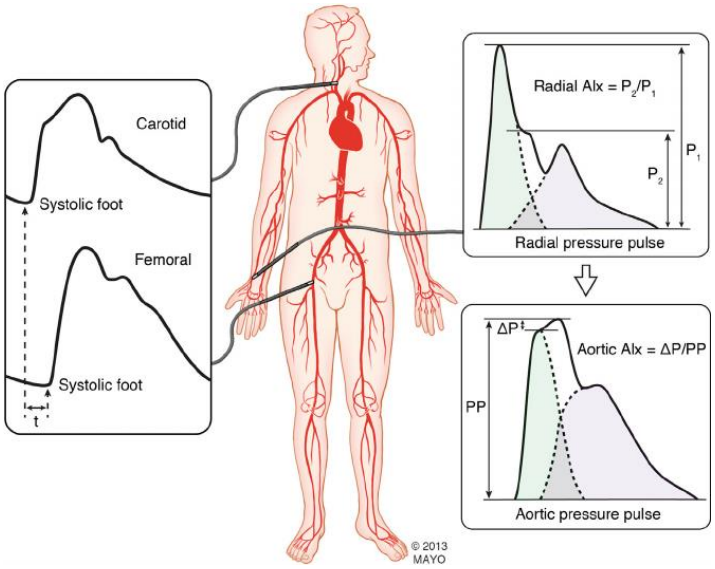

Figure 2.4 Femoral and carotidal estimation PWV.

Variations of PWV values are due to the route of arteries: the final velocity evaluation will depend on the patient arteries characteristic and it will be the average of the blood speed in every crossed vessel [6].
In addition, PWV changes in response to a variation of age, sex, food habits, smoke, and other boundary conditions. The range of a good value is 5-10 m/s, out from this range patient probably might be in pathological condition. ***Table 2.1,*** made by European heart journal, reports the reference value for PWV [7].

Age category	Mean (± 2 SD)	Median (10-90 pc)
<30	6,2 (4,7-7,6)	6,1 (5,3-7,1)
30-39	6,5 (3,8-9,2)	6,4 (5,2-8,0)
40-49	7,2 (4,6-9,8)	6,9 (5,9-8,6)
50-59	8,3 (4,5-12,1)	8,1 (6,3-10,0)
60-69	10,3 (5,5-15,0)	9,7 (7,9-13,1)
≥70	10,9 (5,5-16,3)	10,6 (8,0-14,6)

Table 2.1 Healthy patients PWV reference values according to the age [7].

2.2.1 Devices for PWV Measurement

To non-invasively analyse the cardiovascular system with PWV evaluation, numerous procedures have been designed. In the clinic environment, diagnostic medicine usually used some devices, which have been infrequently employed as screening tools for a massive group of
people. An example of adopted techniques is ultrasonic sensor and magnetic resonance imaging (RMI), but they are too expensive and hard to manage. Recently, other systems for quantifying PWV have been launched onto the market and they are mostly based on pressure sensors as the tonometer.
The gold standard for clinical PWV measurement is a device, Sphygmocor, based on pressure sensors. Momently, this tonometry equipment is mainly diffused in research and clinical environments rather than in ambulatory practise [8].

To better understand how the main PWV estimators work and the signals involved, it is important to briefly mention "the electrocardiogram" (ECG). This bio-signal gives information about the electrical activity of the heart and it detects tiny electric potential differences due to depolarization and repolarization of the cardiac organ's chambers.
Specifically, during the cardiac cycle, the depolarization of some muscular cells and polarization of some others creates a charge separation and relative electric dipole moment. The dipole movement involves the creation of floating electric fields through the tissues. Placing the electrodes on the skin is possible to detect the magnitude of electric fields the rising electrocardiogram [4].

This signal is widely used in the clinical environment for diagnosis, and it is also employed to evaluate pulse wave velocity: it is used as a reference signal for the starting point with which to calculate the pulse transit time.
The main commercialized devices for this application are three and will be briefly described below.

The PulsePen® (DiaTecne, Milan, Italy), is a non-invasive device capable of assessing: central blood pressure, pulse wave velocity and pulse wave analysis. This device has two work methods; the first approach, named "ET", is for PWV estimation and it uses two signals: an electrocardiogram (ECG) and one pressure wave acquired by a tonometer, first in the proximal and then in the distal point. Instead, the upgraded model, called "ETT", allows the PWV evaluation only in one step using two probes for the two sites, in the same instant and without acquiring ECG signal [9].

Figure 2.5 Pulse Pen® device [10].

The *Complior*® (Colson, France) is based on piezoelectric force sensors. The operator simultaneously places the sensors in proximal and distal spots and the device acquires the pressure pulses signal. A benefit is the absence of ECG to measure PWV [11].

Figure 2.6 Complior device [12].

SphygmoCor® and SphygmoCor Xcel® (AtCor Medical, Sydney, Australia) are two devices based on tonometry technology. The gold standard for non-invasive measurement of PWV is the first device. SphygmoCors are able to obtain cardiovascular parameters that cannot be acquired with traditional brachial cuff blood pressure measurements. The first instrument implements PWV evaluation in a two-step approach: tonometer sensor acquires signal from carotid and femoral sites separately and they are referred to ECG signal. Instead, the update device does not use the ECG as reference and it records signals in proximal and distal zones at the same time [13].

Figure 2.7 SphygmoCor device [13].

For PulsePen, Complior, and SphygmoCor the pathway travelled by pulse wave is manually evaluated: the operator, moving far from the patient body to overlook protuberances, projects in air the distance between detection sites and measures it with a common tape measure.

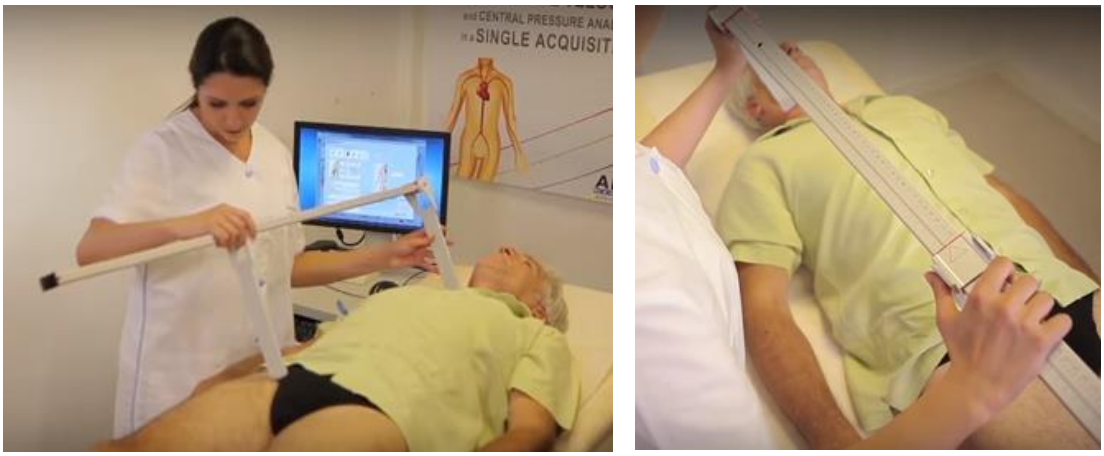

Figure 2.8 Example of how the measurement is made with a measure tape.

As said before, in the clinical environment, the most popular device is the Sphygmocor. But, beyond the three devices described before, there are other techniques to evaluate PWV:

1) *Photoplethysmography*:

This technique is an optical measurement that, uses a light source to send a signal through biological tissue and by measuring the amplitude of the reflected light, it estimates the difference of blood.

This methodology embraces numerous advantages, for example, lower motion artifacts and the option to examine deep tissue using infrared light penetration (important for examining cardiovascular risk in obese subjects). On the other hand, a possible weakness could be the light reflection of bounder tissues around the acquisition points introducing noise on signal.

2) *Ultrasound (US)*:

The US method allows estimating the PWV through the time delay of the diameters waveforms synchronously acquired in two near points on the arteries. The PWV is calculated as the proportion of the longitudinal diameter gradients and temporal gradients [8].

3) *Magnetic Resonance Imaging (MRI)*:

PWV can be measured by MRI technology analysing the data related to the blood flow speed collected by this analysis device. Trough the data are calculated: Δx, it is the distance of aortal arteria pathway from proximal to distal imaging levels; Δt that is the interval time that the pulse wave spends to reach the farther level from the proximal layer. The pulse transit time assessment is an algorithm based on the wave's foot arrival evaluation. So PWV is calculated as $\Delta x/\Delta t$. The intricacy and the cost of this technology have limited its use and diffusion for diagnostic. [8].

It has to be noted that, contrary to all the devices and the approaches here explicated, the best method to make an exact PWV examination is to proceed with an invasive technique of catheterization from a peripheral artery, during an angiography. This technique is not seen as a reference method to use for its invasiveness, except during a vascular procedure or cardiac diagnosis.

2.3 Measure distance of PWV

In this paragraph will be studied and analysed the problems and the actual methods to make the distance measurement in PWV evaluation. In some extent, it has been seen how the uncertainty in the evaluation of the distance between sites increases the probability to get wrong PWV value. In fact, as described before, the distance is directly proportional to the blood velocity.

Although the pulse wave velocity is quite commonly used, there is not a standard method to measure the distance between detection sites. During the last years, several ways for the distance assessments have been addressed. The different ways to calculate the distance of the pathway are due to the need to better describe the curvilinear shape of arteries. It has to be specified how all the methods are a model of the pathway and so an approximation, only imaging and invasive methods give a complete and reliable information.

In assessing the distance there are problems that are not taken into account, but which can lead errors, it is the typology of the study group and the patient conditions.
The subject-specific measures and reference values of PWV change from a centre to another centre, so they are representative for a restricted geographical community. This variance depends by different techniques used between work teams; also, there is a variance inside the centre caused by operator errors [14].

Moreover, not just user errors, but also the patient's health condition adds failings in distance measurements. For example, some health problems, that could lead errors, are diabetes, sclerotic arteries, more fat on the abdominal level, mostly for men, and a larger circumference of bust in women [15] [17].
It has been seen how the diverse methods and uncertainties introduced during the distance valuations could lead an error of PWV of 30 percentage [7].
Additionally, the accuracy of the distance evaluation has different relevance according to the case study. For example, in a scientific study with several measures and operating in only a centre it is less significant. On the other hand, the measurement precision gains importance for the comparison works of various centres for meta-analysis or a simple data matching [16].
Over time, many models have been developed to find a solution to these problems and to get a distance assessment less correlated to bounder conditions.
A list of methods, to approximate the travel of arteria between carotidal and femoral zones and described in the following paragraphs, are:

- Measurement by MRI and invasive methods ("gold standard").

- Direct measure of distance between proximal and distal points by tape measure;
- Combination of direct measures;
- Estimation of distance, not depending on direct measure but as a combination of parameters;

The second and third methods listed are being treated together.

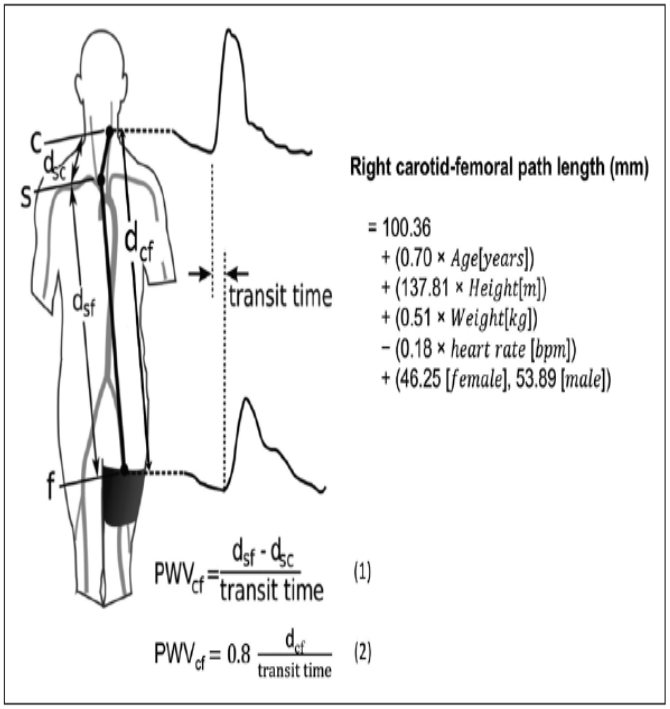

Figure 2.9 Representation of distance in carotidal-femoral pulse wave velocity. Equation (1) are using subtracted methods; Equation (2) are using the total distance between carotidal and femoral zones multiply for the "0.8 parameter"; In right side, there is Weir-McCall et al.'s formula [14].

2.3.1 Measurements distance with invasive method

An angiographic coronary workstation, that can be mono or bi planar, is able to quantify pulse wave velocity in an invasive way. Firstly, the operator inserts a catheter in arteria and fills the vessel with a contrast medium, necessary to evaluate by fluoroscopy the position of external object introduced. After the position check, ECG and pressure wave are recorded in two different sites, ascendance aorta and aortic bifurcation. While the catheter is marked in the signal acquisition points, subsequently its removal, the user can calculate length between the two markers.
Operator evaluates PTT manually or using an informatics algorithm [17].

2.3.2 Measurements distance with MRI

The MRI examination is very accurate to evaluate pulse wave velocity and the distance between acquisition sites. The problems are costs and the time needed for it, which do not allow the device to be a diagnostic and prevention instrument for large-scale analysis, but it is able to validate other methods. Specifically, for calculating the length, vitamin A like contrast medium has to be injected. The vitamin A enables to identify the specific points of bounder surface of arteria to calculate the pathway travelled by pulse wave.
Lastly, in post-processing, the operator manually inserts a point centre for every 2D layer, and evaluates distance point by point, starting from the distal mark and arriving at proximal one [18].

2.3.3 Methods of measure with direct distance

Concerning the methods for the direct distance measurement, they are the ones for the straight distance evaluation between the specific sites. In fact, these measurements can be obtained in a physic-direct way or as a result of a parametric equation.
To better approximate the tortuous path of the circulatory system the first measures employed to evaluate the distance between the two sites where pulses are taken, are:

1. The direct distance from carotidal arteria to femoral one;
2. Distance obtained by the subtraction between carotidal and femoral arteria sites and the carotidal spot-sternal notch length;
3. Distance obtained by the subtraction between the sternal notch-femoral site and the carotidal spot-sternal notch length.

Generally, the study to evaluate the goodness of model is referred to assessment with MRI or invasiveness method [16].
Weber et al. [17], through a study with 135 patients, have verified the distance methods that allow the best fitting between non-invasive PWV and invasive PWV. The best agreement was gotten by the third method listed before.
On the other hand, another work team, Sugawara et al. [18], have made a clinical research with 235 patients; this time the reference chosen for the research was MRI PWV. The collected data show that the second listed method is the best to agree with the reference, as it is possible to see in the following tables. The ***Tables 2.2 and 2.3*** represent statistics of the two just described works.

	Mean difference (m/s)	Spearman's R	P
Invasive vs M1(direct car-fem)	-2,9	0,76	<0,0001
Invasive vs M2 (direct car-fem-car-ssn)	-1,3	0,75	<0,0001
Invasive vs M3 (ssn-fem-car-ssn)	-0,2	0,73	<0,0001
car = carotid; fem = femoral; ssn = suprasternal notch			

Table 2.2 The representation of the difference between the reference value of invasive method and models used [17].

	Arterial path length [mm]	Difference [mm]
MRI	493±35	
car-fem	621±37	128±34
(car-fem) - (ssn-car)	518±31	25±26
(ssn - fem) -(ssn-car)	427±29	-66±24
(ssn -umb- fem) -(ssn-car)	458±30	-35±24
car = carotid; fem = femoral; ssn = suprasternal notch		

Table 2.3 Estimation of the pathway with several methods and difference with the MRI's reference values [18].

A further model to evaluate the pathway is to measure the total distance and multiply it for a constant equal to 0.8. This "optimum" value was found by S. Huybrechts et al. [15], who started from the two labours of Webber et al. and Sugawara et al.
The first group, Webber et al [17] [15], said that the total distance overrates about 20 percent the measure evaluated by invasive PWV, this founded relation was converted to a correction parameter equal of 0.794.
The second group, Sugawara et al. [18] [15], discovered that the direct distance from femoral to carotidal arteria overestimates of about the 25 percentage the real pathway, that is calculated with MRI exam. So, the final correction value was updated to 0.771.
***Table* 2.4** shows some different ways to calculate distance and relative errors, compared with the reference value.

Reference distance [cm]	Tape measure distance [cm]		Tape measure - reference distance [cm]
(AA-FA) -(AA-CA) = 50.7(4.2)	(CA-FA)-(CA-SN)	48.3(4.1)	-2.35(3.8)
	(CA-FA)-(CA-SSN)	53.0(4.1)	2.32(3.8)
	(SN-FA)-(CA-SN)	35.9(4.1)	-14.77(3.9)
	(SSN-FA)-(CA-SSN)	45.8(4.8)	-5.11(3.5)
	(SSN-UMB)-(UMB-FA)	57.7(4.8)	7.18(4.0)
	(CA-FA)	63.6(4.4)	12.99(4.2)
	[(SSN-UMB)+(UMB-FA)]-(CA-SN)	42.3(4.7)	-8.18(4.1)
	[(SSN-UMB)+(UMB-FA)]-(CA-SSN)	47.0(4.7)	-3.51(4.1)
	(CA-FA) X0.8	50.9(3.5)	0.26(3.8)
	Body height/4+C	50.2(2.3)	0.5(3.9)
	Body heightx0.29	49.8(2.5)	0.9(4.0)

Table 2.4 The table shows the reference value in the first column, values measured with several models, and in the third column there is the difference between the reference and the assessment. The table's data are mean and (SD). The acronyms are AA ascending aorta; CA carotid artery; FA femoral artery; SN sternal notch; SSN suprasternal notch [15].

Another team, J. Vermeerscha et al. [19], developed two equations: the first to extract the direct distance from the subtracted one, i.e. the difference between the distance femoral site-sternal notch and the carotidal arteria-sternal notch, and a second equation to make reverse the first function.
Moreover, these equations introduce a correction feature depending on the subject's height. The described equations are depicted by the following formula:

$$X_{\text{direct}} = 0.45 * X_{\text{subtracted}} + 0.21 * \text{height} + 0.08\ (\text{m}) \quad (2.2)$$

$$X_{\text{subtracted}} = 1.04 * X_{\text{direct}} - 0.11 * \text{height} - 0.02\ (\text{m}) \quad (2.3)$$

This case study advises that to obtain a good value of PWV, starting from distance subtraction and using the total distance obtained with the previous equation, it is better to correct the final value multiplying it for a correction factor 0.8 [19].

2.3.4 Methods of measure with anthropometric parameter

The methods to obtain the distance between acquisition sites shown in this paragraph, are defines as some approaches to evaluate distance with no direct measurement, but that let to extract a quite reliable point-to-point measurement using algorithms based on anthropometric parameters. This methodology should eliminate the variability inter-center, improve the possibility to compare the data, decrease the measurements errors and the uncertainty due to used models and operator. As written previously, inter-center variability means the errors due to the operator during the measurement, the different models used, the methodology to acquire the measure and the various boundary conditions. Everything listed brings a variability and therefore a difficulty in comparing data of different centers. Now some works will be presented describing methods for measuring distance with anthropometric parameters.

Webber et al. [17], have formulated an example of indirect method; it is simple and depends only on patients' height. The knowledge behind the formulation was induced by the quarter-wavelength relationship. The equation (below presented) was identified from the pulse wave reflection works.

$$\mathrm{X\,[cm]} = \frac{\mathrm{Height\,[cm]}}{4} + 7.29\,; \quad (2.4)$$

Analysing the invasive pulse wave velocity, the Webber's work team produced this mathematical relationship threated in [17], but there is not a validation of the function in the above-mentioned paper. Whereas, Huybrechts et al. [15] has tested the function; the results are shown in Table 2.*4* where the values related to the length are the second most similar to the reference.
As it could be seen, the problem for this procedure is that this theoretical relationship deviates from reality when some or all patient's factors change; as the body mass index, cardiovascular pathologies, and diabetes.

Lastly, likewise, Weir-McCall et al. in [14], focused to eliminate the measured distance and to link the distance between acquisition sites only to anthropometric parameters, such as age, height, weight, heart rate, and sex.
Starting from a dataset, proceeding with a regressive method, they extracted these equations:

$$\mathrm{RCFP} = 100.36 + (0.70 * \mathrm{Age[years]}) + (137.81 * \mathrm{height[m]}) + (0.51 * \mathrm{Weight[Kg]}) - (0.18 * \mathrm{heart\ rate[bpm]}) + (46.25[\text{if female}], 53.89[\text{if male}]) \quad (2.5)$$

$$\mathrm{LCFP} = 61.03 + (0.81 * \mathrm{Age[years]}) + (132.5 * \mathrm{height[m]}) + (0.59 * \mathrm{Weight[Kg]}) + (0.21 * \mathrm{DBP[mm\ Hg]}) - (0.14 * \mathrm{heart\ rate[bpm]}) + (60.51[\text{if female}], 68.48[\text{if male}]) \quad (2.6)$$

Where, for RCFP is intended the “Right Carotidal Femoral Path length” and for LCFP the “Left Carotidal Femoral Path length”.
The last work decreases the variation inter-center as “the 0.8 method”, previously described in **2.3.3**. The main problem is that the anthropometric parameters vary by changing the population from which the dataset is extracted. Consequently, the other problem is the lack of threshold values of PWV calculated with this model to identify the patient condition [14].

2.4 Sound Propagation

The sound is a mechanical perturbation of an equilibrium state and it is transmitted through an elastic material. In the air, sound travels as a longitudinal wave, formed by mechanics vibrations. The periodical alternation of compression and relaxation of this material produces a sound wave at a specific speed.

To try to describe this phenomenon through a model, the first assumption is to represent the sound as a planar wave to simplify the math formulation. But this approximation is not real, because wave produced from a source moves in a sequence of spherical wavefronts and not in straight pathway.

The essential mechanism of sound wave's propagation is identified as Huygens' Principle, for which "every point on a wave is a source of spherical waves in its own right" [22]. By this statement the wavelets combine together in the frontward trend to produce a novel wavefront, and interfere destructively in the retrograde path; so doing the waves keep propagation forward direction.

Starting from the approximation said before, the sound wave can be described as a sinusoidal curve, is a mathematical representation of planar waves.
The simplest formula is:

$$y(x,t) = A\sin\left(2\pi ft - \frac{x}{\lambda}\right). \quad (2.7)$$

The specific distance between a pressure wave variation and another same is called *wavelength*, its symbol is λ and its unit of measurement is the meter (m). An additional parameter used to describe a wave is *period*, denoted by *T*: it represents the time passed from a pressure wave variation and another. The period inverse is the *frequency(f)*, which is calculated in Hertz (Hz, equivalent to fractions of a second) and consists of the number of wavelengths going across a point into space.

The relation between a wave's frequency and its period is:

$$fT = 1 \text{ or } f = \frac{1}{T}. \quad (2.8)$$

Additionally, the relation between the wavelength and its frequency or period gives information about the *speed* of the wave (*S*):

$$S = f\lambda = \frac{\lambda}{T} \quad (2.9)$$

As it could be seen from the last relation, frequencies and periods are inversely proportional. Moreover, the intensity of a sound wave depends on its amplitude. The Acoustic *intensity* is defined as "the average rate of energy transmission per unit area perpendicular to the direction of propagation of the wave", and its formula is

$$I = \frac{A^2}{2\rho S} \quad (2.10)$$

The ρ is the density of air [Kg/m^3], the S represents the speed of sound [m/s], and, indeed, I is the intensity [W/m^2].

Wave velocity of sound is reformulated like the square root of the ratio of the elastic modulus of the medium and its density or inverse of density multiply for compressibility of gas:

$$S = \sqrt{\frac{B}{\rho}} = \sqrt{\frac{1}{\rho K}}; \quad (2.11) \qquad B = \frac{1}{K}; \quad (2.12)$$

In the formulation of speed B is the elastic modulus of the medium, K the compressibility of gas. Approximating aria as an ideal gas and using gas laws, sound speed can be expressed in two formulas, depending on pressure or temperature*:*

$$S = \sqrt{\frac{\gamma P}{\rho}} \quad (2.13) \qquad or \quad S = \sqrt{\frac{\gamma R\theta}{M}} \quad (2.14)$$

Where: P is pressure [Pa], ρ the density [Kg/m^3], θ is absolute temperature [K], R represents gas constant [J/ (m*K)], M is molecular weight of the gas [g/mol], and indeed γ is the ratio between the specific heat at a constant pressure and the specific heat at a constant volume.

$$\gamma = \sqrt{\frac{C_p}{C_v}} \qquad (2.15)$$

Starting from the equation of the sound speed related to the temperature, replacing inside the values of the constants for the air and switching the temperature from the Kelvin scale to the Celsius scale, the preview formula becomes:

$$S = 331.3\sqrt{1 + \frac{\theta}{273.15}} \qquad (2.16)$$

In this new equation, the sound speed is determined by the temperature parameter and is independent of the pressure, this happens because of the introduced approximation for an ideal gas.

Furthermore, the previous equations of speed are not correlated with the frequency, so the velocity of a sound wave is the same at every frequency. This is again due to the ideal gas hypothesis, but if gasses are at high pressures, this assumption is not more valid because there are effects such as absorption, dispersion, diffraction, and reflection, which will be described following [22].

Sound absorption

The physical processes that dissipate an amount of sound wave are denoted as "*Sound absorption*" when the signal is traveling into the air or another medium and this could happen for two different causes.
Firstly, the most important process is the energy transfer from mechanical vibration to thermic, as heat into the medium. Secondly, this phenomenon is produced by the transformation from a coherent molecular motion of the wave to incoherent molecular motion in the propagation material.
The viscosity of a fluid medium, for example, caused dissipation by the second type of dissipation origin. The combination of these two phenomena causes the attenuation of sound wave amplitude [22]:

$$A(x) = A_0 e^{-\alpha x} \qquad (2.17)$$

In the formula above, A_o *is* the original amplitude of the wave, $A(x)$ is the amplitude after distance x through the medium, and α is attenuation of medium proportional to square frequency, humidity, and temperature.

Diffraction

The *diffraction* property has derived by Huygens' wavelets construction, it is the ability of sound waves to curve around angles and to expand when they pass through a tiny gap.
The diffraction property of a sound's wave decreases when frequency increases and wavelength rises down.
When a sound wave collides with a surface, a part of it is reflected and the other part is propagated and or diffracted. The size of colliding obstacle and wave's wavelength influence the reflection of the acoustic wave. If the obstacle and the wave wavelength have the same size, diffraction can take place, and this would influence the diffracted waves with interferences. If this happens, some spaces, called acoustic shadows, will form zones with greater or lesser sound intensity [22].

Reflection

The property of reflection for sound waves can lead to echoes creation. This phenomenon happens every time an acoustic wave crosses two or more different mediums. To be exact, the reflection happens every time the speed parameter is modified, or the sound's propagation pathway significantly changes. For the effect of the reflection, the direction of propagation varies perpendicularly to the wavefront of all the Huygens' wavelet [22].

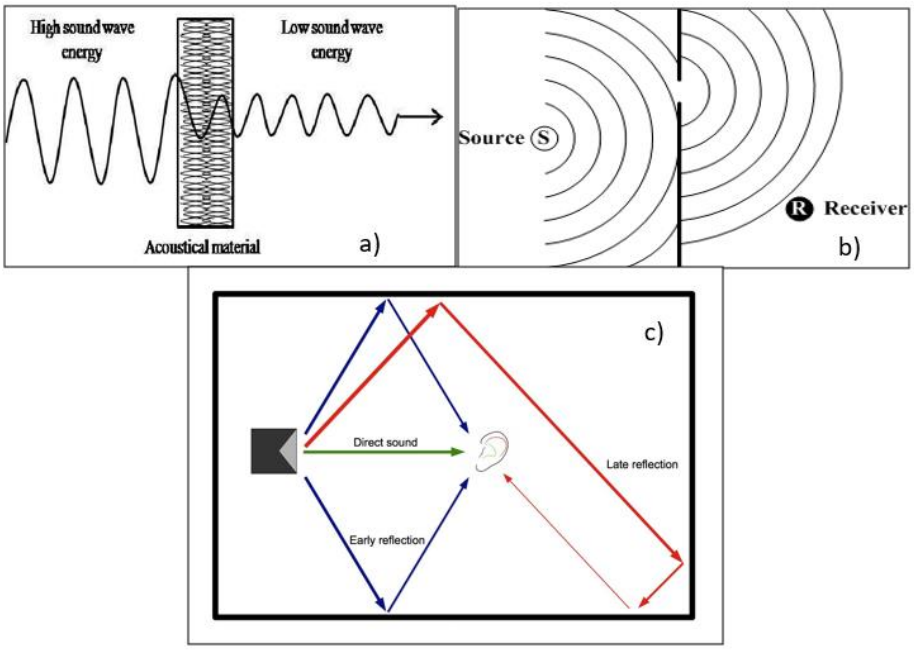

Figure 2.10 Absorption effect b) diffraction effect c) Reflection effect.

2.5 TDE: Time delay estimation

The aim of this thesis work is to design a system for the automatic distance measurement for the estimation of pulse wave velocity (PWV). For this purpose, the basic principles of time delay estimation (TDE) are here exploited. This paragraph describes some models and problems that can be addressed in the sound propagation delay evaluation.

The time delay estimation (TDE) can be considered as the first step of a larger blockchain, able to detect, identify and locate the source of an acoustic signal. The TDE can be applied to various waveform types and found application in several technology fields as sonar, radar, geophysics, ultrasonic, seismology, and communications. Depending on the goal and the boundary conditions of the application where it has to be used, there are two different approaches for Time delay estimation:

- the time of arrival (TOA) estimation;
- the time difference of arrival (TDOA) estimation.

TOA and TDOA are correlated because have similar targets; nevertheless, their critical aspects are deeply different.
Commonly, the source of the signal is placed in an environment, where noise is always present, and it is impossible to eliminate.

Moreover, the signal acquired is often a sum of copies of the original wave. Copies, caused by reflection, that are delayed and attenuated compared to the reference.
The formation of many propagations multipath creates echoes effect and spectral distortion and they will degrade the signal. Another condition that adds difficulty in the evaluation of time delay is the movement of the source; because if it changes position in the space, in the same moment time delay will vary. For this reason, time delay estimation is a complex and stimulating problem and researchers have tried to resolve it using different techniques and different models of the received signals [23].

The following paragraphs provide an overview of the patterns used to approximate the signal, considering each acoustical phenomenon, and, lastly, the two main ways for location method: TOA and TDOA.

2.5.1 The ideal single-path propagation model

The first proposed signal propagation model is the simplest. It is an ideal representation of the sound wave propagation in which there is a single signal that arrives at the microphone. Supposing to have an array of *N* sensors that acquire the signal, the received acoustic wave is similar the original one, but it is reduced in amplitude, it is delayed in time, and it is affected by noise. Mathematically the formula is:

$$x(t) = a_n s(t - \tau_n) + w_n(t); \qquad n = 1,2, \dots N \qquad (2.18)$$

In the equation is present: an attenuation factor a_n ,for the n-th sensor, that multiplies the source signal s(t) function; $w_n(t)$ is the nth sensor-additional noise signal and it is unrelated to the source signal, indeed, τ represents the delay between source and *nth* sensor [23] [24]. According to this model, the signal follows only a direction and only the absorption is considered, but there are other effects that deteriorate the acoustic sound as seen in **Paragraph 2.4**. All this increases the problem complexity, making other schemes necessary.

2.5.2 The multipath propagation model

The multipath model is widely used in physical applications like radar, sonar, and geophysics. In this sound propagation description, the acquired signal is the combination of a single emitted wave that has travelled several pathways ***Figure 2.9***. In addition, the signal recorded depends on the delay of every way, attenuation of the original signal and the noise added. The formula produced for a single sensor is:

$$r(t) = \sum_{K=1}^{M} a_k s(t - tk) + w(t); \qquad (2.19)$$

Where s(t) is the source signal; a_k is attenuation factor for pathway travelled, and τ_k is time delay for the k-th path. All is summed with the w(t), a white Gaussian noise.
This model, like the first in 2.5.1, is an approximation and they both are not usable for every location. Moreover, in these models, scattering effects are not considered and if there are several paths the delays are difficult to evaluate [25] [26].

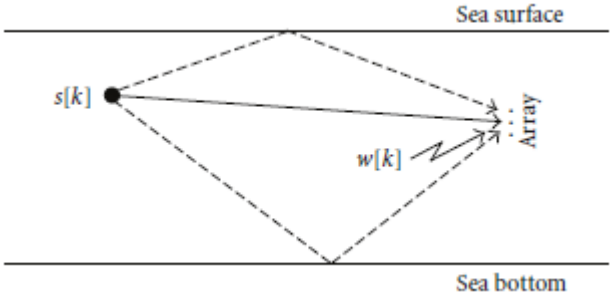

Figure 2.11 Multipath model of a sound signal.

2.5.3 The reverberation model

Lastly, the propagation model presented in this paragraph is the system which evaluates reverberation effects. In this case, the complexity of the model is bigger. The signal is the combination of a single waveform that has been reflected with objects and edges of the room. In fact, before reaching the sensor, the sound can be reflected several times. The model, which takes into account reverberation, is mathematically expressed like:

$$x_n(k) = h_n * s(k) + w_n(k) \quad (2.20)$$

Where: the * operator means convolution, h_n represents channel impulse responses from the origin of signal to the microphone, the signal generated is referred as s(k). At the end is added a $w_n(k)$ white Gaussian noise, and all let to obtain the total signal recorded $x_n(k)$.
In this model (**Figure 2.10**), the time delay is not clearly expressed, and this causes difficulties to resolve TDE problems. To get the delay time, firstly, the channels' impulse responses is evaluated, then the direct propagation pathway is researched. If there is no information about the source signal, the only evidence that can be used is the acquired data, then the channel impulse responses will be extracted in a blind mode [27].

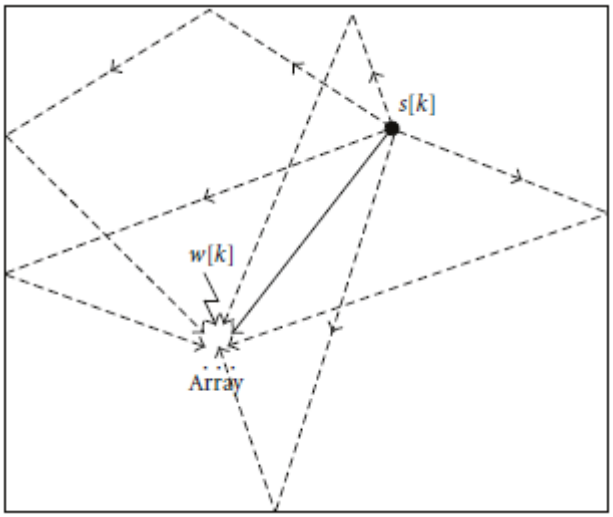

Figure 2.12 Reverberation model of a sound signal

2.5.4 TOA: Time of arrival

The aim of the TOA technique is to measure the time delay between the instant in which a pulse signal is emitted and the arrival time of its echo. This is of primary importance for technologies as radar, active sonar and commonly for any active location system.
The most significant feature of the system based on TOA is the knowledge of transmitted signal, also called "clean" reference signal. Accordingly, to evaluate the time delay is needed a generator of signals, as a speaker, and a single sensor to record signal. TOA (Time of arrival) is the period passed between the conduction of a pulse and its revelation, in last instance, the distance, travelled by wave's front end, can be extrapolated.
The resolution, or localization precision, is subject to the TOA assessment accuracy and the knowledge of sound velocity in the medium. In fact, the temperature influences the speed of sound and the thermic effect of the environment must be compensated [28].
The process starts from an ideal situation, where there are not reverberation effects and echoes, and white Gaussian noise is uncorrelated with the original signals. Therefore, the signals used to get the time delay and distance are: the original signal (x_1) as a reference and the signal recorded that is amplitude attenuated and time delayed (x_2):

$$x_1(t) = s(t) + w_1(t) \qquad (2.21)$$
$$x_2(t) = \alpha s(t-\tau) + w_2(t) \qquad (2.22)$$

Making crosscorrelation between two signals:

$$R_{x_1x_2}(\tau) = E[x_1(t)x_2(t-\tau)] \qquad (2.23)$$
$$R_{x_1x_2}(\tau) = \frac{1}{T-\tau}\int_{\tau}^{T} x_1(t)x_2(t-\tau)dt; \qquad (2.24)$$

The time delay (τ) will be the argument that maximizing the crosscorrelation function. From this interval, according to the sound speed (c for a specific temperature) is possible to estimate the distance (δ) between the speaker and the sensor:

$$t_0 = \arg\max(R_{x_1x_2}(\tau) \qquad (2.25)$$

$$\delta = c * to \qquad (2.26)$$

2.5.5 TDOA: Time delay of arrival

The time delay of arrival (TDOA) tries to assess the time employed by wavefront to travel between two different acquiring sensors spaced between them. Typically, this approach is related to passive systems such as microphone array systems or passive sonars. Contrary to the TOA, here the reference signal is unknown; in this instance, the delay approximated is the difference between wave's arrival times at two spatially separated sensors.
The signal s(t) spreads out through a medium, where there are noise and interferences, that change s(t) in the two signals acquired by sensors $x_1(t)$ and $x_2(t)$:

$$x_1(t) = \alpha s(t - \tau_1) + w_1(t) \quad (2.27)$$
$$x_2(t) = \alpha s(t - \tau_2) + w_2(t) \quad (2.28)$$

Where: $x_1(t)$ is the signal acquired by the first sensor, $x_2(t)$ is signal acquired by the second sensor, and τ_1 and τ_2 are the delay time due to the travelled path for signal x_1 and x_2.
Taking the signal with the smallest delay as the reference signal, mathematical formulas become:

$$x_1(t) = s(t) + w_1(t) \quad (2.29)$$
$$x_2(t) = \alpha s(t + D) + w_2(t) \quad (2.30)$$

Where:

$$D = \tau_2 - \tau_1 \quad (2.31)$$

As in the TOA case, in particular condition, the simplest way to obtain D is performed by a cross-correlation function.

$$R_{x_1x_2}(\tau) = E[x_1(t)x_2(t - \tau)] \quad (2.32)$$
$$R_{x_1x_2}(\tau) = \frac{1}{T - \tau}\int_{\tau}^{T} x_1(t)x_2(t - \tau)dt \quad (2.33)$$

And the final distance, as said before, could be obtained in this way:

$$t_0 = \arg\max(R_{x_1x_2}(\tau)) = D \quad (2.34)$$
$$\delta = c * to \quad (2.35)$$

The TDOA evaluation, when the received signals are purely delayed and muted, is an easy assignment.
But, as mentioned above, cross-correlation, in many real cases, is not the best technique to achieve a quantitive valuation of time delay because reverberation, noise and interference damage the signal. Many algorithms had been made for surmounting problems that afflict signal.

2.6 Employed Devices and Tools

In order to measure the distance between PWV acquisition sites addressing an automated and inexpensive approach, different STMicroelectronics devices have been considered for our goal.
The adopted devices are:

1. The STM32F429 Discovery Kit allowed to supervise and control the whole distance acquisition process and the data transmission to PC through an USB interface
2. The MP3AB01H analog MEMS microphone
3. A 8Ω miniaturized speaker
4. The LM386N Audio Amplifier allowed driving the sound speaker

For the firmware and algorithms implementation, the following software tools have been adopted: KEIL µVision5 for ARM microcontrollers and the Matlab™R2018a numerical computing environment from MathWorks.

2.6.1 Analog microphone MP33AB01H

The MP33AB01H is a compact, low-power MEMS microphone assembled with a low-profile sensing component. The sensing component, capable of detecting acoustic waves, is manufactured using a specialized silicon micromachining process for audio sensors production.
The main acoustic and electrical characteristics are listed in ***Table. 2.5*** and are specified for a Vdd=2.2 V [31].

Characteristic	**Value**
Current consumption (**Idd**)	0,25 mA
Sensitivity at 1kHz (**SO**)	-38dBV
Signal-to-noise ratio at 1kHz (**SNR**):	66 dB
Distortion at 125 dBSPL (THD)	10%
acoustic overload point	125 dBSPL
Operating temperature range	-30°C to +100°C

Table 2.5 Acoustic and electrical characteristics of the MP33AB01H microphone [31].

Distinctive frequency response normalized at 1 kHz is reported in ***Figure 2.11***.

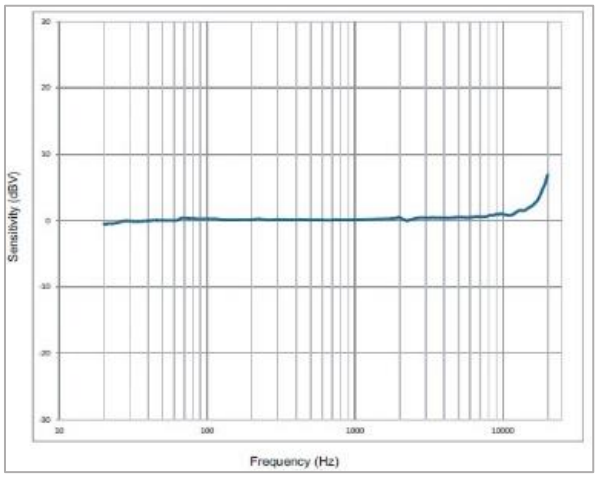

Figure 2.13 MP33AB01H typical frequency response [31].

2.6.2 Speaker RS PRO 8Ω

Miniaturized speaker RS Pro is a compact and low-power speaker realized in Polyether ether ketone (PEEK). It is ideal for PDA, smartphones and medical device.
The specifications for this device are shown in **Table 2.6** [32].

Characteristic	**Value**
Dimensions	9 x 16 x 3 mm
Rated impedance	8 Ω
rated input power	0.7 W
frequency range	200Hz - 10KHz
operating temperature	-30 a +70°C
sound pressure level at 2Vrms/0,1m	88 dB

Table 2.6 The acoustic and electrical characteristics of speaker RS PRO 8 Ω [32].

Frequency response curve at 2.0Vrms/10cm in 1cc box is represented in ***Figure 2.12***.

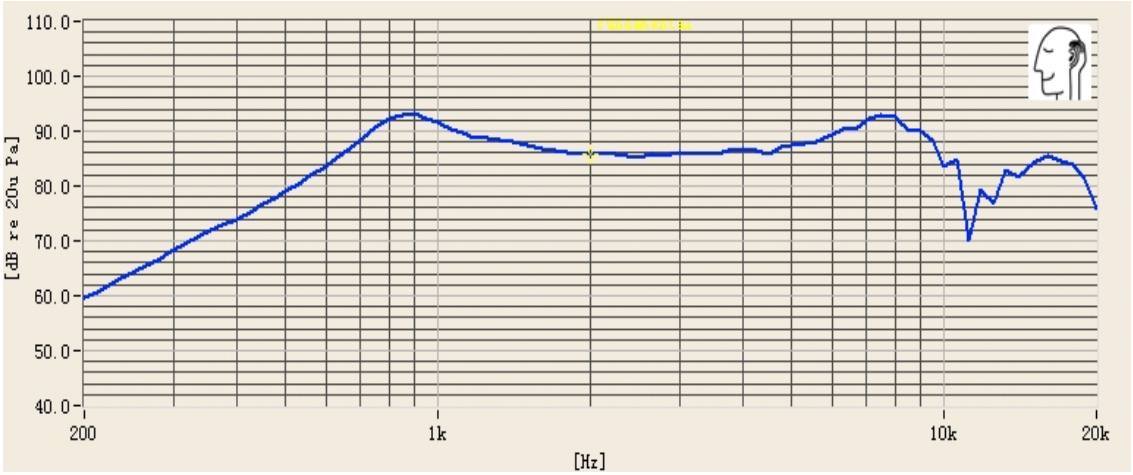

Figure 2.14 Speaker RS PRO 8Ω typical frequency response [32].

2.6.3 Audio power amplifier

The LM386N-3 is a power amplifier designed to be used in low voltage consumer applications. The gain is user configurable in the range from 20 to 200. A gain of 20 can be achieved without additional components while introducing a capacitor and a resistor between pins 1 and 8 it is possible to increase the gain up to 200 [33].

The recommended Operating Conditions reported in the datasheet are shown in ***Table 2.7:***

Supply voltage range	4-12 V
Quiescent current drain	4 mA
Voltage Gains	20-200
Total Harmonic Distortion (THD) (condition: AV=20, VS=6 V, RL 8Ω, PO=125 mW, f = 1 kHz.)	0,20%

Table 2.7 LM386N-3 recommended operating conditions [33].

In ***Figure 2.15*** it is shown a simple schematic of the internal circuit of the power amplifiers.

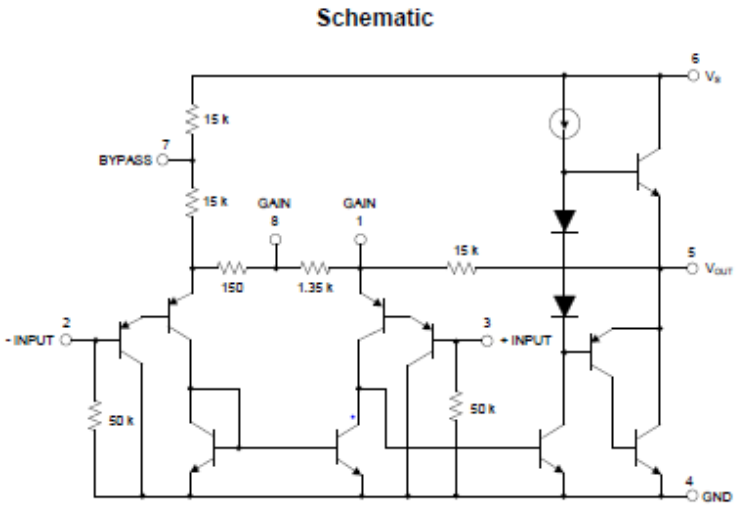

Figure 2.15 Simple schematic of the internal circuit of the power amplifiers

2.6.4 Discovery Kit STM32F429 and STM32F429ZIT6 Micro

The STM32F429 Discovery Kit development board (**Figure 2.14**) comprises several components:

- STM32F429ZIT6 microcontroller unit implementing a Cortex®-M4 core Arm®
- 2.4” QVGA TFT LCD display
- ST- LINK/V2 embedded debug circuit
- External 64-Mbit SDRAM
- Two USB connectors (for debugging, programming and application needs)
- Push-buttons (user and reset) and indication LEDs

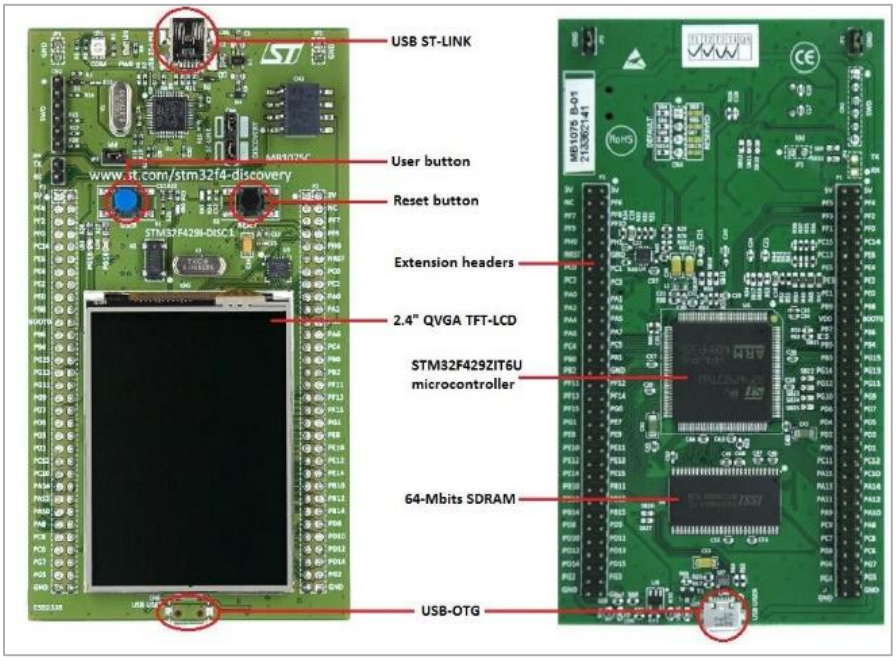

Figure 2.16 Discovery Kit STM32F429 board.

A USB cable linked to a host PC or an external 5V source can be used to provide the power supply to the development board [34].
The STM32F429ZIT6 microcontroller unit (MCU) is the main component of the Discovery Kit. It is based on an ARM Cortex-M4 32-bit RISC core with a single precision hardware Floating point unit (FPU). The MCU is rated for max operating frequency of 180 MHz.
The microcontroller integrates into his circuit high-speed memories: 2 Mbytes of flash memory for storing code and data and 256 Kbytes of SRAM. Furthermore, there could be up to 164 fast I/Os coupled to two Advanced Peripheral Buses (APB), two Advanced High-performance Buses (AHB) and a 32-bit multi-AHB bus matrix.
On STM32F429 discovery board are available 114 GPIO fast input/outputs, which can be independently set by software as input or output.
Additionally, this MCU offers: two 12-bit Digital Analogic converter (DAC), three 12-bit Analogic digital converter (ADC).

- The 12-bit analog-to-digital converters are linked to 16 external channels, that can operate in single-shot or scan mode. Scan mode performs automatic conversion on a group of signals to acquire.

- The 12-bit buffered DAC channel converts a digital signal in an analog signal as output. There are two DAC linked to two output channels that can work simultaneously and independently from each other. The DAC can work in conjunction with internal timers and DMA for fast memory transfer and waveform generation *[34] [35]*.

2.6.5 KEIL-µVision5 and Matlab™ R2018a

Keil-µVision5, an integrated advanced development environment made by ARM, was used to create a program for setting and managing the microcontroller unit and all the embedded peripherals such as: interrupt controller, DMA controller, timers, GPIO, ADC, DAC, etc….
This software is designed to operate in windows system and incorporates all the tools needed to develop firmware for several applications. It includes a compiler for C and C++ languages, a macro assembler and an object code linker. In addition, it offers highly optimize run-time libraries and an advanced debugger with flash memory firmware download capability.
Matlab™R2018a was used to analyse the acquired sound signals and to develop a specific algorithm able to compute the physical distance between speaker and microphone by evaluating the sound signal propagation delay.

Chapter 3 Signals management

The automated distance evaluation for pulse wave velocity estimation is based on a sound wave that will be generated and simultaneously acquired from the designed system. The delay between the generated and acquired signal will allow computing the linear distance existing between the signal source (speaker) and signal sensor (microphone).
In order to obtain useful signals for the described purpose, the speaker and the microphone biasing and control circuitry has to be carefully designed for the purpose. So, for the device management, it was necessary to create a specific hardware together with a relative control firmware, able to manage the waveforms and the signal chosen.

The hardware is composed of two independents channels:

- Microphone conditioning channel;
- Speaker conditioning channel.

They will be managed by three microcontroller peripherals, two are input for signal acquisition and one is an output for signal generation. The following paragraphs will describe the hardware and firmware implementation, which allow to create, acquire and to process the required signals.

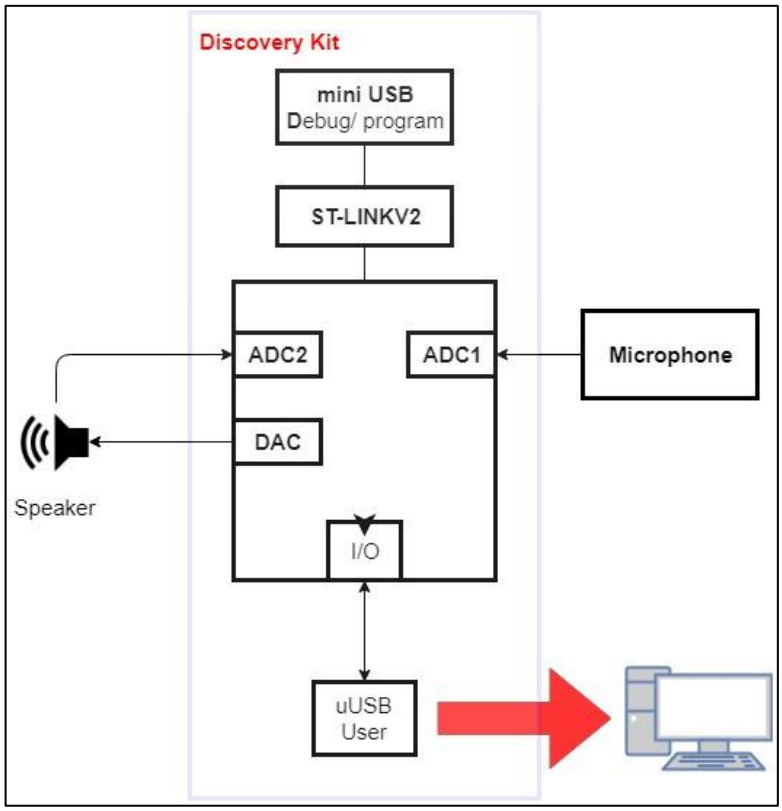

Figure 3.1 Board interfacing diagram

3.1 Speaker Emission

The first step is to generate a sound signal by means of a speaker. The sound wave is realized by filtering and amplifying a signal generated by a Digital to Analog. The employed DAC is hosted by the MCU STM32F429ZIT6 present on the Discovery Kit

The conditioning circuit, between the DAC and the speaker, is useful for the sound generation because it adapts the signal for our needs. In fact, the analog circuit shapes the analog signal controlling its amplitude, limiting the output power, and removing the DC component.
The following paragraphs will describe the conditioning circuit and the firmware procedure adopted for signal generation and emission.

3.1.1 Hardware for speaker

Few elements were used to manage the speaker for the sound generation. An integrated audio amplifier, useful to properly drive the sound speaker. A first order high passes filter allows to remove the DC offsets introduced and detrimental for the speaker. Then, in order to make possible the comparison between the generated and acquired sound signals, the voltage on the speaker is feed in input to an ADC channel. But, to take advantage of the ADC input dynamic range, the speaker signal has to be centered in 1.5V.
Below are briefly described the components adopted in the signal generation stage.

LM317 Adjustable Regulator

The developed system requires a stable reference voltage of 1.5V. This voltage value has been chosen because it represents the middle of the ADC and DAC dynamic range. The LM317 adjustable regulator is used to obtain the reference voltage of 1.5V.
This three-pin device can provide adjustable voltage from 1.25V up to 37V [36].
The nominal output voltage is obtained thanks to a voltage divider placed between the output pin, the adjustable pin, and ground. In addition to the potentiometer, decoupling capacitors were used as recommended in the device application note.

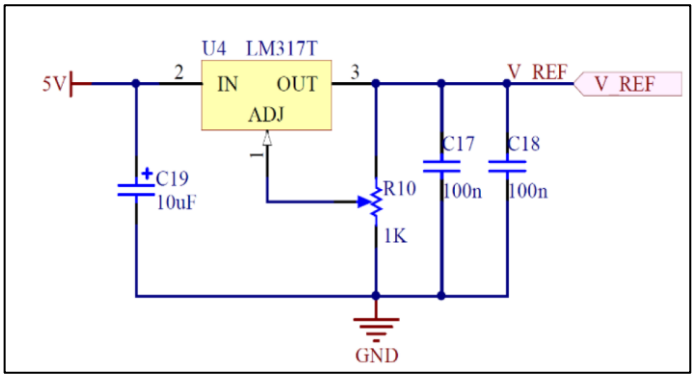

Figure 3.2 Circuit for reference signal based on LM317 Adjustable Regulator.

High pass and Voltage divide

The analog signal generated by DAC passed into a first order high-passes filter to remove its DC component and a voltage divider attenuates the signal. So, these units of the conditioning circuit allow avoiding saturation on the audio power amplifier input stage.

LM386 Low Voltage Audio Power Amplifier

To generate an output signal compliant with the selected speaker specification the LM386 low voltage audio power amplifier, introduced in **Chapter 2.6.3**, has been adopted. In our case, the audio amplifier is powered by the 5V power supply present on the Discovery kit board. In addition, it has been selected the configuration able to grant a 20x gain, allowing to keep pin 1 and 8 floating as indicated on the amplifier datasheet. In this way, the maximum output power is limited to 1W.

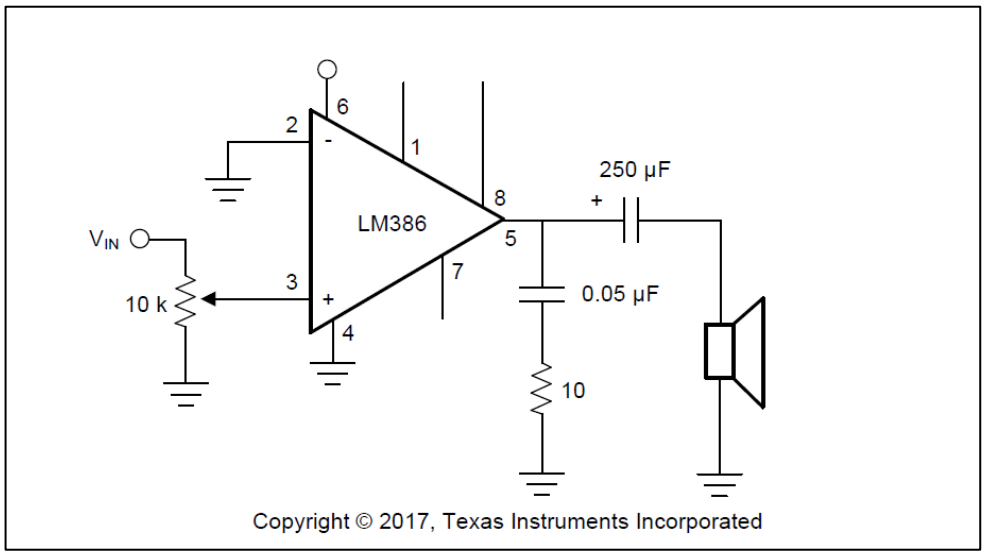

Figure 3.3 LM386 configuration addressing a 20x gain.

Voltage Divider

This section of the conditioning circuit allows to add a continuous component of 1.5V to the speaker signal, so to have it centered in the 0 and 3V range, which is the operating input range of the ADC. A divider (referring to the voltage of 1.5V generated by the LM317) adds the offset to the signal and attenuates it, to avoid saturation on the ADC input stage.

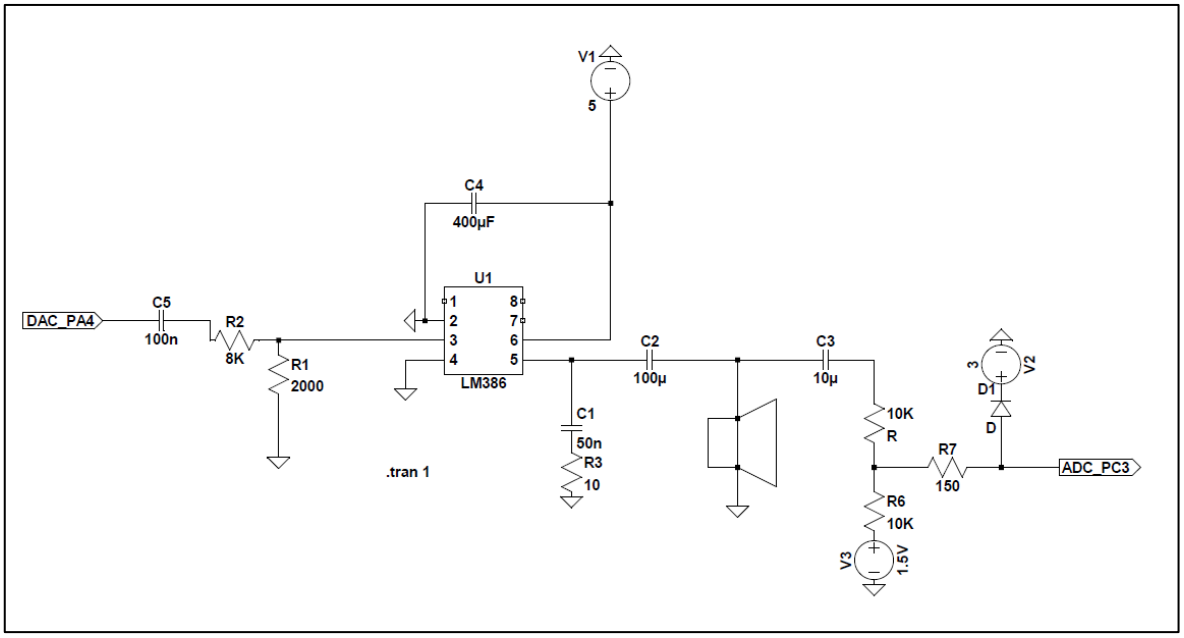

Figure 3.4 Speaker conditioning circuit.

3.1.2 Firmware for speaker

For the speaker audio signal generation and feedback control, several MCU peripheral are involved and requires to be properly configured. The following paragraphs describe the firmware procedures implemented to address the ADC, DAC, DMA and Timer configuration.

Digital to analog converter (DAC)

To generate the desired waveform the DAC1 is used, its output is connected to the port GPIO PA4 and it is configured with a 12-bit resolution. The signal to be generated is built ad the system start-up and stored in the MCU internal SRAM. Then, each time it is required, the pre-built samples are transferred from the SRAM to the DAC by configuring in circular mode a proper stream on the predefined DMA channel. In particular, due to MCU architectural constrains it has been chosen the Stream 5 on channel 7 of the first DMA peripheral (DMA1)

The DMA transfer trigger and consequently the timing on which the DAC generate the desired signal, is controlled by configuring an internal MCU Timer (TIM2).
The TIMER is set according to the following formula:

$$\text{period} = \frac{\text{TIMCLK}}{2*n*fp} \qquad \text{fs} = \frac{\text{TIMCLK}}{2*\text{period}}$$

The TIMCLK is equal to 168MHz and corresponds to the MCU system clock frequency, n is the number of digital samples that compose a period of the digital signal and f_p is the carrier frequency.

Analog-to-Digital Converter (ADC)

To compute the time delay which characterizes the signal on the microphone, it is important to acquire also the reference signal generated by the speaker.
This is done by acquiring the voltage on the speaker by the channel 13 of the ADC1, corresponding to port PC3 on the Discovery Kit board.
The ADC configuration and its functional mode will be better detailed in Paragraph 3.2.2

3.2 Microphone signal acquisition

A conditioning circuit was designed to manage the signal that comes from ST analog MEMS microphones MP33AB01H before to be acquired by the ADC. This stage is required to reduce signal noise and to select the proper working bandwidth.
The signal acquisition sub-system, as well as the part concerning the Speaker driver, consists of a hardware circuit and some firmware procedures. They will be described in the following sections.

3.2.1 Microphone acquisition circuit

The MP33AB01H MEMS microphone has been chosen because it has a good sensitivity (-38 dBV), a Signal to Noise Ratio (SNR) higher than 64 dB and implements an analog output. The microphone analog output permits a wide flexibility on the signal processing, this kind of versatility is not always possible using digital output compact MEMS microphones.
The first stage is composed of a high pass filter to eliminate the low frequencies and DC-bias introduced by the microphone. Next, there are two-second order low-pass filters and two amplifiers preceded by a first-order high-pass filter.
For the amplifying and filtering stages, the following components were used:

- TLV2464 opAmp

A four channels low-power rail-to-rail input/output operational amplifier with the main features listed in Table 3.1 [37]:

Power supply	Up to 6 V
Gain Bandwidth product (GBW)	6.4 MHz
Input voltage offset (Vio)	100 μV
Output current (Io)	±40 mA

Table 3.1 Primary features operational amplifier TLV2464

- OPA2244 opAmp

A two channels low-power operational amplifier with the main features listed below in Table 3.2:

Power supply	Up to 36 V
Gain Bandwidth product (GBW)	430 KHz
Input voltage offset (Vio)	700 μV

Table 3.2 Primary features operational amplifier OPA 2244.

- LM317

The same component was employed for the sound wave emission and it was described in **section 3.1.1**. It provides the reference voltage of 1.5 V for the system.

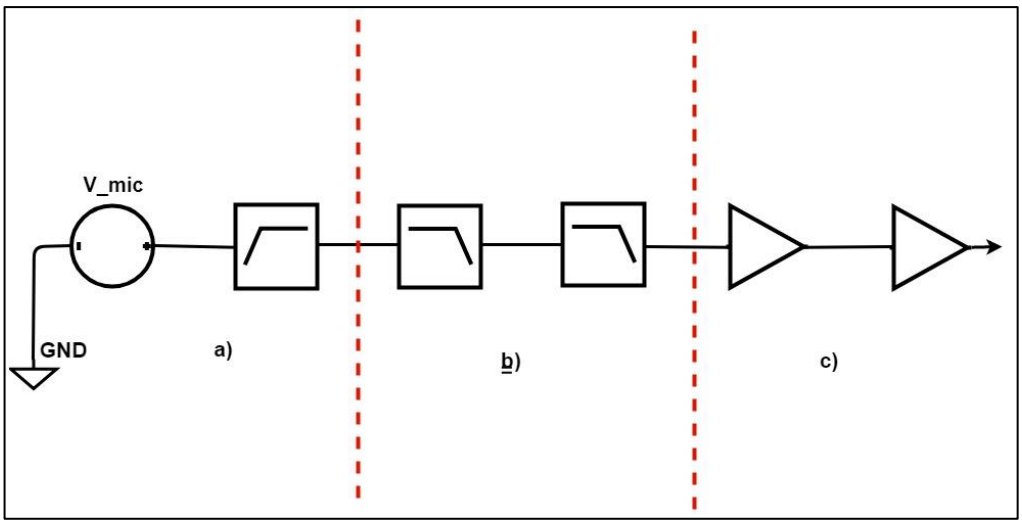

Figure 3.5 Microphone's conditioning block diagram.

a) Mics summing & high pass filter

One or more microphone devices can be used for the audio signal acquisition. The advantage in the usage of multiple sensors is that by doubling the number of microphones it is possible to increase the SNR by 3dB. For simplicity, this addressed system uses only one microphone. Hence, this stage consists of a high pass filter that attenuates the recorded signal of 5 dB and filters all the frequencies below 1KHz. The correspondent cut-off frequency can be obtained by:

$$f_c = \frac{1}{2*\pi*R*C} = \frac{1}{2*\pi*1.5K*100n} = 1{,}061\ KHz$$

b) Low pass filter

The low pass filter is required to avoid aliasing in the analog to digital conversion.
The corner frequency is at 25 KHz and a fourth order filter in obtained implementing two second order stage. The band pass gain is set equal to the unity while the attenuation at the Nyquist's frequency is at least 30dB, that is enough to grant the expected system performances.

c) Amplifiers

To be able to exploit the input dynamic of the ADC and to maximize the usage of its 12bit resolution, the signal must be strongly amplified. It has to be considered that the microphone's output is of the order of few mV. Therefore, two cascade gain stages were implemented and controlled with two potentiometers for totally configurable amplification. In addition, a high pass first order RC filter is put at the input of each gain stage in order to remove the effect of the op-amp input offset, preventing in this way the saturation of the high gain amplification stages.

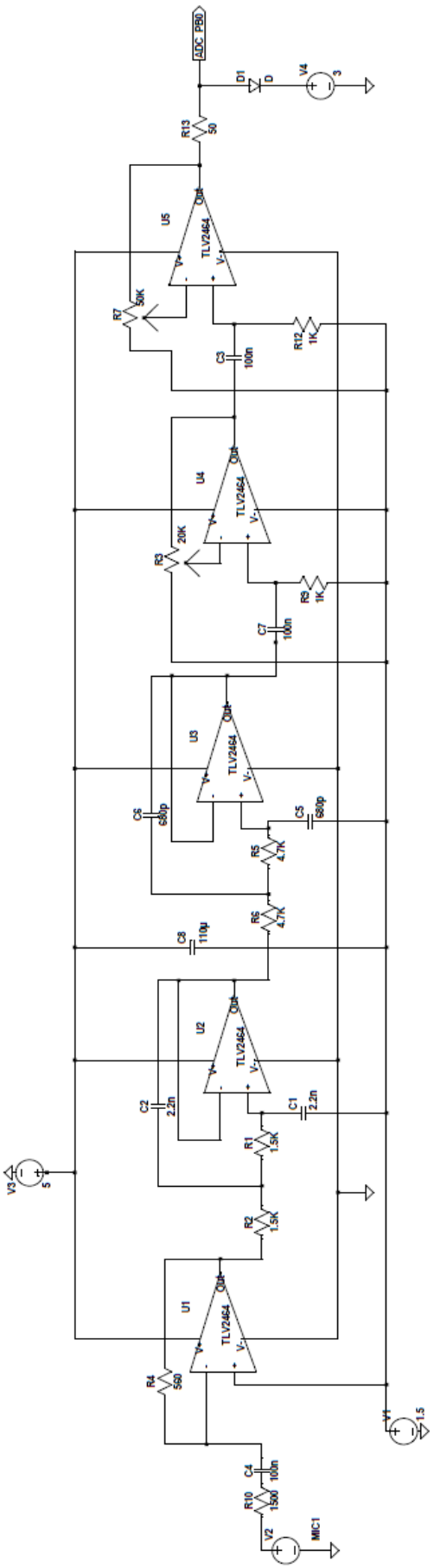

Figure 3.6 Microphone amplification chain.

3.2.2Microphone management firmware

For the microphone's signal acquisition, some MCU peripheral are involved and requires to be correctly configured. The following section explains the firmware actions executed to address the ADCs, DMA and Timer setting.
To acquires the desired waveforms the ADC1 and ADC2 are used, their inputs are linked to the ports GPIO PA0 and PC3, they are set with a 12-bit resolution. The two ADCs operate in dual multi-mode for a simultaneous acquisition of the two signal inputs. After the conversion, the two analog digital converter peripheral transcribe data on a 32-bit common register, named ADC_CDR. Whereby, the values converted by the ADC1 will be fixed on the bits 0-15, instead the value converted by the ADC2 will be transcribed on the bits 16-31.

Then, each time it is required, the samples are transferred from the ADC_CDR to a buffer memory by configuring in circular mode a proper stream on the predefined DMA channel. For MCU architectural constrains it has been selected the Stream 0 on channel 0 of the second DMA peripheral (DMA2).
The ADC conversion trigger and subsequently the timing on which the DMA transfer the samples of the digital signal, is controlled by configuring an internal MCU Timer at frequency 218.750KHz.

3.3 Hardware related issues

During the first signal acquisitions, the presence of a parasitic noise was detected. It periodically affected the microphone conditioning branch.
This noise is due to the ground imbalance, when the speaker is generating the acoustic pulse. It was necessary to improve the hardware implementation paying attention to better decouple the power supply rails. For this reason, decoupling capacitors have been increased and others inserted, trying to balance them as much as possible. The changes made did not completely solve the problem, but the parasitic noise was strongly decreased. The interference has not fully eliminated but it has been reduced enough to do not affect the following digital processing stages. One of the possible causes of this can be found in the parasite inductance of cable and wires.

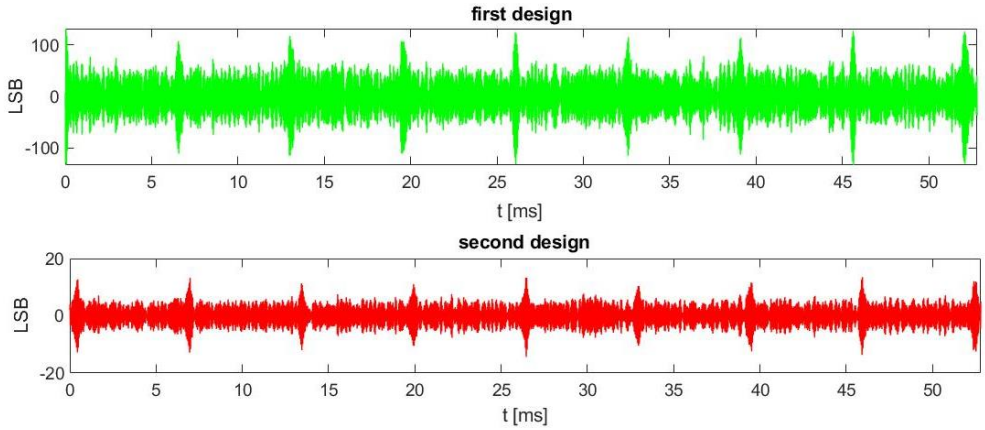

Figure 3.7 The plot above depicted the noise before and after the action to adjust the capacitors.

Chapter 4 Algorithm based on amplitude modulation

After the hardware and firmware implementation, how to calculate a time delay between the acquired signals was approached; because a good time delay estimation leads to a better distance evaluation. To achieve a satisfactory result, in the algorithm implementations some factors have to be considered; such as: the wave's amplitude, the signal frequency, and the emitted waveform.
The fourth and fifth chapters address the algorithms and strategies to realize a good measurement of the time of arrival (TOA) (paragraph 2.5.4). In particular, two different ways were employed to address the problem:

- Algorithms based on amplitude modulation;
- An algorithm based on frequency modulation.

The following pages will describe the used techniques for amplitude modulated signal. The techniques considered are four and all have a low computational cost. They are based on techniques developed in origin for ultrasound produced by piezoelectric systems and are:

1) Distance max (Dmax);
2) Threshold (Ths);
3) Two-point parable fit (2pointsParable);
4) Iterative parable fit (Parable Fit).

4.1 Amplitude modulation

Generally, amplitude modulation (AM) is a transmission technique that is implemented to broadcast information using a radio frequency signal as a carrier.

This consists in modulating the amplitude of the signal that is designed to be used for the transmission (called Carrier) proportional to the signal amplitude is intended to transmit (modulating) and which contains information. It is a simple method; therefore, it has been used since the radio broadcast was born. In the case of a binary transmission, a power low corresponds to the zero while at a high-power match to the number one.

The method has some drawbacks, the main is the extreme sensitivity to the noise and the propagation conditions. Therefore, any disturbance and variations in the random attenuation are added on the signal amplitude during its diffusion in the medium distorting the In this thesis work, amplitude modulation was performed by sound waves and not by radio waves. This modulation technique has been used to improve the preservation of the waveform during the flight time. Another purpose for which it is used is to exploit a carrier with a frequency hardly perceptible to the human ear, about 20KHz that also it is less affected by the surrounding acoustic noise.

In general, to make a good modulation is needed to sum and generate two different signals:

A sinusoidal carrier V_p , with amplitude A and frequency f_p

$$V_p = A\cos(2\pi f_p t); \quad (4.1)$$

A modulating signal $V_{m,}$, with amplitude B and frequency f_m

$$V_m = B\cos(2\pi f_m t); \quad (4.2)$$

So, the final signal V_{am} will have an amplitude A_m:

$$A_m = [A + B\cos(2\pi f_m t)] \quad (4.3) \text{ then}$$

$$V_{am} = A_m * \cos(2\pi f_p t); \quad (4.4)$$

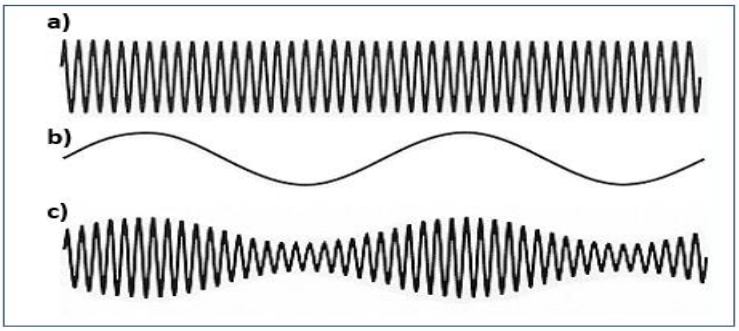

Figure 4.1 Amplitude modulation example, a) carrier signal, b) modulating signal, c) modulated signal.

In some circumstances, there may be more modulating frequencies or be used signals that are not sinusoidal as this design. For example, Gaussian, triangular, and rectangular window are employed for attending the designed system's aims.
For this thesis purpose, the next paragraph briefly defines the waveforms emitted by the sound speaker and explains the reason for their use.

4.1.1 The Waveforms

Three waveforms (triangular, Gaussian and rectangular) have been tested to evaluate which one provides the best result for this application. Nevertheless, their differences, there is a feature in common for all the modulated signals: the emission duration of 2s, containing 200 pulses. This means that between one pulse and another pass about 7 ms, having a rate of about 155 Hz. The three types of waveforms are shown in figure 4.2.

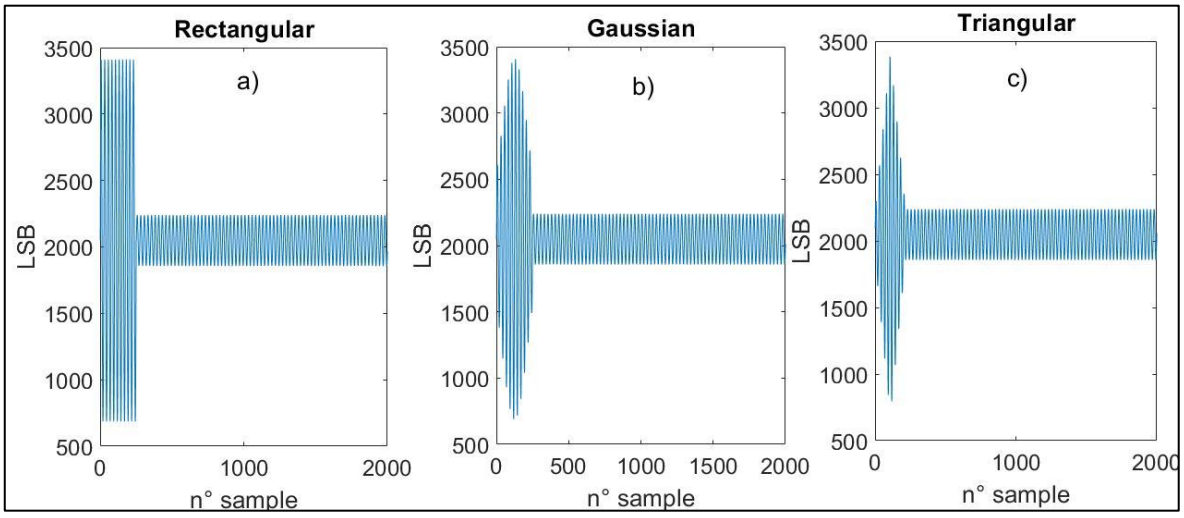

Figure 4.2 a) Triangular waveform, b) Gaussian waveform, c) rectangular waveform.

Waveforms detected by MEMS microphone have been tested to find the most approximated one by the equation written below.

$$y(t) = x(t - t_0)\sin[2\pi f_0(t - t_0)] + n(t); \quad (4.5)$$

In which $x(t - t_0)$ is the envelope of the impulsive signal part.

$$x(t - t_0) = a_0 e^{-a_1(t-t_0)}(t - t_0)^2 \quad (4.6)$$

This last equation expresses the envelope of the recorded wave, the a_0 e a_1 components are related to the shape and attenuation of the signal due to the crossed medium and the t_0 is the time delay. Also, the sinusoidal component is the oscillating carrier at the chosen frequency. Lastly, the *n(t)* is white Gaussian noise as a result of the acoustic noise in the environment, electrical noise, and thermal noise. This acquired wave approximation derived from the propagation low of a wave in a fluid. However, it is only valid in the initial part of the sound impulse assuming there is no reflection of the waveforms or another distorting effect, specifically the range is $[t_o : t_o + 1/2a_1]$ [38].
The above mentioned equation is the theoretical rule on which the subsequently implemented algorithms are based, they will be analyzed in the following subchapter.

4.2 Algorithms

4.2.1 Digital Signals pre-processing

The signal given to the speaker and the one read by the microphone and then filtered (see Chapter 3) are lastly sent to the laptop, where they are processed in MATLAB environment. The main purpose of software algorithms implementation is to extract the time of arrival values (TOA), also called time of flight (TOF), between the microphone and the speaker waves, that are simultaneously processed.
Before everything, the four procedures used (Dmax, Ths, 2pointsParable, ParableFit) have the first steps in common:

1. As the data transfer finishes, the first USB buffer is deleted to cut possible noise or non-clean signals;
2. The mean values are removed from both the waves;
3. The microphone signal is filtered to remove noise and frequency components that have not been eliminated from the implemented conditioning circuit;
4. The two envelopes of the signals are extracted;
5. The signal is segmented in windows, each one containing a burst.

Concerning the third step, the microphone signal filtering, a bandpass IIR filter has been adopted and designed with the "*fdesign.passband"* Matlab function, which provides a flat bandwidth and a high attenuation. This function needs as inputs the filter order, the useful corner frequencies and the sampling rate.
In this case, the corner frequencies are 16KHz and 24KHz and they have been chosen through a spectral analysis, to preserve as much as possible the informative components and the morphology of the signal useful for the purpose, as could be seen in Figure 4.4.

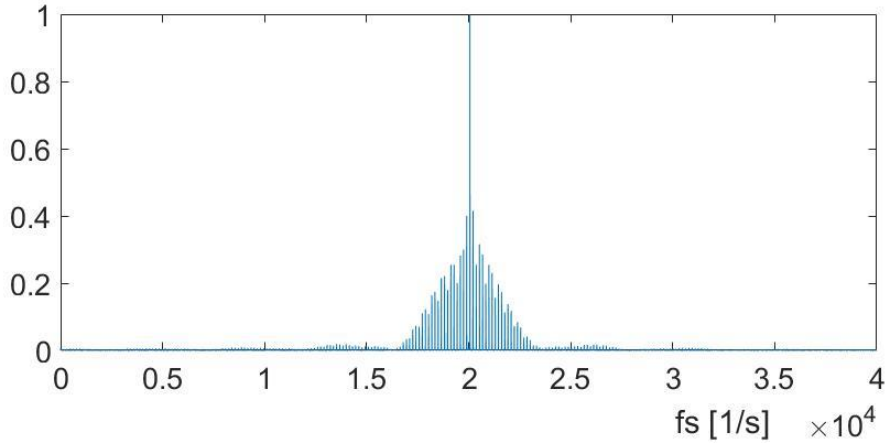

Figure 4.3 Spectral analysis of a signal at 20KHz and triangular modulation.

The *fdesign* only provides the filter specifications, a function called *design* is used to get the filter project, it returns a structure in which the second order section (SOS) matrix and the vector G are presented. The vector array and the signal to be filtered are the input to the *filtfilt* function. This instruction filters twice the signal in two forward and backward directions, so performing a zero-phase filter.

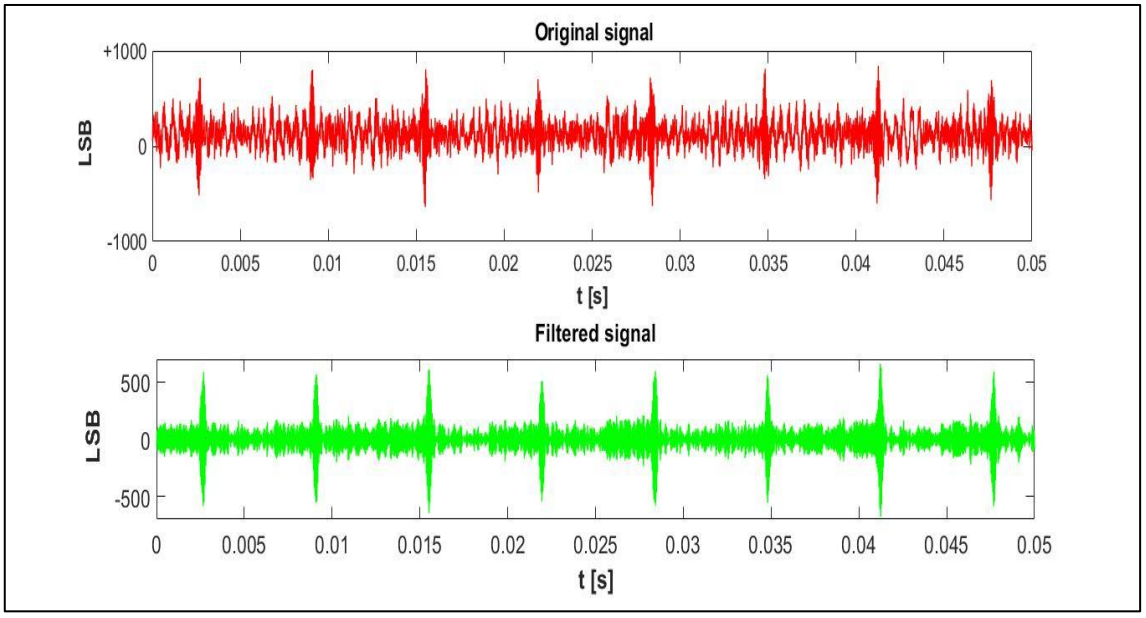

Figure 4.4 Microphone signal before digital filtering and after.

The fourth step aim is to extrapolate the signal envelopes. This time, after both signals are squared, a low pass sixth-order IIR filter is implemented; its specifications are obtained by the *fdesign* function seen before, but with the *lowpass* indication (*lowpass*,*fdesign*). The bandwidth cut-off frequency is 8KHz to obtain a precise envelope. Then, the same functions of the previous step are used to extrapolate the *SOS matrix* and *vector G* and to filter with *filtfilt instruction*.

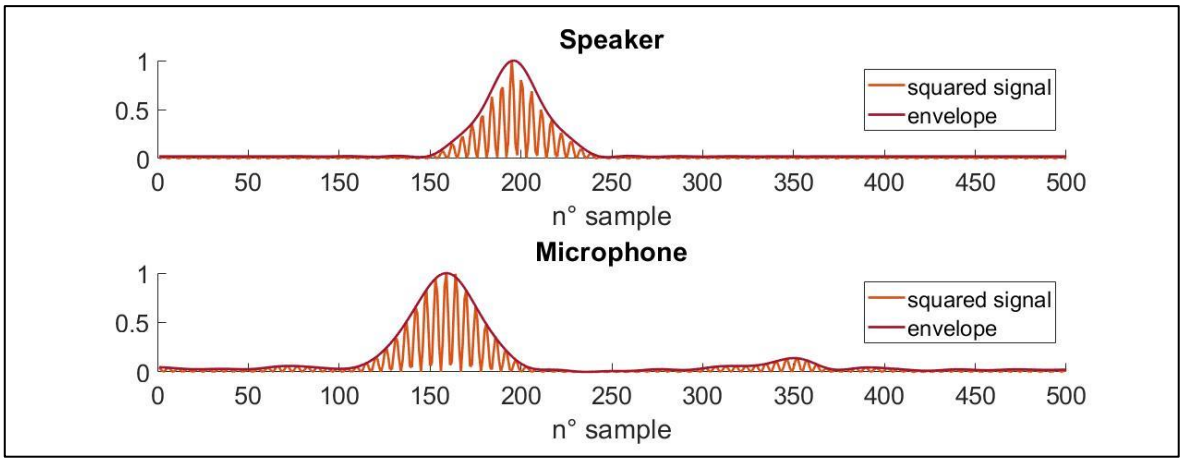

Figure 4.5 Squared signals and relative envelope.

The last fifth common stadium is focused on the signal's sectioning in time windows. To do the division, the event start time is detected from the speaker's signal.
In details, in the envelope, the position where the impulse begins is discovered descending from the maximum of the event towards the left slope until the first local minimum is founded. Finally, from that instant, the next 1400 samples are taken. The number of samples derives from the ratio of the 155hz event frequency and the sampling rate of 218,750 KHz leading to the result of about 1400 samples.

$$\text{N° samples} = \frac{f_s}{f_v} = \frac{218.750\ \text{KHz}}{155\ \text{Hz}} \approx 1400 \quad (4.7)$$

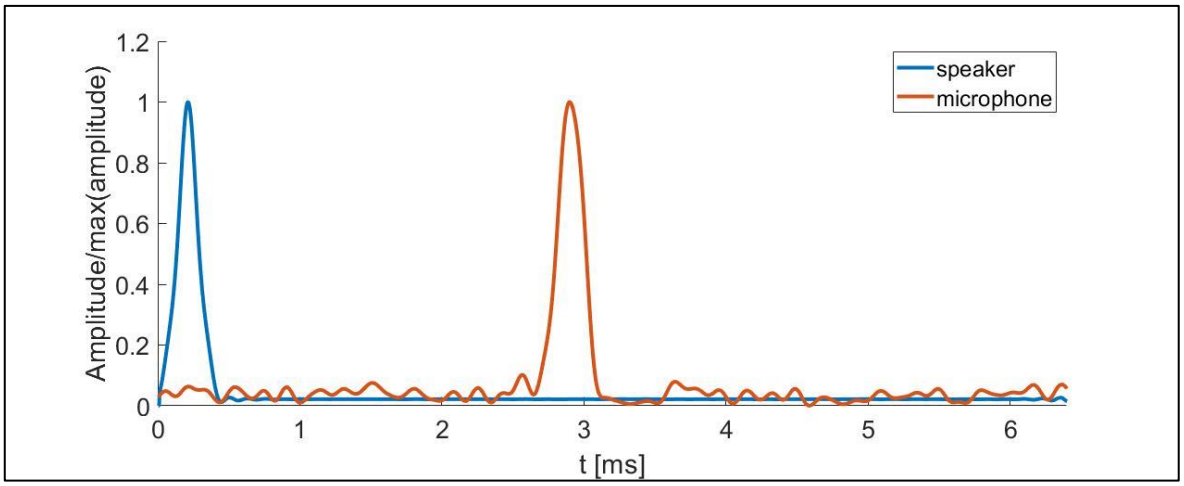

Figure 4.6 Signal section illustration, the speaker's wave envelope is the blue line and the red line is the microphone's envelope.

The last image represents a single window with the two waves envelopes, for each acquired signal 200 of these windows are extracted and then, singularly, given as input to the next

algorithm phase. Lastly, all the results of each window are converted to cm ant the mean value is calculated in order to compare data with the other methods.

As said before, to estimate as accurately as possible the temporal delay and so the distance by the sound velocity in the air four different techniques have been adopted. These are explained in the following sections of this chapter.

4.2.2 Distance between Peak

The first method addressed is one of the most obvious and simpler.
The time delay between the two envelopes, the first emitted by the speaker and the other obtained from the signal acquired by the microphone is estimated by means of the distance between their peaks.

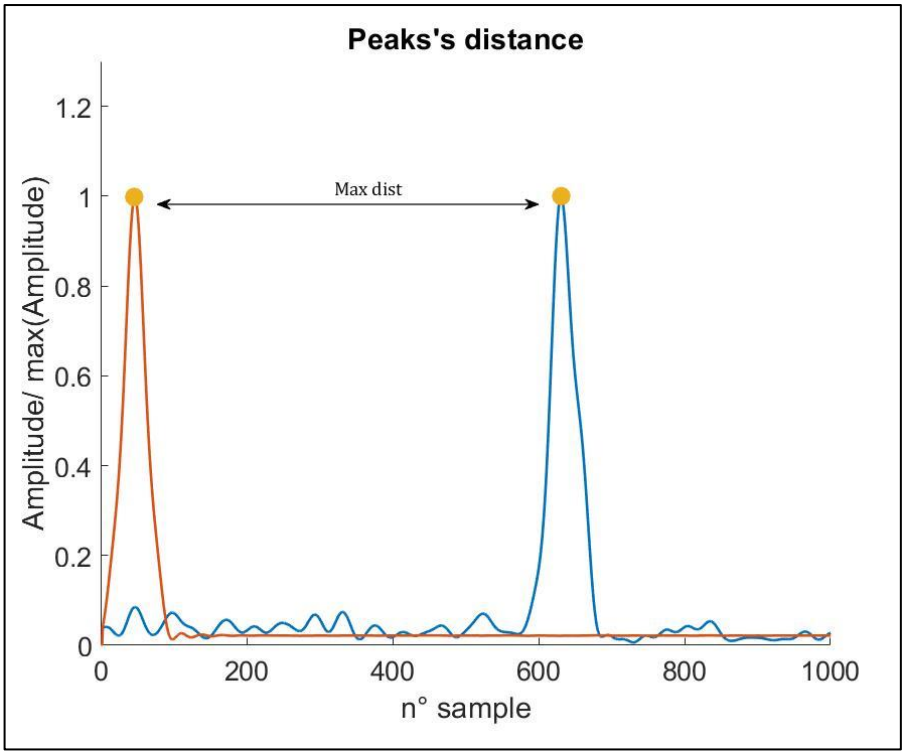

Figure 4.7 Representation of cross correlation and peaks' distance.

The number of samples between impulse peaks is calculated and, according to the sampling frequency, the time delay is evaluated.
With this method, if the source of the signal is in a space where there is no noise and there are no diffraction and reflection effects that corrupt the signal (model **Paragraph 2.5.1.**) the estimation is good. But For a sound wave that propagates in the environment that follows the multipath model explained in **paragraph 2.5.2**, the method makes errors estimation because the signal maximum peak shifts over time.

4.2.3 Threshold

The threshold method is one of the simplest for detecting the time of flight (T_f). When the echo envelope grows up, a threshold level must be set to determine the starting point. This limit can be identified based on two different values:

- Proportional to the deviation standard of signa before the impulse, i.e. of the signal noise (it is supposed that the signal components are present only in the envelope)
- The maximum value reached by the signal envelope before the burst response, where it is supposed to be zero in the ideal case.

The algorithm used takes as a reference point the first one, that exceeds the level in the slopes of the peak of interest.

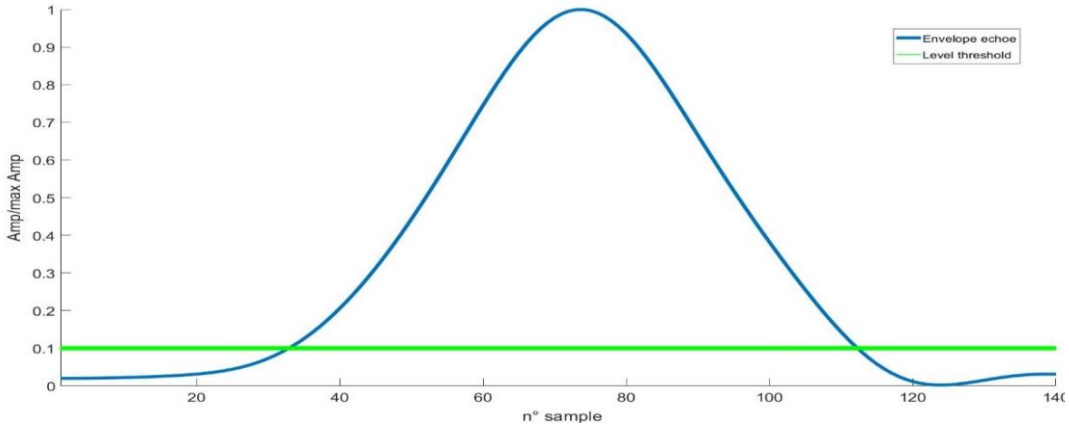

Figure 4.8 Threshold method

The processed signal is the signal acquired by the microphone previously elaborated by the steps described in **section 4.2.1**, with the final detected windows like that depicted in Figure 4.6

The algorithm processes 200 intervals equal to 200 emitted pulses, so the same number of Time Delay estimation will be generated.

The method implementation must carry out simple but fundamental steps starting from the envelope of the digital signal, the sequence is portrayed in the workflow in Error! Reference source not found..

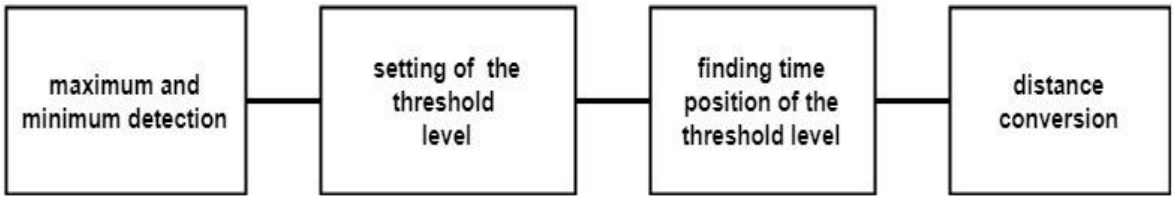

Figure 4.9 Workflow threshold method.

The first step is based on the detection of the absolute maximum peak and the local minimum before the recorded sound event. The maximum is detected simply taking the highest point in the window and its relative position that will be saved in a vector. From the maximum point, the algorithm scans to the left, sample by sample, until it reaches the nearest local minimum, whose position is saved.

The second phase is the most relevant stage: the system sets the threshold level τ to detect the TOF (Time of flight). The τ level will be established as the max amplitude of the noise present before the impulse. This threshold value is taken as the maximum of the signal from the first value of the examination window to the minimum of the envelope rise.

The following stage is the one that detects the position of the sample equal to the threshold value. However, being a discrete signal and not continuous, many times there is not a sample that is equal to the reference value: the value nearest to the detected edge is considered. So, starting from the global peak the procedure goes left down and it stops when the first sample that is lower than the chosen threshold occurs.

At the end, to better understand the results, the TOF measurement performed is converted in physical distance, in centimetre, according to the sound speed obtained through the formula discussed in paragraph 4.1.1.

On the one hand, the considered algorithm is easy to be implemented and it does not have a big computational cost, but, on the other hand, it introduces a bias equivalent to the expression:

$$B[t_f] = \sqrt{\frac{\tau}{a_0}} + \frac{T_s}{2} \quad (4.8)$$

The above equation consists of a sum between two main components. The first due to the signal shape, where τ is the level of threshold and a_0 is the parable concavity that approximates the signal ascent slope. The second depends on the sampling frequency of the signal, in fact, Ts is the sampling period.
Because it depends on the morphology of the envelope that varies for each impulse, this bias cannot be corrected [38].

4.2.4 Parable approximation

This implemented method for time delay estimation is an improvement of the one described in the previous paragraph. In fact, even this case is founded on approximations that lead to a bias lower than the previous one. The logic behind the procedure is explained below.

This algorithm assumes that the envelope rises, that goes up forming the impulsive response, can be approximated as a parabola to be shown in section 4.1.1

$$v(t) = \alpha(t - t_0)^2; \qquad (4.9)$$

The mathematical expression contains "*a*", that indicates the parabolic pattern, and the parabola apex "t_o".
The aim of this technique is to discover a fit parabola for the half envelope shape (from the maximum to the left minimum), once it is founded its apex will be used for the distance evaluation.

To adopt this procedure, two thresholds and two corresponding points in the left peak slope have to be chosen they can be so expressed:

$$v_1 = \alpha(t_1 - t_0)^2; \qquad (4.10)$$

$$v_2 = \alpha(t_2 - t_0)^2; \qquad (4.11)$$

These two v1 e v2 values are chosen by implementing some fundamental passages that will be explained in detail little further.
From the two equation above derive the final formulation:

$$t_0 = \frac{V^{1/2}(t_1 - t_2)}{V^{1/2} - 1} \qquad (4.12)$$

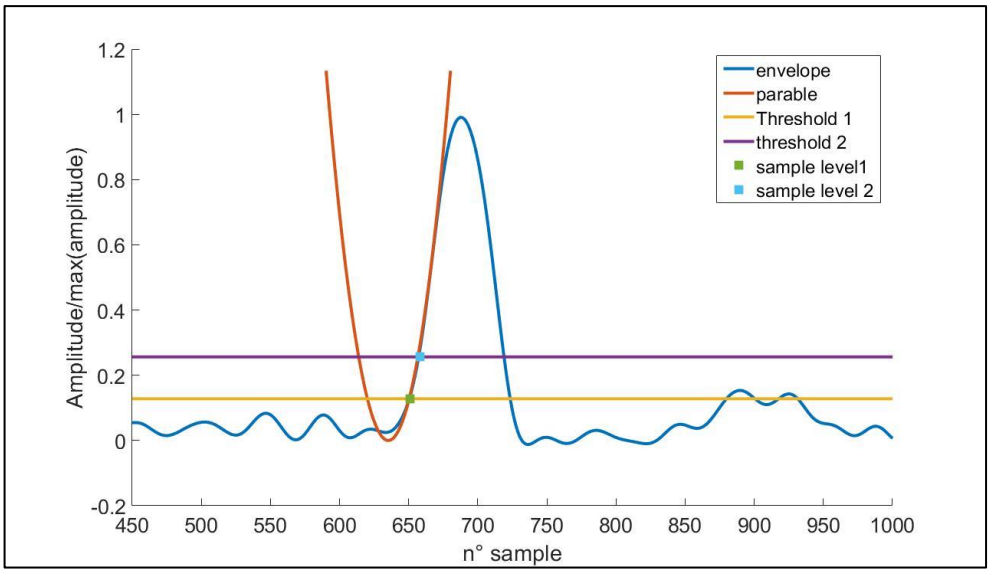

Figure 4.10 Representation of the double threshold parable fit technique.

From the above mathematical equality can be understood that the apex of the parabola does not depend on the signal amplitude but on V. The V is the ratio between the v1 and v2 the two thresholds values. Instead, t_1e t_2 represent the moments when the function assumes the two amplitudes [39].

Also in this case, the algorithm takes as input the 200 windows of the signal and each one is processed following this steps

- The first threshold is chosen following the "threshold method", seen in Paragraph 4.2.3;
- A second threshold level is calculated by setting the relation: $v_2 = V * v_1$, where V is a proportional coefficient set at the beginning;
- The obtained instant time "t_o" is converted from second to a physical distance, in cm;

The value of V and v_1 must be appropriately chosen because they are the two elements responsible for a good result and that can affect the evaluation with errors. Therefore, if v_1 is too small it can be corrupted by noise or be lower than t_o and bring a deviation from the real origin. In the same way, a too large v1 threshold and a big V ratio lead to a v2 level closer to the final peak of the impulse that differs more from the parabola approximation.
For this reason, contrary to the first method, there are controls for which if the first threshold is not included in an established range, it is forced to a default value of 0.2.

The multiplication value V is chosen equal to 2, how it is recommended by the proposing method article; this allows to have a not too high and far v_2 value [39].

In the end, both the temporal points t_1 and t_2 are achieved. In the last step, the t_1 and t_2 are put in the equation obtaining the sound flight time t_o and so the distance between the source and the microphone.

4.2.5 Iterative method

This is the last method, based on amplitude modulated signals, is the most complex among those seen and should achieve greater accuracy, because the bias introduced in the estimation is minor. This technique is valid until the hypothesis that the recorded impulse has a parabolic pattern in its first part is true as see in Paragraph 4.1.1. Where there are no echoes or interference due to phenomena of reflection and diffraction that generally have a greater delay.

The process is an iterative algorithm based on Marquardt's "An algorithm for least square estimation of nonlinear parameter" [40] and its purpose is to fit the real signal pattern with a parabolic function in the range: [t_f : t_f+1/2a1]
Where t_f is the starting point of the pulse's envelope and a_1 is a parameter due to the attenuation, it is explained better in paragraph 4.1.1
In order to get the best result, the algorithm minimizes the Quadratic error function, that is the sum of the square difference composed of two elements.

$$[\varepsilon^2] = \sum_k [s_k - a_0(t_k - t_f)^2] \quad (4.13)$$

The first element s_k is a portion of the envelope chosen arbitrarily. Instead, the second member is the parabola equation approximation.
In this mathematical function there are: t_k which is the position of the k-th sample, a_0 represents the trend of the parabola that is unknown and is updated at each iteration, as well as the parabola apex corresponding to the sound propagation delay t_f.

The first supposition made is to have *20* samples (the segment sk), of the wave envelope, between the time interval [tf:tf+1/2a1]. The process starts with initial deductions of a_o, and t_f, where the starting vertex position is established equal to the value derived by the threshold detection obtained with method 4.2.3. Meanwhile the shape parameter a_0 is equivalent to the half of the signal derivate at the same position of the threshold value.
With these opening values, the squared error objective function is computed.

After initialization, the algorithm performs an iteration loop that lasts until the target function is decreased ($\varepsilon_i^{2}{}_{+1} < \varepsilon_i^2$).
An adjustable step gradient method is employed to produce a provisional parameter by Marquardt's algorithm. The square function is estimated by means of these trial values, and the variation is evaluated:

$$t_f^{(n)} = \begin{cases} t_f^{(n-1)} + \Delta t_f^{(n-1)} & \text{if } [\varepsilon^2]^{(n)} < [\varepsilon^2]^{(n-1)} \\ t_f^{(n-1)} & \text{if } [\varepsilon^2]^{(n)} \geq [\varepsilon^2]^{(n-1)} \end{cases} \quad (4.14)$$

The same thing is done for a_0

$$a_0^{(n)} = \begin{cases} a_0^{(n-1)} + \Delta a_0^{(n-1)} & \text{if } [\varepsilon^2]^{(n)} < [\varepsilon^2]^{(n-1)} \\ a_0^{(n-1)} & \text{if } [\varepsilon^2]^{(n)} \geq [\varepsilon^2]^{(n-1)} \end{cases} \quad (4.15)$$

Where, $\Delta a_0^{(n-1)}$ and $\Delta t_f^{(n-1)}$ are related to the Jacobian of the objective function and two arbitrarily chosen constants, these two parameters are update each iteration tending to diminish.

To reduce computational cost, this interactive algorithm is forced to be arrested when one of three conditions is reached:

1. Minor time Step 10-4 's,
2. N Cycles are passed with no quadratic error variation,
3. The objective function is less than 0.01%.

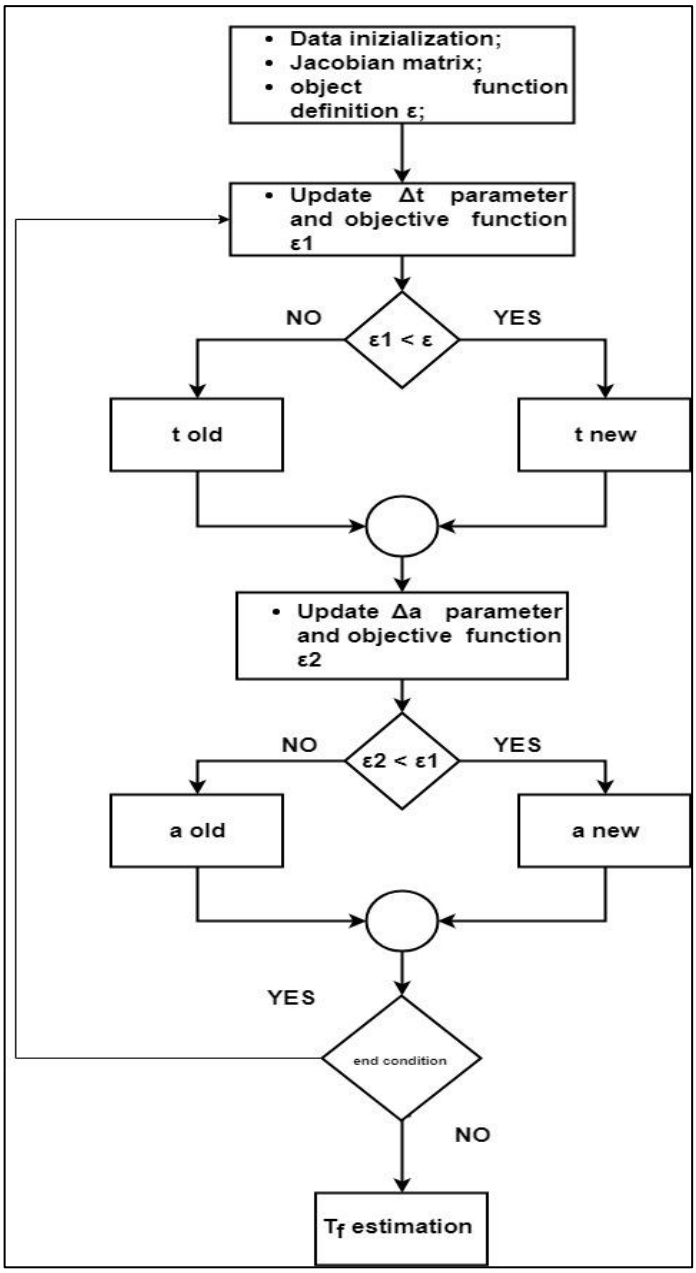

Figure 4.11 Iterative algorithm's workflow diagram.

The first step is to initialize the parameters a_o^0, t_f^0 and select the envelope segment S_k to approximate. As described above, t_f^0 is set as the result of a threshold method seen in Paragraph 4.2.3. It will also be the central sample of the window S_k which contains 20 samples. Finally, a_o is initialized by calculating the half-derivative at the threshold point. The objective function and its Jacobian are calculated to update the unknown parameters during the iteration loop.

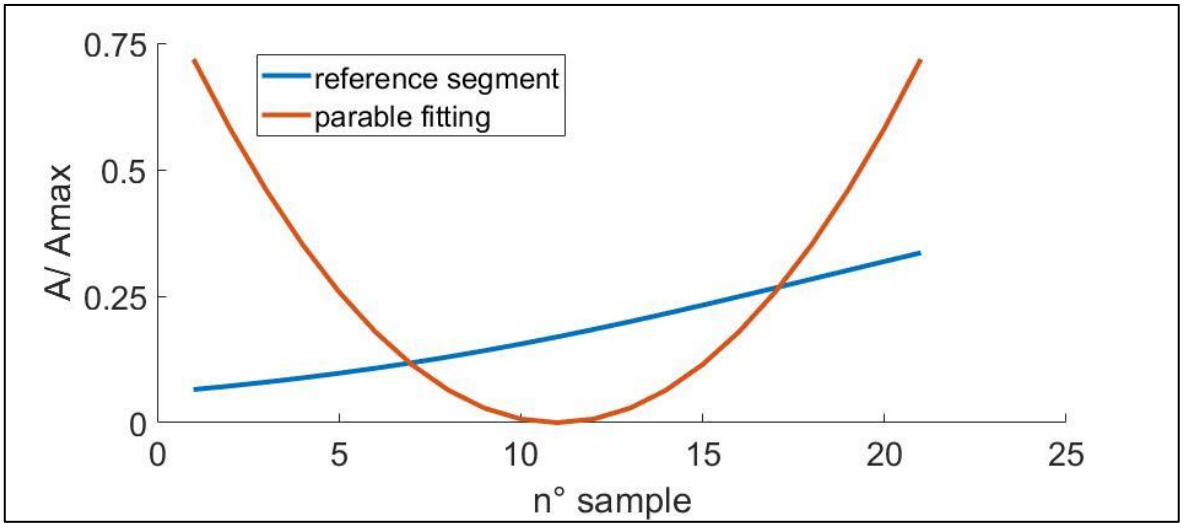

Figure 4.12 Envelope parabolic approximation at first iteration.

In each iteration, the first step is the calculation of the t_f that is correlated to the inverse of the time partial derivative of the objective function.
The adopted method is a minimization process and the closer it is to the solution the smaller becomes the step, increasing accuracy.
In addition to this, there is a constant λ which also varies depending on whether the square error decreases or not.

$$t_f^{i+1} = t_f^i + \Delta t_f \quad \text{or} \quad \Delta t_f = -\frac{\delta(\varepsilon^2)}{\delta t_f} * \lambda; \quad (4.16)$$

After updating the parameter t_f the algorithm calculates the square error and compares it to the previous one. If it is less, the parabola summit is updated with the new value, otherwise, it is restored to the value of the previous iteration.
The same way the system proceeds to update the value of α_0, checking whether the quadratic error decreases or not.

$$a_0^{i+1} = a_0^i + \Delta a_0 \quad \text{or} \quad \Delta a_0 = -\frac{\delta(\varepsilon^2)}{\delta a_0} * \lambda_1; \quad (4.17)$$

The values λ and λ_1 are arbitrarily chosen are equal to 1 and 0.5. If the objective function does not vary in an iteration, the two values are halved.
At the end of the process, the signal is approximated as it can be seen in Figure 4.13.
It will not be the same, but the approximation is high.

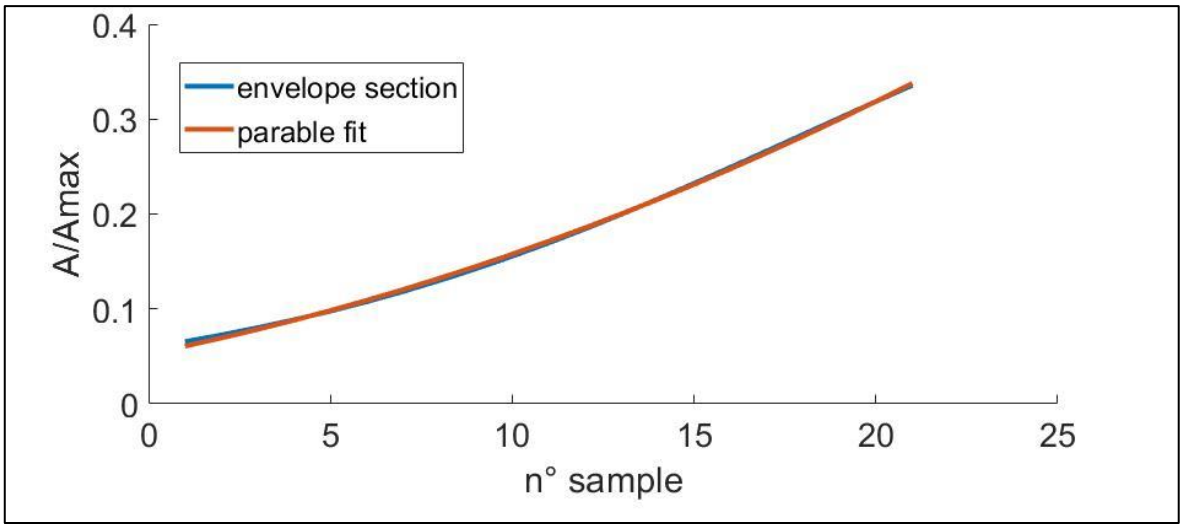

Figure 4.13 Envelope parabolic approximation at last iteration.

About this method, to make it stronger to the noise and to decrease the computational weight of the system, inspired by the technique of averaging, all the envelope of 200 windows are mediate obtaining only one. So, Noise-related peaks that do not have a periodicity were attenuated, instead, it does not happen with the peak related to emitted pulse.

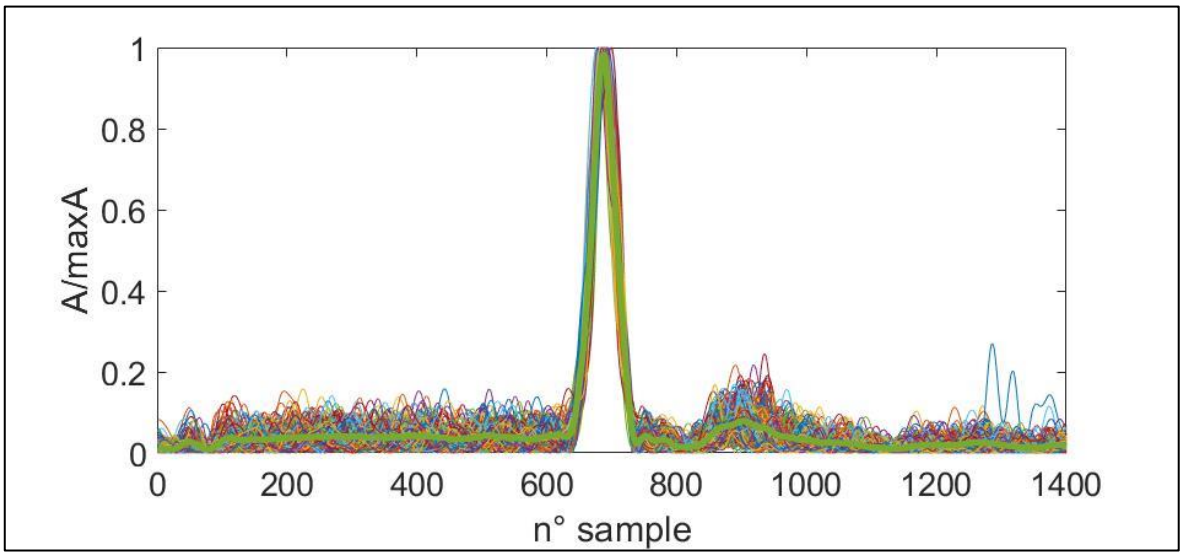

Figure 4.14 Average window in green and 200 envelope windows.

Chapter 5 Algorithm based on frequency modulation

In addition, the amplitude modulation-based algorithms have been compared to the results obtained applying the frequency modulation.
With this aim, a simple and easily-implementable technique has been developed to quickly assess the time delay evaluation. The used algorithm, the addressed problems to choose the right frequencies of the signal, the processing of the envelope and the estimation defects of time delay will be approached in this chapter.

5.1 Frequency shift keying (FSK)

Frequency modulation (FM) is normally used in the telecommunications field. It is one of the transmission techniques that operate to exchange information employing the frequency variation of the carrier signal. In fact, as suggested by the name, in FM there is a tight link between frequency deviation and message. As follow, some simplistic concepts of frequency modulation, useful to better understand the method implemented in this work, will be explained.

$$f_i(t) = f_c + k_f m(t) \qquad (5.1)$$

Where: K_f is a constant named "the frequency sensitivity factor of the modulator",
$m(t)$ is the modulating signal and f_c is the frequency of the unmodulated carrier.
The *instantaneous phase(ϑ_1)* of the modulated wave can be written as:

$$\vartheta_i = f_c + k_f \int_0^t m(\tau)d\tau \qquad (5.2)$$

So, the modulated signal will have the form :

$$y(t) = A_c \cos\left(2\pi f_c t + 2\pi k_f \int_0^t m(\tau)d\tau\right) \qquad (5.3)$$

The system designed during this thesis work employs the technique called Frequency-shift Keying, acronym FSK. It is exploited in the field of computer science and telecommunications and it is a scheme of numerical frequency modulation. This technique contains information by shifting the carrier frequency between two predetermined values.
In particular, in this case, it was thought to use this modulation not to transmit data but to preserve a signal morphological characteristic and only two modulating frequencies were adopted. Secondly, a feature is chosen to evaluate the delay between the time the signal is emitted by the speaker and the one when it is received by the microphone. In the last step, this delay is, as usual, transformed into a distance.

5.1.1 Frequencies of signal

The first step of this method is to select the right frequencies to use and the right signal sequence variation, as will be described in this section.

In particular, the two frequencies were selected analyzing the frequency response of the entire developed system, composed by the sound speaker and the analog microphone MEMS, as described in Chapter 3. The only imposed restriction has been that all the frequencies must be difficult to perceive for the human ear. Moreover, if they are not audible sounds, they are little affected by the environment acoustic noise.
However, the intrinsic limits of the component specifications, as it is possible to see from the frequency response graphs in Figure 2.13 and Figure 2.14, lead to having an indication of the frequency response of the total system. With this purpose, a waveform that varies its frequency over time but not the amplitude has been emitted. In
Figure 5.1 are shown the two signals acquired by the system: the one emitted by the speaker (at the top) and the other captured by the microphone, after the analog conditioning circuit.

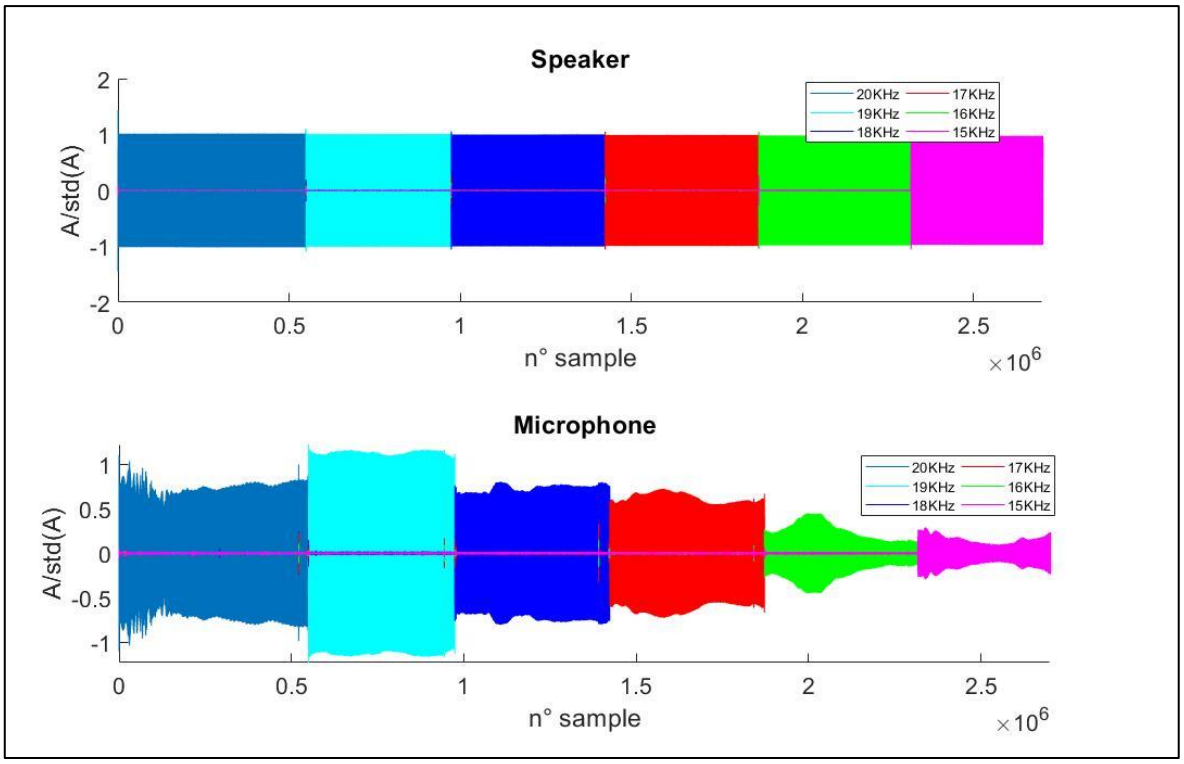

Figure 5.1 Frequencies analysis of the developed system.

So, in the above diagram, the two most opportune frequencies to use could be assessed: they must be spaced, at least 2 KHz, and not be highly distorted. The frequencies chosen to create an FSK signal are 17 and 19 KHz.
The highest frequency at 19 KHz corresponds to the space frequency equivalent to the value 0 and the 17 KHz corresponds to the mark frequency equal to the value 1. The emitted signal

is a sequence of 1 and 0, and each pulse is composed by a precision sequence “0101”, as shown in Figure 5.2.

The signal released by the speaker is acquired by a single microphone. The emission duration is about 2 second, inside there are 121 bursts. The bursting rate is 58Hz, corresponding to 17 ms for each impulse. So, the entire 2 second acquisition is segmented in 17ms-window in which the microphone’s response can fall.

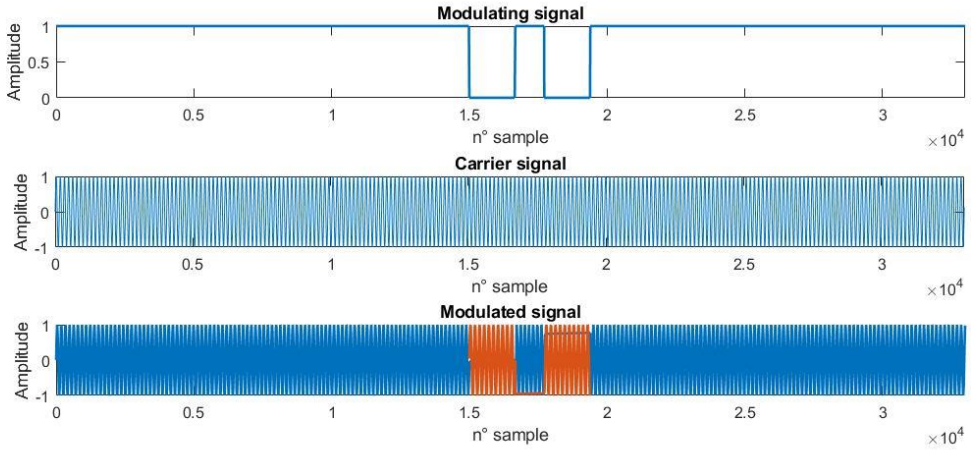

Figure 5.2 Frequency modulated signal emitted by the sound speaker.

5.2 Algorithm Implementation

In this case, the Algorithm for the TOA valuation is simple. It is based on the shape characteristics of the modulated waveform analyzed in the preceding paragraph.
As for the other amplitude algorithms, it investigates the signal delay in each window, evaluating the sample distance between two envelopes signals through a feature that will be described later. The envelopes are taken out from the two signals of both the Speaker's and microphone's branch acquired in sync. The digital data of the speaker are used to estimate the emission moment, instead those of the microphone to evaluate the arrival instant.
Moreover, also this algorithm has been implemented in Matlab environment.
The process can be identified in two basic steps:

1. Signal demodulation;
2. Feature identification.

In the following paragraphs, how the distance has been extracted from the acquired and digitalized signals will be explained.

5.2.1 Signal Demodulation

In the first step, the useful signal is extrapolated by frequency demodulation, schematized in Figure 5.3. Later, its envelope will be obtained for feature extraction.
As it is shown, two ramifications and two envelopes for each signal are realized. For this project aim, they are not both utilized because a frequency is more affected by the noise and so this decreases the quality of the distance estimation.

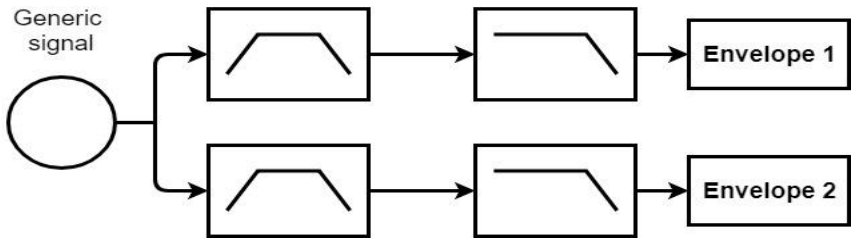

Figure 5.3 FSK signal demodulation Workflow.

In the practice, after eliminating the average, the generic signal is filtered by two IIR bandpass filters, always implemented with *fdesign.passband* and *design* Matlab functions, as previously explained in paragraph 4.2.1.
One pass band stage is centered at 17KHz and the second is placed around the 19 KHz. For both, the 6^{-th} order passband is 1 KHz wide. So, proceeding, two clean signals with only the component equal to the filter's central frequency are extracted (Figure 5.4).

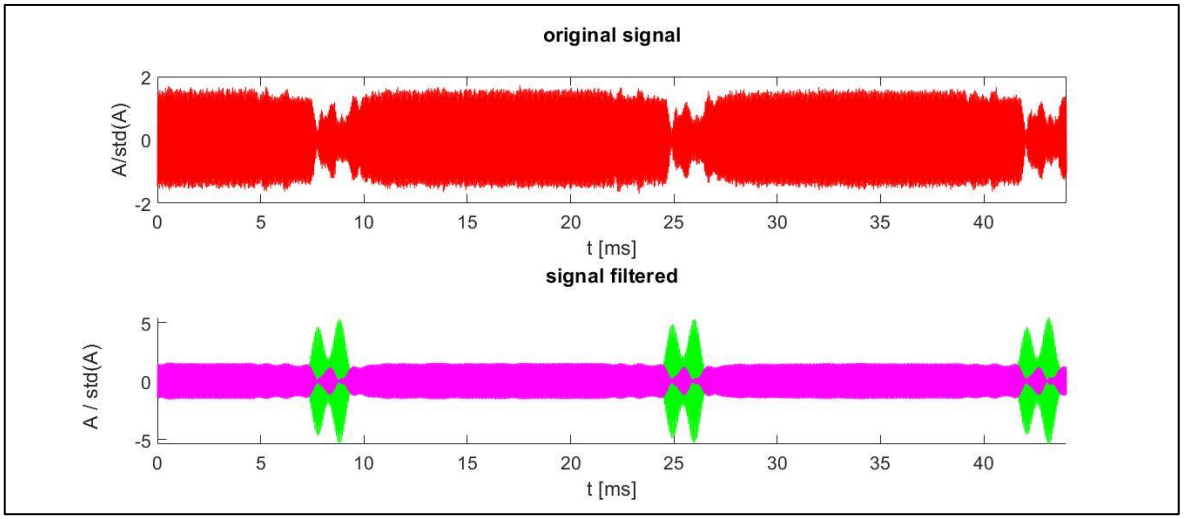

Figure 5.4 FSK Signal filtering.

From the previous step, the two output signals have one (17 KHz) or the other (19 KHz) frequency present. Now, to obtain their envelopes, other filters are applied to the square of both.

This time, the filters are 6^{-th} order low pass with a cut-off frequency of 2 KHz or 2,250 KHz. The first is for the waveform centered at 17 KHz, while the highest one is for the pulse train centered at 19KHz. The design filters are always made by the functions *fdesign.lowpass, design* to obtain the SOS matrixes and the G vectors; instead, the *filtfilt* function is for the filtering.

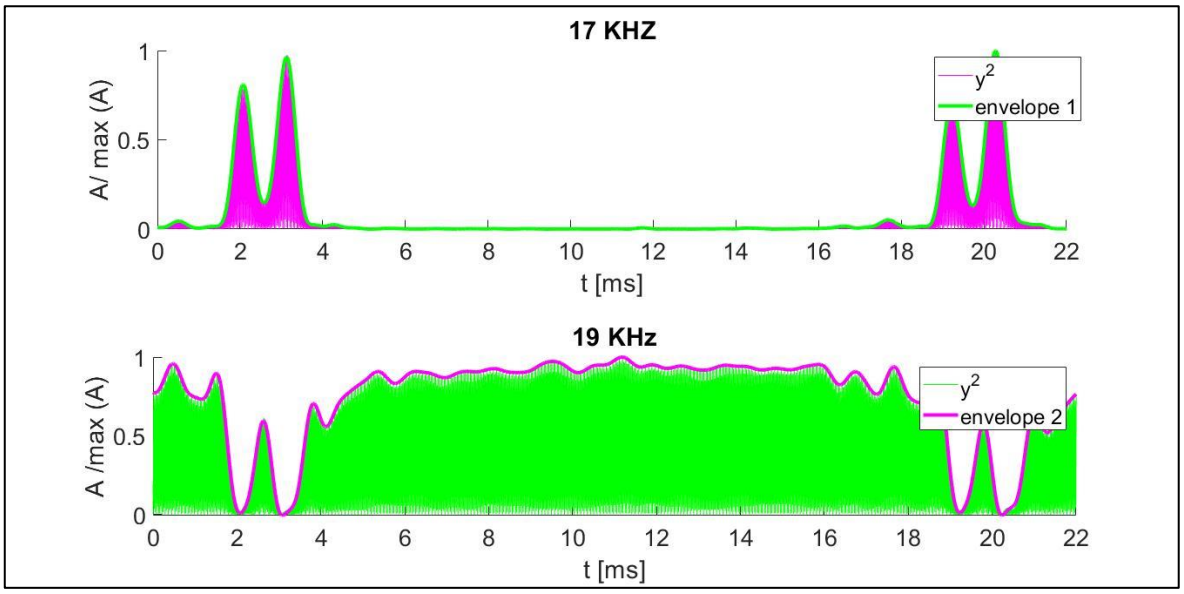

Figure 5.5 FSK signal demodulation example

With this last passage, the envelope 1 relative to the frequency at 17 KHz and the envelope 2 for the high frequency are produced.
Looking at Figure 5.5 , the envelope 1 seems less deformed than the 2 and measurements in the distance estimation had confirmed the hypothesis.
The 19 KHz frequency will have been more subject to external interference, even though it was the one best conserved by the system, as it was evidenced by the frequency analysis made on Figure 5.1
For this, the following algorithm works using only the envelope 1 of the two signals (microphone and the speaker).

5.2.2 Feature identification

For the feature identification, the minimum between the two peaks present in the envelope, corresponding at the zero phase in the variation “101” made by the modulated sequence, was chosen.
For the proper functioning of the algorithm, the division into windows is important. To achieve this task, the envelope 1 of the speaker is used.
The characteristic, to be found, is the position of the "0" which corresponds to the minimum between the two peaks (as you can see in Figure 5.6)

The search for the minimum takes place in two steps:
1. Find the peak signal pairs.
2. Find the minimum between the two peaks.

For the first step is very simple, handling the signal of the speaker, it is enough to detect all the maximum values and divide them into pairs of two.
To find the minimum, consider the sample period between the two maximums where the point with the lowest value is found and its position is saved in a vector.
Then the signals are divided into windows in which to observe the presence of the microphone responses.
The division takes place starting from the minimum value previously found and considering the 3000 successive samples.
The number of samples was obtained considering f_v the frequency variation rate of the signal and considering the system sampling rate f_s. This relationship is described in the formula below (5.4).

$$\text{N°sample} = \frac{f_s}{f_v} = \frac{218.750\ \text{KHz}}{58\ \text{Hz}} \approx 3500 \qquad (5.4)$$

Having found the minimum corresponding to the position of the value "0" in the envelope of the speaker and divided the signal in temporal windows, it is possible to move on to the response identification of the frequency variation in the microphone.

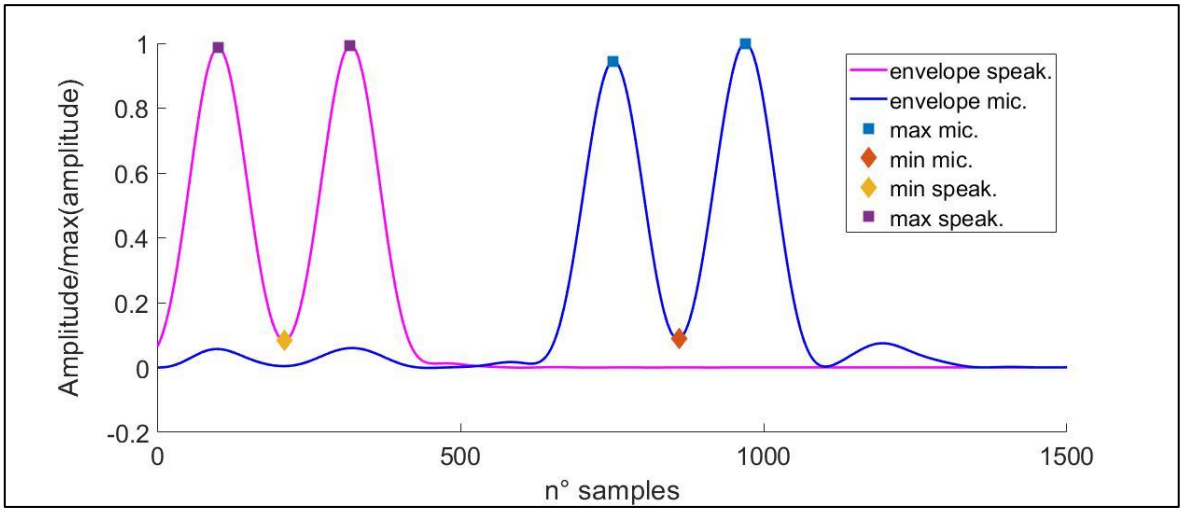

Figure 5.6 Generic FSK signal window after detected max e min points

Once the subdivision in windows has been carried out, it is possible to find the zero position offsets over time of the microphone signal. As with the speaker's signal, the maximum values are identified first. But in this circumstance, noise-related maxima can be detected, for these two checks have been created to determine if this maximum is admissible or not. These two evaluation criteria are:

- Evaluate the maximum width reached by the peak. If this amplitude is less than an arbitrarily chosen threshold, it is discarded. This threshold has been identified by experimental tests and its value is 0.6.
- The second check consists in evaluating when it is a peak from the next. If the peak is more than 500 samples distant from the next it is not taken into account in the search.

After these checks for the maximum permissible pairs, the algorithm looks for the minimum in the same way performed for the speaker's signal.
Finally, the meters distance will be proportional to the sampling rate, the sound speed in air, and the difference between the two positions of minimums found.

Chapter 6 Results Discussion

In this chapter of the thesis, all the results obtained by the designed system in distance measurement will be explained.
As previously written, in order to find the algorithm that better performs distance evaluation, different signals were acquired and analyzed with the implemented methods.
Firstly, different wave signals for amplitude modulation have been compared and, in a second moment, the best one was compared with the results obtained by FSK method.

As said before, the developed device is able to acquire with one microphone the signal emitted by the speaker. To evaluate if this developed system could be suitable for distance measurement between peripherical sites in PWV evaluation, all the acquisitions here reported were done in a setting as ideal as possible, to not include interferences or noise not yet under control. The main purpose of these acquisitions, in fact, was to evaluate the possible feasibility of the proposed idea.

For every acquisition the system has been set in this way: the speaker was locked in a point on a table, flanked by a measuring tape, and the microphone has been moved along the defined line. In this way, all the measurements were instantaneously checked with the meter.
In
Figure 6.1 is shown the final setting: the outdistanced microphone and speaker, the measuring tape and the acquisition board, which transmits data to the laptop for signal elaboration.

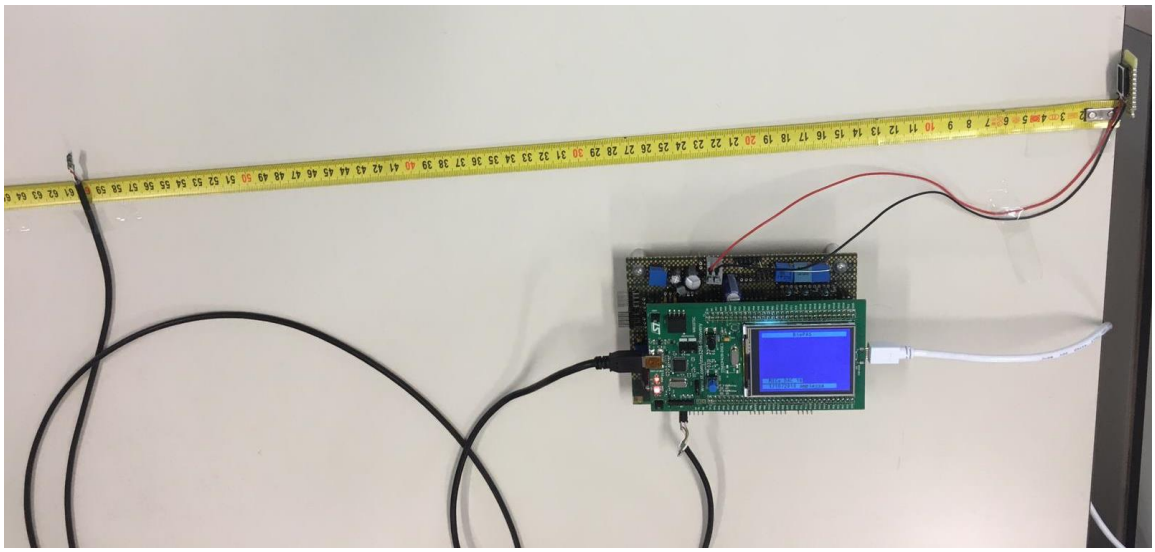

Figure 6.1 System setting for the tests.

In the following paragraphs, the results are so presented:

- The best waveform for AM algorithms evaluation
- the best algorithm chooses between the ones based on AM signals.
- AM system limits and performances.
- FM system limits and performances.

All the distances are expressed as an average value and standard deviation. These two quantities are derived from the N signal windows from which are extrapolated N evaluations of distance.
Before the results, something about the errors and the significant digit has to be mentioned. The millimeter is the last significant digit here reported, this choice was made for two reasons. The first is that for this work aim, the further clinical application, there is not the need to have a greater accuracy than a millimeter. The other one is more related to the limits of the system, it has a sampling frequency of 218.750 KHz and so the maximum resolution in time is 4.57 us.
Moreover, there are other secondary factors that may introduce a more or less predictable error: the delay relative to analog circuit filtering in the microphone branch (about 11.25 us, estimated with LTspice software) and the error due to the sound velocity in the air, because of its dependence on temperature (see equation (2.16)), not under perfect control in our measurements.

6.1 Results of AM algorithms

Concerning the AM signals and their usage for this application purpose, several deductions were done.
In the following paragraphs, the results obtained through the four different algorithms with the three different modulated signals (rectangular, Gaussian and the triangular) and their relative collected data are presented.
After the speaker's and microphone's signals are acquired for 2 seconds by the system, they have been processed with the four algorithms developed (Distance Max, Threshold, Parabolic double threshold fitting, Iterative parabolic fitting), obtaining 200 measurements for each digital wave, from which the mean value and standard deviation are derived. In particular, the distance evaluations were taken every 10 cm in the range between 10 and 100 cm, the useful range for the application purpose.
Then, in the last paragraph, the best signal with the best parameter extraction is performed in a wider range of measurements to evaluate the precision, the accuracy, the repeatability, and the resolution.

6.1.1 Rectangular Window

The first waveform tested is the amplitude modulated signal with a rectangular window, depicted in Figure 6.2.

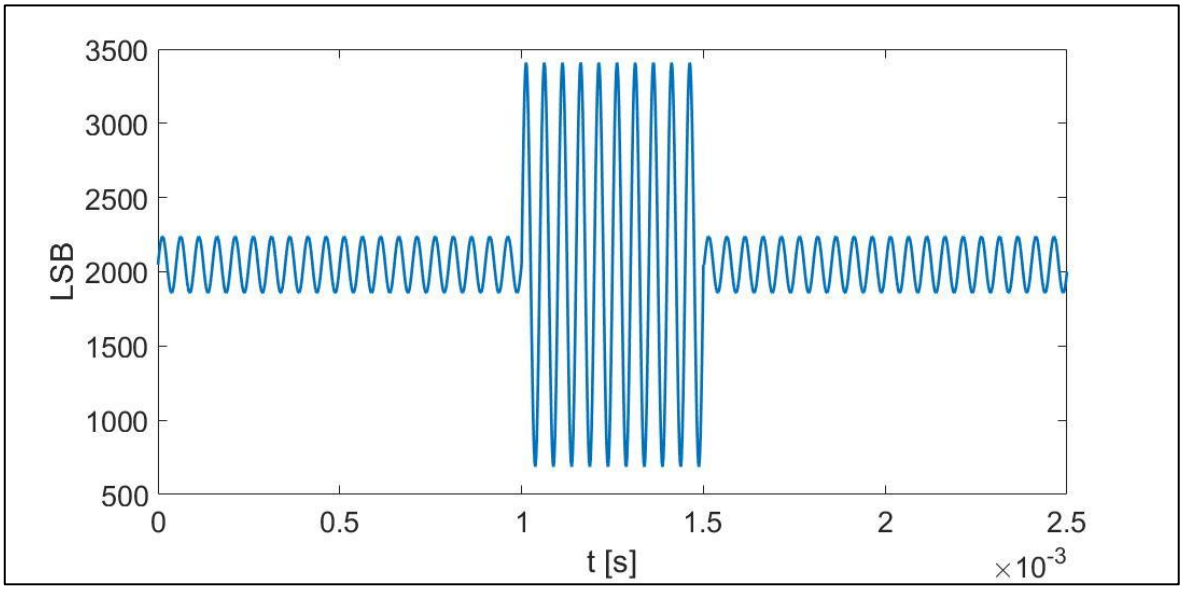

Figure 6.2 Rectangular wave.

With this wave shape, the mean distance values of the 200 windows and the relative difference with the reference value, for all the implemented algorithms, are reported in Table 6.1. In all the table reported in this chapter: "DIFmax" is the distance between the peaks, "THR" is the simple threshold method, "TDLFP" means the threshold double level parable fit and "IPF" is iterative parable fit; all described in Chapter 4.

	Methods				mean-reference			
Reference	DIF.MAX	THR	TDLPF	IPF	DIF.MAX	THR	TDLPF	IPF
10.0	11.9	14.3	8.4	8.7	1.9	4.3	-1.6	-1.3
20.0	21.6	24.0	18.3	18.7	1.6	4.0	-1.7	-1.3
30.0	30.6	33.3	27.9	28.1	0.6	3.3	-2.1	-1.9
40.0	40.1	42.8	37.2	37.5	0.1	2.8	-2.8	-2.5
50.0	51.6	53.6	47.5	47.9	1.6	3.6	-2.5	-2.1
60.0	60.3	62.9	57.4	57.8	0.3	2.9	-2.6	-2.2
70.0	70.6	73.1	67.3	67.7	0.6	3.1	-2.7	-2.3
80.0	80.3	82.6	76.7	77.0	0.3	2.6	-3.3	-3.0
90.0	90.1	93.6	82.1	86.3	0.1	3.6	-7.9	-3.7
100.0	99.5	103.1	92.0	96.1	-0.5	3.1	-8.0	-3.9

Table 6.1 Rectangular waveform's distance estimation for the four algorithms.

From these averages, it can be noted that the closer values to the reference are those of the "DIFmax" method, that theoretically should have been the weakest one.
Instead, the other methods overestimate the measure, as the Simple thresholding (THR), or underestimate, as in the case of TDLPF and IPF.
In any case, the algorithm that most moves away from the real values is the two-point estimation.

6.1.2 Gaussian window

The second type of signal tested is the one modulated with a Gaussian window (Figure 6.3). Also, in this case, the signal analysis took place as previously described.

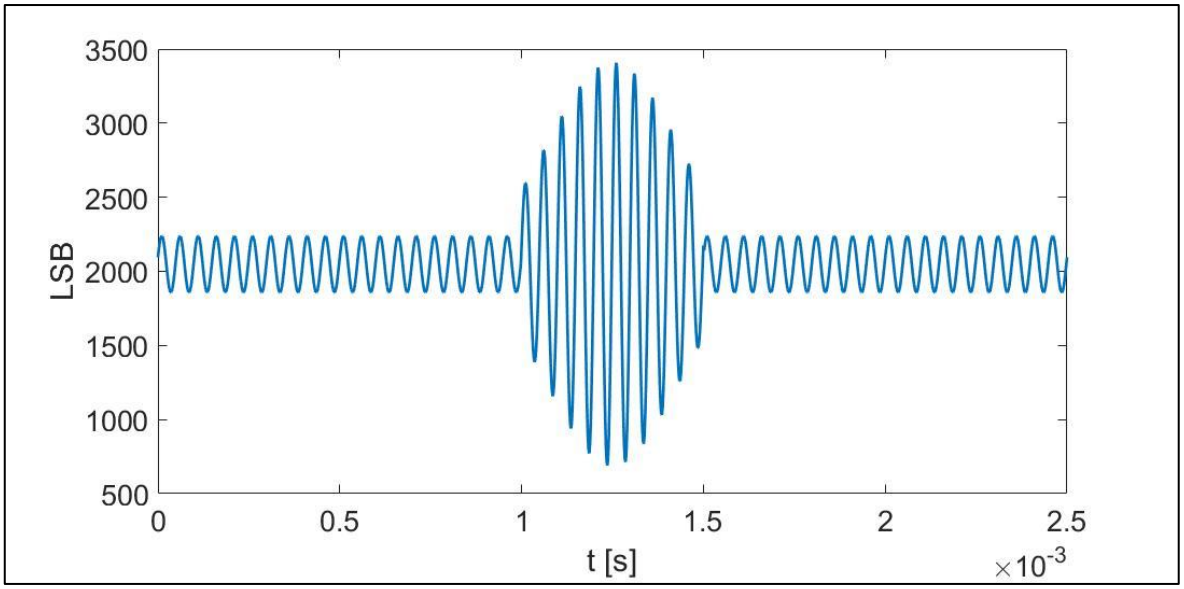

Figure 6.3 Gaussian wave.

As said, the data, presented in Table 6.2, are the average value of the 200 windows. Moreover, the tests are carried out once again along the range [10 cm :100 cm] with steps of 10 centimeters.

	Methods				mean-reference			
dimension	DIF.MAX	THR.	TDLPF	IPF	DIFF.MAX	THR.	TDLPF	IPF
10	12.4	13.8	6.0	7.2	2.4	3.8	-4.0	-2.8
20	19.0	23.4	13.2	15.3	-1.0	3.4	-6.8	-4.7
30	30.0	32.3	25.5	26.4	0.0	2.3	-4.5	-3.6
40	40.8	42.8	35.6	36.6	0.8	2.8	-4.4	-3.4
50	49.1	51.7	45.0	45.8	-0.9	1.7	-5.0	-4.2
60	59.3	61.7	54.7	55.6	-0.7	1.7	-5.3	-4.4
70	68.6	70.7	63.7	64.6	-1.4	0.7	-6.3	-5.4
80	79.6	81.5	74.3	75.3	-0.4	1.5	-5.7	-4.7
90	89.2	91.8	85.0	85.8	-0.8	1.8	-5.0	-4.2
100	-	-	-	-	-	-	-	-

Table 6.2 Gaussian waveform's distance estimation for the four algorithms**.**

From the data presented above, the first drawback is that the system has not been able to obtain a 100 cm distance estimation.
In addition to that, as in the case of the previous shape wave, the most effective method is the difference between the peak positions (DIFF. MAX). In fact, the other three methods behave worse: the THR overestimates values and the other two methods underestimate, as in the preceding case.

6.1.3 Triangular window

The last signal tested to better approximate the equation (4.6) is a sound wave with a frequency at 20KHz and a triangular amplitude modulating (Figure 6.4).

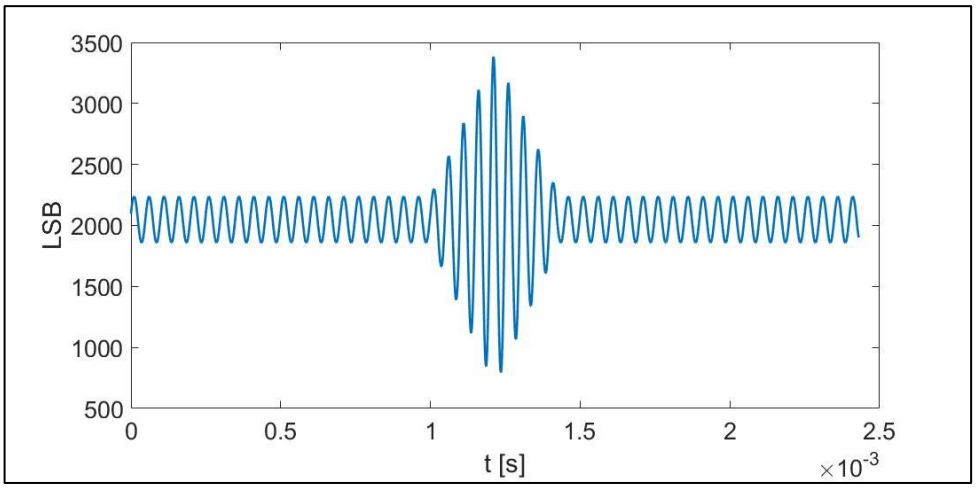

Figure 6.4 Triangular wave.

In the same way as the two past cases, the table concerning the 4 methods along the range 10-100 cm is shown (Table 6.3).

	Methods				mean-reference			
Reference	DIF.MAX	THR	TDLPF	IPF	DIF.MAX	THR	TDLPF	IPF
10.0	12.7	16.0	10.5	10.7	2.7	6.0	0.5	0.7
20.0	21.5	25.3	19.9	20.1	1.5	5.3	-0.1	0.1
30.0	30.9	35.3	30.0	30.1	0.9	5.3	0.0	0.1
40.0	40.9	45.3	39.9	40.0	0.9	5.3	-0.1	0.0
50.0	50.9	55.0	49.5	49.6	0.9	5.0	-0.5	-0.4
60.0	60.8	64.7	59.4	59.5	0.8	4.7	-0.6	-0.5
70.0	71.3	74.5	69.1	69.2	1.3	4.5	-0.9	-0.8
80.0	80.8	84.9	79.4	79.6	0.8	4.9	-0.6	-0.4
90.0	91.4	94.5	89.1	89.2	1.4	4.5	-0.9	-0.8
100.0	98.8	104.2	99.0	99.1	-1.2	4.2	-1.0	-0.9

Table 6.3 Triangular waveform's distance estimation for the four algorithms.

The above tabled data are generally improved for almost all the algorithms, except for the threshold (THR) where there is the highest overestimation.
This THR error is probably due to the not ideal conditions of the acquisition environment, acoustic noise and signal distortion effects. In fact, unlike the others, the threshold algorithm is closely related to the noise before the peak and this leads an increase in the measure uncertainty.

The best software process results to be the parabolic iterative fitting (IPF). Also, the double threshold parable fit algorithm (TDLPF) obtains good results, if compared with the reference values, and the greater error is for the 100 cm (1 cm underestimated).

Conclusions between the various waveforms

With the aim of making a comparison between the three presented waveforms, the best-performing method for each signal has been taken and depicted in Figure 6.5. From this, the differences between the three systems could be noticed.

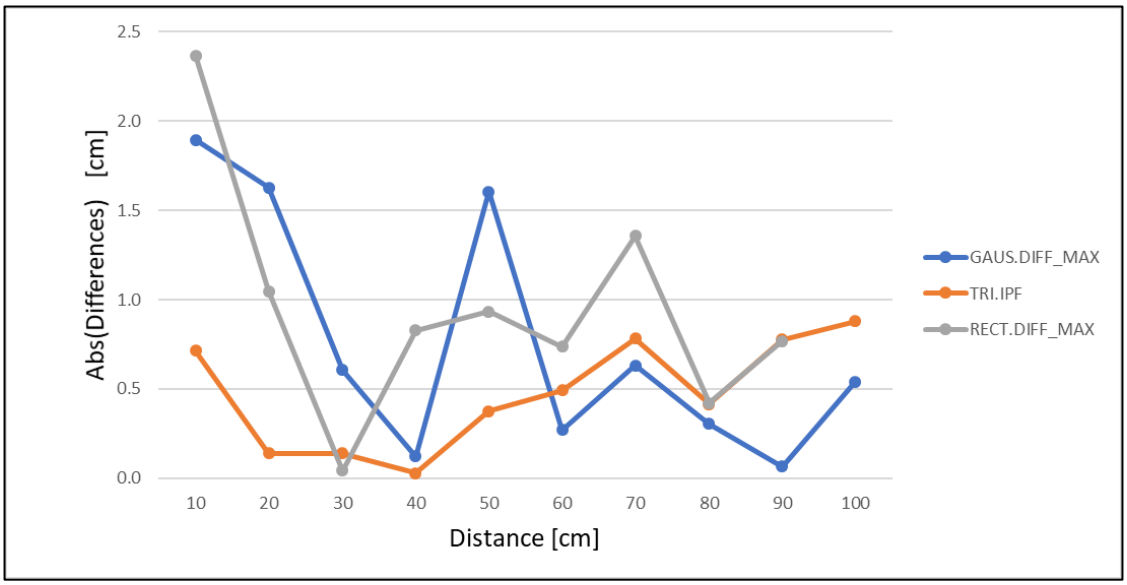

Figure 6.5 The best algorithm for each waveform

Considering all three waveforms tested and according to the papers in support and the experimental data, it has been chosen the one that gives the values closer to reference.
As could be seen, the triangular signal is the one that best performed, with the maximum error is less than 1 cm.

After this choice, the triangular waveform has been tested on the 4 algorithms but on a wider range of distances, as reported in the following paragraph.

6.2 Results of AM technique

This paragraph contains all the results obtained using the waveform chosen in the previous evaluation. This waveform is the amplitude modulated signal with a triangular shape.
To clarify, the estimations were obtained always using the conformation seen in the introduction (Figure 6.1).

The time delay calculated in samples, according to the sampling rate and the sound speed, obtained from the formula (2.16), provides a distance estimation, that is always assessed by comparing it to the measurement of the measuring tape.

6.2.1 Accuracy and precision

The first results are useful to verify which method, among the four was, the most performing in the range between the 30 and 190 cm.
The lower limit 30 cm is imposed by the circuit saturation, instead, the upper limit is due to the lack of interest for project purpose. So, the optimum trade-off has to be found, in this case, the analog circuit amplification has been calibrated at about 36 dB.

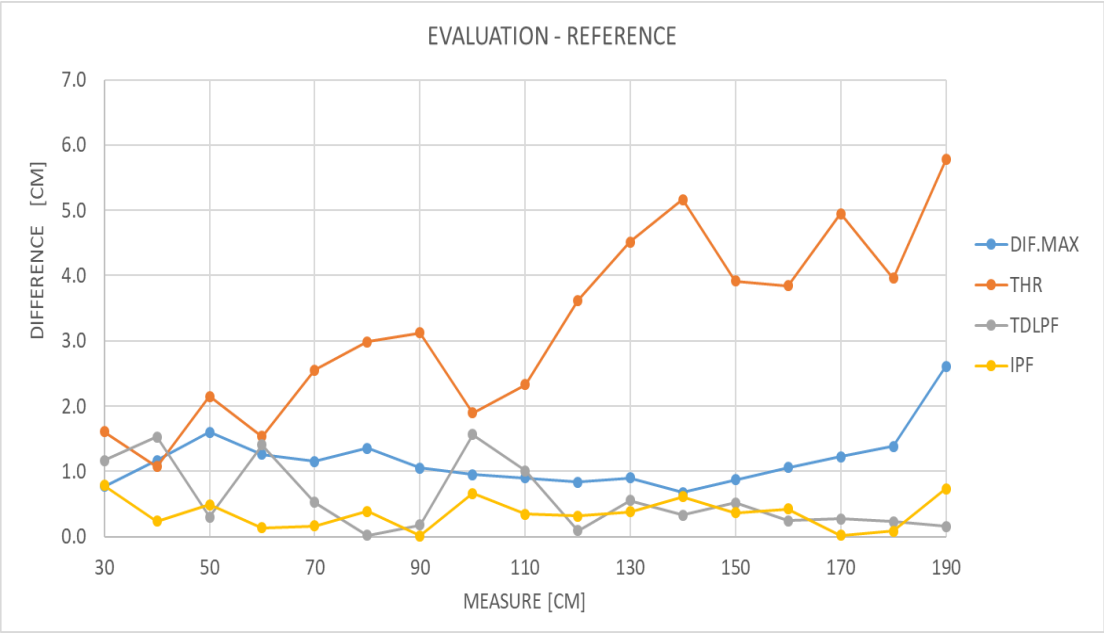

Figure 6.6 Triangular signal's distance estimations for all algorithms.

Looking at the graph above that shows the trend of the difference between the estimated value and the real one, it can be said that generally, the trend of the threshold method is to increase. The error in estimations follows the growth of distance.
The method of difference between maxima (DIF.MAX) is mostly constant except in the last distances over the 150 cm in which it has a tendency to increase.
Finally, the remaining two methods have a constant tendency, but the iterative method (IPF) is more accurate than the fitting passing through two points (TDLPF).

From this analysis the most accurate is the parabolic iterative method, in fact, all the made distance estimations have an error less than one centimeter.
Instead, for evaluating the method precision, the standard deviations in Table 6.4 is considered. Observing that the precision decreases to the increase of the distance between speaker and microphone. Looking at the graph above, that shows the trend of the difference between the estimated value and the real one, it can be said that, generally, the threshold method has an increasing trend. The error in estimations, in fact, follows the growth of distance.

The method of difference between maxima (DIF.MAX) is mostly constant except in the last distances over the 150 cm, where it tends to increase.
Finally, the remaining two methods have a constant tendency, but the iterative method (IPF) is more accurate than the fitting passing through two points (TDLPF).

From this analysis the most accurate algorithm results to be the parabolic iterative method; in fact, all the distance estimations done have an error less than one centimeter.

On the other hand, to evaluate the method precision the standard deviations in Table 6.4 is considered. Observing that the precision decreases as the distance between speaker and microphone increases.

REF	STD	REF	STD
30	0.2	120	1.6
40	0.3	130	1.5
50	0.4	140	3.5
60	0.6	150	1.9
70	0.7	160	1.5
80	0.6	170	1.7
90	1.0	180	1.7
100	1.5	190	2.0
110	1.7		

Table 6.4 Standard deviation obtained by the 200 values derived from the iterative method

6.2.2 Measurement repeatability

To verify the measurement repeatability for the amplitude modulated signal, several assessments were made in the range between 40cm and 180cm every 20 cm.
The measurements were repeated five times for every reference value and these results are reported in Table 6.5 and depicted in Figure 6.7.

RIF.	VAL.	STD	DIFF	STD. DIFF	RIF.	VAL.	STD	DIFF	STD. DIFF
	40.3	0.3	0.3			120.5	1.1	0.5	
	40.1	0.4	0.1			120.1	5.8	0.1	
40.0	40.2	0.3	0.2	0.1	120.0	120.0	1.6	0.0	0.4
	40.4	0.3	0.4			120.7	0.9	0.7	
	40.3	0.4	0.3			120.8	1.1	0.8	
	60.4	0.5	0.4			139.9	1.4	0.1	
	60.6	0.5	0.6			139.7	1.4	0.3	
60.0	60.6	0.5	0.6	0.2	140.0	139.5	2.0	0.5	0.3
	60.2	0.5	0.2			140.4	1.1	0.4	
	60.8	0.5	0.8			139.9	1.3	0.1	
	80.1	0.8	0.1			160.2	1.7	0.2	
	79.9	0.7	0.1			160.9	1.1	0.9	
80.0	80.4	0.6	0.4	0.4	160.0	160.4	1.4	0.4	0.4
	80.9	0.6	0.9			160.1	1.7	0.1	
	80.6	0.6	0.6			160.0	1.6	0.0	
	100.5	0.8	0.5			180.4	1.7	0.4	
	100.2	0.8	0.2			180.8	1.4	0.8	
100.0	100.3	0.9	0.3	0.2	180.0	179.5	1.8	0.5	0.6
	100.3	0.8	0.3			180.1	1.8	0.1	
	100.1	1.2	0.1			179.5	3.1	0.5	

Table 6.5 Results for evaluating measurement repeatability.

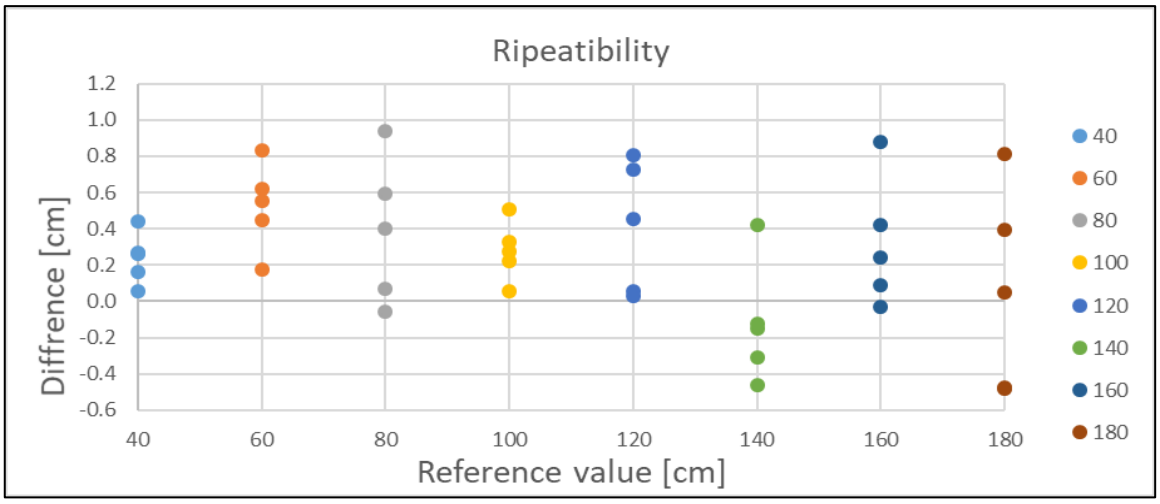

Figure 6.7 The five differences for every reference value in range [40 cm : 180cm].

From the data collected, it could be seen how the system repeats easily measurements at some determinates distance (for example 40cm and 100 cm). The distance at which the maximum divergence among the various measurements could be noticed is 180 cm, where the standard deviation of the 5 differences is about 0.6.

Immediately after and considering the target application, a second range was tested to see how the system operates in the short distances. For this, to avoid saturation effects, the project gain has been lowered at about 25 /27 dB.
The specific range was from 5 to 30 cm, moving through 5 cm steps (Table 6.6 and Figure 6.8).

RIF.	VAL.	STD	DIFF	STD DIFF.	RIF.	VAL.	STD	DIFF	STD DIFF.
	4.7	0.0	-0.3			20.9	0.2	0.9	
	4.3	0.1	-0.7			19.9	0.4	-0.1	
5.0	4.3	0.1	-0.7	0.3	20.0	20.5	0.2	0.5	0.3
	4.9	0.2	-0.1			20.3	0.3	0.3	
	4.6	0.2	-0.4			20.3	0.3	0.3	
	10.5	0.1	0.5			25.2	0.3	0.2	
	10.5	0.1	0.5			25.3	0.4	0.3	
10.0	10.4	0.1	0.4	0.1	25.0	25.2	0.3	0.2	0.1
	10.3	0.2	0.3			25.3	0.3	0.3	
	10.3	0.2	0.3			25.0	0.3	0.0	
	15.7	0.1	0.7			30.0	0.4	0.0	
	15.4	0.2	0.4			29.9	0.4	-0.1	
15.0	15.2	0.2	0.2	0.2	30.0	30.5	0.3	0.5	0.3
	15.4	0.2	0.4			30.6	0.3	0.6	
	15.4	0.2	0.4			30.1	0.4	0.1	

Table 6.6 Repeatability data in the range between 5 and 30 cm.

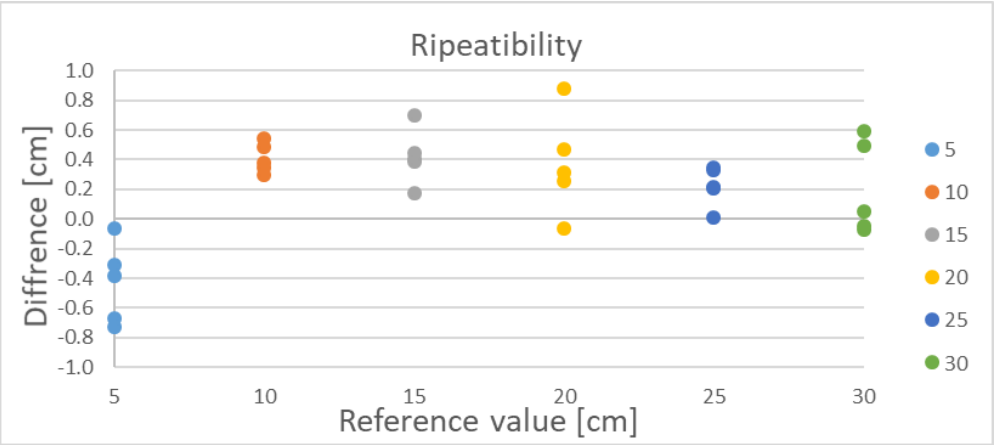

Figure 6.8 The five differences for every reference value in the range [5 cm: 30 cm].

Analyzing the data written in the table and observing the graph, it is seen how the measure is easily repeated. the maximum values of standard deviation are for the 5, 20 and 30 cm which are 0.3.

6.2.3 System Resolution

Still, on the triangular signal AM, it has been verified how much the resolution varies in the very short distance. In fact, considering the destination of this system, for clinics and operator, who are evaluating Pulse Wave Velocity, it becomes important to distinguish among very close distance measurement to increase the total system accuracy.
So, to better test the designed system, in addition to the measures from 30 to 180 cm every 10 cm (the central values) distances were also evaluated 1 cm first and one centimeter later; i.e. at 100 cm the measurements carried out are for 99, 100, and 101cm.
The results obtained through these tests are shown in Table 6.7 and for a better comprehension in Figure 6.9

REFERECE	ESTIM.	STD	DIFF	REFERECE	ESTIM.	STD	DIFF	REFERECE	ESTIM.	STD	DIFF
29.0	29.4	0.2	-0.6	89.0	89.4	0.8	-0.6	149.0	149.2	1.5	-0.8
30.0	30.1	0.3	0.1	90.0	90.3	1.0	0.3	150.0	149.8	3.0	-0.2
31.0	30.9	0.2	0.9	91.0	90.8	0.8	0.8	151.0	151.5	1.6	1.5
39.0	39.2	0.3	-0.8	99.0	98.5	0.9	-1.5	159.0	159.1	1.9	-0.9
40.0	40.4	0.4	0.4	100.0	99.8	0.8	-0.2	160.0	160.0	1.6	0.0
41.0	41.5	0.3	1.5	101.0	101.2	0.8	1.2	161.0	160.8	1.9	0.8
49.0	49.3	0.4	-0.7	109.0	108.8	1.3	-1.2	169.0	169.0	1.5	-1.0
50.0	50.2	0.5	0.2	110.0	110.2	1.3	0.2	170.0	170.2	1.6	0.2
51.0	51.4	0.5	1.4	111.0	111.5	1.0	1.5	171.0	170.8	2.0	0.8
59.0	58.9	0.5	-1.1	119.0	118.7	1.4	-1.3	179.0	179.2	2.1	-0.8
60.0	60.2	0.5	0.2	120.0	120.4	1.0	0.4	180.0	180.3	1.8	0.3
61.0	61.2	0.6	1.2	121.0	120.7	1.3	0.7	181.0	181.5	2.2	1.5
69.0	69.0	0.7	-1.0	129.0	128.6	1.6	-1.4	189.0	189.2	1.8	-0.8
70.0	70.2	0.7	0.2	130.0	130.2	1.9	0.2	190.0	190.3	2.2	0.3
71.0	71.3	0.7	1.3	131.0	130.7	1.7	0.7	191.0	191.6	1.6	1.6
79.0	78.9	0.8	-1.1	139.0	139.2	1.4	-0.8	-	-	-	-
80.0	80.6	0.6	0.6	140.0	140.0	2.1	0.0	-	-	-	-
81.0	80.9	0.7	0.9	141.0	140.7	1.8	0.7	-	-	-	-
Reference=reference value, estim=estimation,std=standard deviation,diff=estimation-central reference value											

Table 6.7 The table illustrates the collected data for the resolution estimation

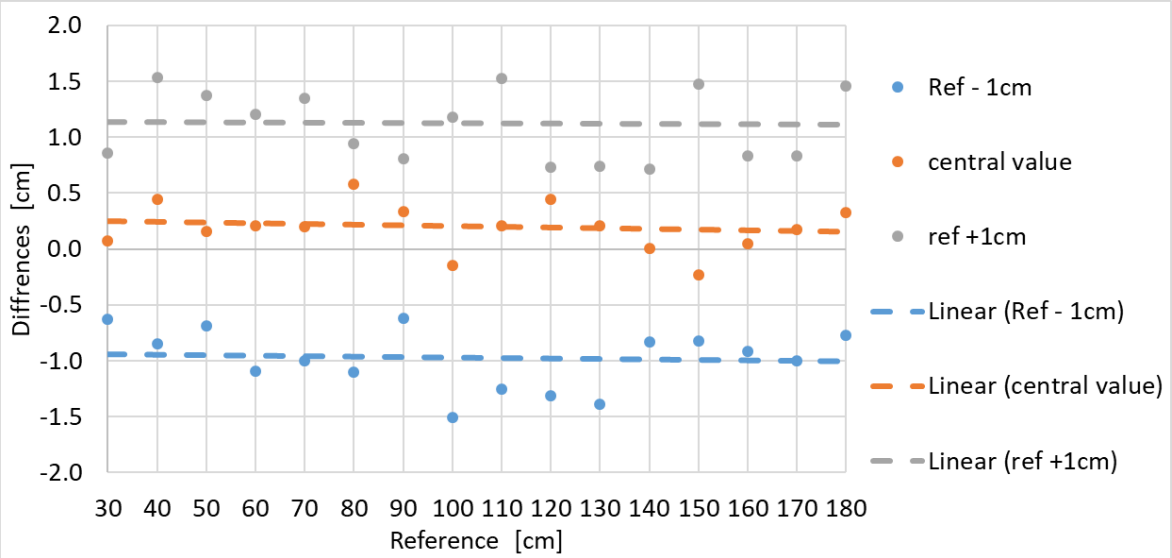

Figure 6.9 Differences between central value and estimation, the linear functions are the trend lines of the differences made for the +1cm, -1cm and central value.

The graph shows the results of the difference from the central value. In the ideal case, there would be only three series of values, the first centered at +1 cm, one centered at 0 and the other centered at -1. In the practice, data are distributed around these three values.
So, for a better and simpler analysis of the three series of measures, the linear trends were produced. The analysis is also done by evaluating the position of the individual tests in relation to the ideal value.
The first linear function should be centered at 1 cm, but from the experimental data, it differs by 1 mm from the reference value.

Instead, the orange trend relative to the center values should be centered at 0; nevertheless, it diverges from that center axis by a maximum 3 mm.
Finally, there is the blue trendline, it corresponds to the lower measurements and its position is roughly at -1 cm as it should be.

It was also tried to evaluate the 1-cm-resolution under the value of 30 cm. To do this the gain of the conditioning circuit has again been lowered to a value of 25 / 26 dB to avoid saturation. In this case, tests have been made from 6 to 30 cm with a step of 1 cm. The results of these estimations are in Table 6.8.

REFER.	ESTIM.	STD	DIFF	REFER.	EVAL.	STD	DIFF
6.0	6.1	0.1	0.1	19.0	19.6	0.2	0.6
7.0	7.4	0.1	0.4	20.0	20.6	0.2	0.6
8.0	7.9	0.1	-0.1	21.0	21.3	0.3	0.3
9.0	8.7	0.1	-0.3	22.0	22.2	0.3	0.2
10.0	9.9	0.1	-0.1	23.0	23.6	0.3	0.6
11.0	11.3	0.1	0.3	24.0	24.4	0.3	0.4
12.0	12.4	0.1	0.4	25.0	25.3	0.4	0.3
13.0	13.4	0.1	0.4	26.0	26.0	0.4	0.0
14.0	14.4	0.2	0.4	27.0	27.1	0.4	0.1
15.0	15.4	0.2	0.4	28.0	27.9	0.4	-0.1
16.0	16.3	0.2	0.3	29.0	29.4	0.5	0.4
17.0	17.2	0.2	0.2	30.0	29.7	0.5	-0.3
Refer.=reference value, estim=estimation,std=standard deviation,diff=estimation-reference value							

Table 6.8 Data for the resolution evaluation in the range between 6 and 30 centimeters.

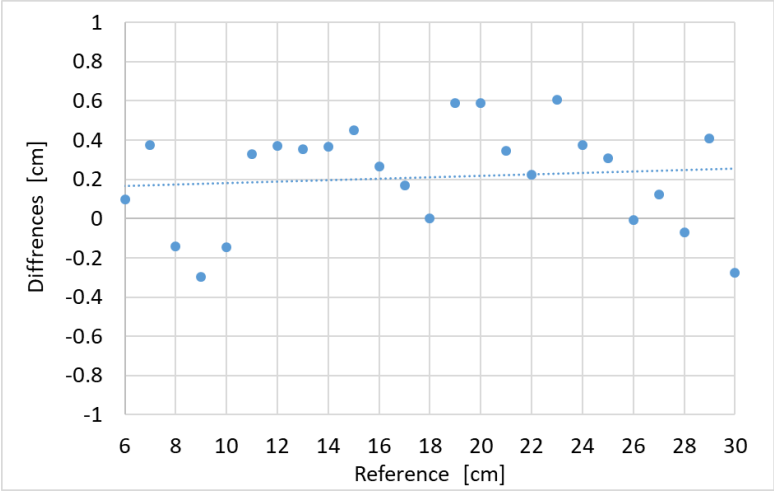

Figure 6.10 Differences between the estimated distance and reference value and the trendline of the results.

This last data showed how the system in most cases differs less than 5 mm from the real value; only for the 19, 20, and 23 centimeters, the error is greater, about 6 mm.
These differences can be due to a wrong temperature estimation or to a positioning error of the speaker or microphone that have been placed in a manual mode.

6.3 Results of FSK technique

For the frequency variation algorithm, the evaluations carried out are different. The waveform should not be chosen, but the best of the developed algorithm is simply tested, and then compared to the best AM algorithms.

With the intent of evaluating the various aspects of the system and its characteristics, in the same way as the AM algorithms, a test set was chosen. This has not been modified during the acquisition and it is represented at the beginning of Chapter 6, Figure 6.1.
Furthermore, the gain of the analog conditioning circuit has been varied to avoid saturation of the ADC and not to incur measurement errors.
The last thing to remember is that the results obtained are the standard deviation and the average value of every distance derived from 121 estimates, each one concerning a window burst.

6.3.1 Precision and accuracy

The first test made was to check the precision and accuracy of the system for the FSK signal. These assessments are carried out by examining the average value that must be as close as possible to the benchmark. Instead, the standard deviation is evaluated for the precision.
For this purpose, two type of tests are developed:

- The first test takes place in the range between 80 cm and 200 cm in steps of 10 cm, using a conditioning system gain of about 35dB.
- The second is done in the range between 20 and 100 cm always in steps of 10 cm with an amplification of 25 dB.

The results are listed in Table 6.9 and Table 6.10:

REF.	ESTIM.	STD	DIFF
80.0	80.7	0.2	0.7
90.0	89.5	0.2	-0.5
100.0	99.8	0.2	-0.2
110.0	110.0	0.3	0.0
120.0	120.3	0.2	0.3
130.0	130.7	0.4	0.7
140.0	140.6	0.3	0.6
150.0	150.3	0.4	0.3
160.0	160.3	0.3	0.3
170.0	169.8	0.3	-0.2
180.0	179.6	0.3	-0.4
190.0	190.8	0.6	0.8
200.0	200.6	0.5	0.6

Table 6.9 FSK signal's Data collected for precision and accuracy range [80-200cm].

REF.	ESTIM.	STD	DIFF
20.0	20.6	0.1	0.6
30.0	30.3	0.1	0.3
40.0	40.9	0.1	0.9
50.0	51.0	0.1	1.0
60.0	61.1	0.1	1.1
70.0	69.9	0.2	-0.1
80.0	80.1	0.2	0.1
90.0	89.5	0.2	-0.5
100.0	100.6	0.3	0.6

Table 6.10 FSK signal's Data collected for precision and accuracy range [20-100cm].

The data contained in the two tables above were summarized into the following Figure 6.11.

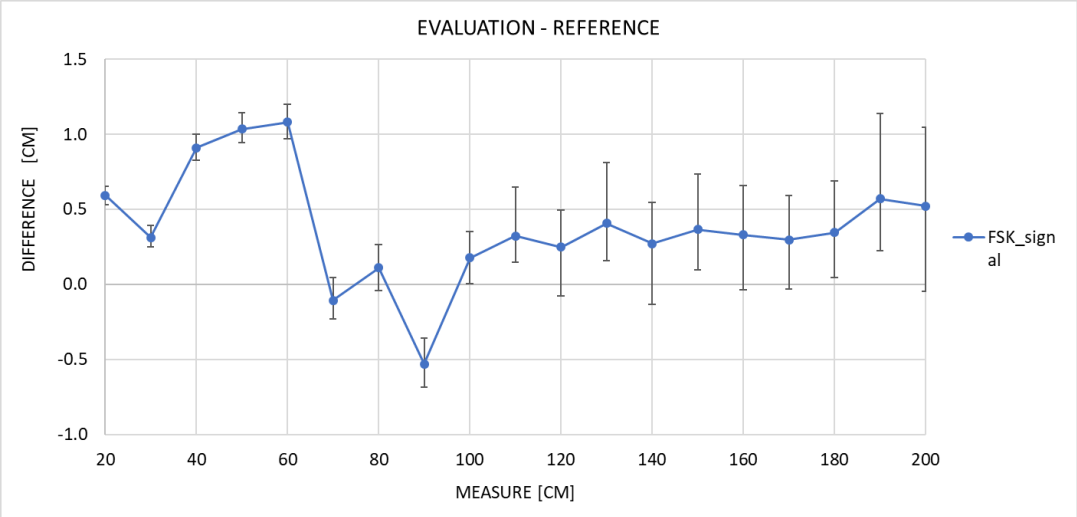

Figure 6.11 Differences between distance estimations and reference value and relative standard deviation for an FSK signal.

The chart shows how this method is not very accurate especially for the signals below the 70 cm, where the values of 40, 50 and 60 cm make an error up to 1 cm; thereafter the differences decrease reaching approximately 5 mm. So, making a speculation, when the distance increases the accuracy improves a little.
As concerns the precision: the more distance increases the more the standard deviation increases and with this decreases the precision. A hypothesis explaining this is that when the distance increases the signal noise ratio decreases along with the estimation precision.

6.3.2Measure repeatability

Secondly, repeatability has been tested using the same approach used for amplitude modulated signals. In order to evaluate the measurement repeatability, the distance estimation is repeated for 5 times every 20 cm-step.
The first interval was defined between 100 and 180 cm. Distances above 180 cm were not investigated because the gain was not enough, but more they are not interesting distances for the work purposes. Unlike long distances, those below 100 cm are interested in this application goal. Consequently, the gain was decreased to test the system in a second range between 20 and 100 cm.
The data collected in these two trials (20-100, 100-80) are summarized by the graph depicted in Figure 6.12

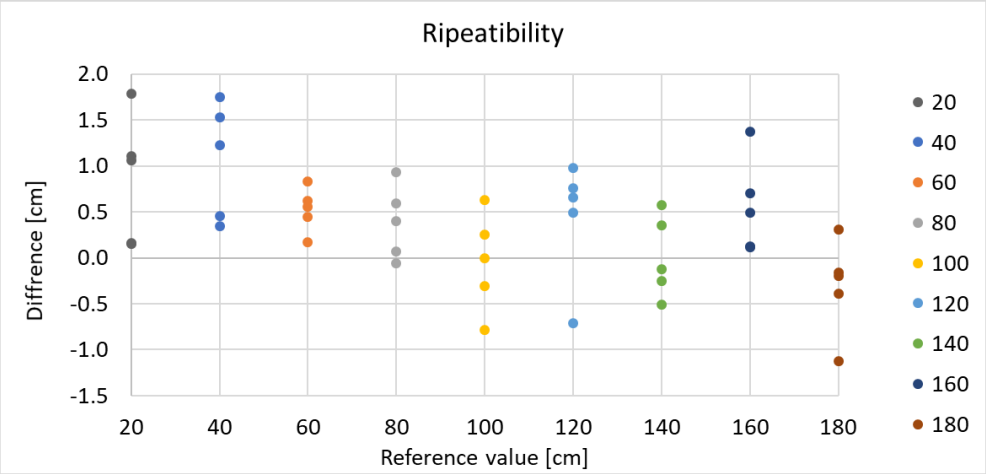

Figure 6.12 The five differences for every reference value in the range [20 cm: 180cm] for repeatability evaluation.

The graph in Figure 6.12 was extracted from the data in the tables below (Table 6.11):

RIF.	VAL.	STD	DIFF	STD DIFF	RIF.	VAL.	STD	DIFF	STD DIFF
	21.8	0.2	1.8			119.3	0.4	-0.7	
	21.1	0.2	1.1			120.5	0.2	0.5	
20.0	21.1	0.2	1.1	0.7	120.0	120.7	0.2	0.7	0.7
	20.2	0.2	0.2			120.8	0.2	0.8	
	20.1	0.1	0.1			121.0	0.3	1.0	
	41.2	0.2	1.2			140.6	0.3	0.6	
	41.7	0.2	1.7			139.5	0.3	-0.5	
40.0	41.5	0.2	1.5	0.6	140.0	140.4	0.3	0.4	0.4
	40.3	0.7	0.3			139.9	0.3	-0.1	
	40.5	1.0	0.5			139.7	0.3	-0.3	
	59.6	0.3	-0.4			161.4	11.1	1.4	
	59.6	0.2	-0.4			160.7	0.3	0.7	
60.0	59.3	0.4	-0.7	0.3	160.0	160.5	0.3	0.5	0.5
	59.9	0.4	-0.1			160.1	0.3	0.1	
	60.2	0.6	0.2			160.1	0.5	0.1	
	80.8	0.4	0.8			179.8	0.3	-0.2	
	79.4	0.2	-0.6			180.3	0.4	0.3	
80.0	79.9	0.2	-0.1	0.6	180.0	179.6	0.4	-0.4	0.5
	79.2	0.2	-0.8			179.8	0.3	-0.2	
	79.8	0.2	-0.2			178.9	0.5	-1.1	
	100.0	0.4	0.0						
	100.3	0.3	0.3						
100.0	99.2	0.2	-0.8	0.5					
	99.7	0.5	-0.3						
	100.6	0.2	0.6						

Table 6.11 FSK signal's repeatability data in the range between 80 and 180 cm.

Analyzing all the data shown, it could be noted that for most of the measurements there is a standard deviation, calculated on the difference from the reference measurement, greater than 5 mm. Only for the 40 and 140 cm, the standard deviation values are lower than 5 mm and therefore acceptable.

6.3.3 System Resolution

Once again, as for the AM, other tests have been made to evaluate the resolution by measuring every ten centimeters 3 distances that differ by one centimeter from each other.

The values obtained are tabulated in Table 6.12 and represented in the chart in Figure 6.13, in which ideally there are values that produce trendlines positioned respectively at 1cm, at 0 cm, and at -1cm.

REFERECE	ESTIM.	STD	DIFF	REFERECE	ESTIM.	STD	DIFF	REFERECE	ESTIM.	STD	DIFF
29.0	29.6	0.1	-0.4	89.0	88.8	0.3	-1.2	149.0	148.2	0.3	-1.8
30.0	29.7	0.1	-0.3	90.0	89.7	0.4	-0.3	150.0	149.3	0.5	-0.7
31.0	32.4	0.2	2.4	91.0	90.7	0.2	0.7	151.0	150.9	0.2	0.9
39.0	39.7	0.1	-0.3	99.0	99.1	0.3	-0.9	159.0	158.6	0.6	-1.4
40.0	39.8	0.1	-0.2	100.0	100.0	0.4	0.0	160.0	159.6	0.6	-0.4
41.0	41.3	0.1	1.3	101.0	100.8	0.2	0.8	161.0	161.6	0.4	1.6
49.0	48.9	0.1	-1.1	109.0	109.1	0.3	-0.9	169.0	169.1	0.4	-0.9
50.0	49.8	0.1	-0.2	110.0	109.8	0.3	-0.2	170.0	169.3	0.3	-0.7
51.0	51.6	0.1	1.6	111.0	110.5	0.4	0.5	171.0	171.9	0.5	1.9
59.0	59.1	0.2	-0.9	119.0	119.5	0.2	-0.5	179.0	179.2	0.5	-0.8
60.0	60.2	0.2	0.2	120.0	119.7	0.2	-0.3	180.0	179.2	0.5	-0.8
61.0	61.0	0.3	1.0	121.0	120.7	0.2	0.7	181.0	180.7	0.5	0.7
69.0	68.7	0.2	-1.3	129.0	128.6	0.3	-1.4	189.0	188.8	0.7	-1.2
70.0	70.0	0.2	0.0	130.0	130.5	0.3	0.5	190.0	190.6	0.5	0.6
71.0	71.1	0.2	1.1	131.0	131.2	0.3	1.2	191.0	191.4	0.5	1.4
79.0	79.2	0.2	-0.8	139.0	138.5	0.3	-1.5	-	-	-	-
80.0	79.7	0.2	-0.3	140.0	139.8	0.4	-0.2	-	-	-	-
81.0	81.1	0.3	1.1	141.0	140.7	0.3	0.7	-	-	-	-
Reference=reference value, estim=estimation,std=standard deviation,diff=estimation-central reference value											

Table 6.12 The table illustrates the FSK signals' data collected for the resolution estimation

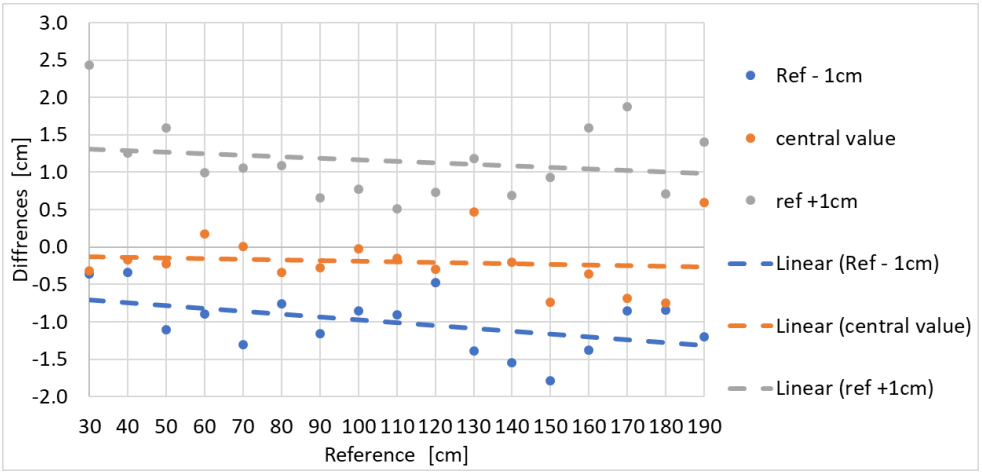

Figure 6.13 Differences between central value and estimation, the linear functions are the trend lines of the differences made for the +1cm, -1cm and central value for the FSK signals.

According to the graph in Figure 6.13, it is noted that, contrary to expectations, the values are distributed in a scattered manner, producing trend lines that deviate from the prefixed value.

A linear trend could be observed only for the central value; instead, the others follow a decreasing tendency that varies with the variation of the distance.

6.4 AM method vs FSK method

In this paragraph, after having observed and analyzed the results of the two types of signal modulations, their algorithms and the results obtained, a comparison between the two will be made.
In particular, the two are compared according to the methods:

- Accuracy and Precision;
- Resolution;
- Repeatability.

For simplicity, concerning AM approach, the results used in this paragraph are referred to the iterative method (IPF), which provides more satisfactory results.

6.4.1 Accuracy and precision.

The first comparison made (Figure 6.14
Figure 6.14) is about precision and accuracy, giving more emphasis to the latter.

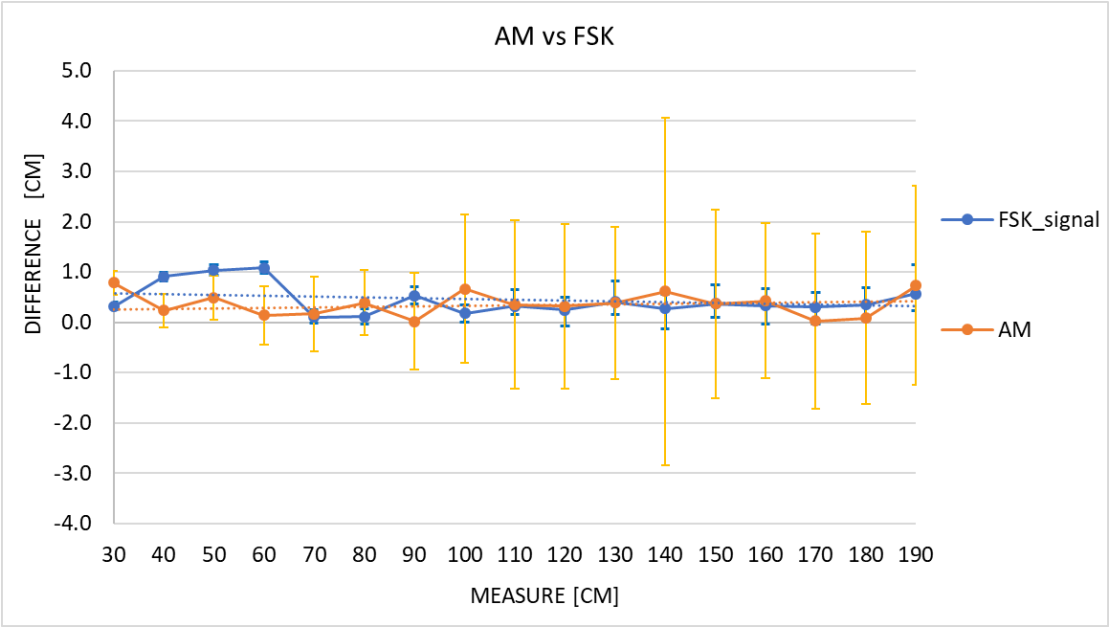

Figure 6.14 Matching data between the FSK signal and AM signal.

The results of the two different approaches, depicted in the figure above, are very similar to each other since the various quantities evaluated have comparable trends.

For the accuracy, the difference between the measured and the reference value is estimated. In the range between 100 and 190 cm, the estimation errors are overlapped, whereas between the 30 and 90 cm the FSK commits a greater error, sometimes over 1 centimeter.

So, after this analysis for the accuracy, it seems that the iterative method based on amplitude modulation has a better performance.

On the other hand, the standard deviation is assessed for the precision. It is visible, for both algorithm's types, how it decreases as the distance increases.

6.4.2 Resolution comparison

The second evaluation concerns the resolution of the system. In order to compare this feature as simple as possible, the trend lines of the results of Figure 6.9 and figure 6.13 were shown in the same graph, obtaining Figure 6.15.

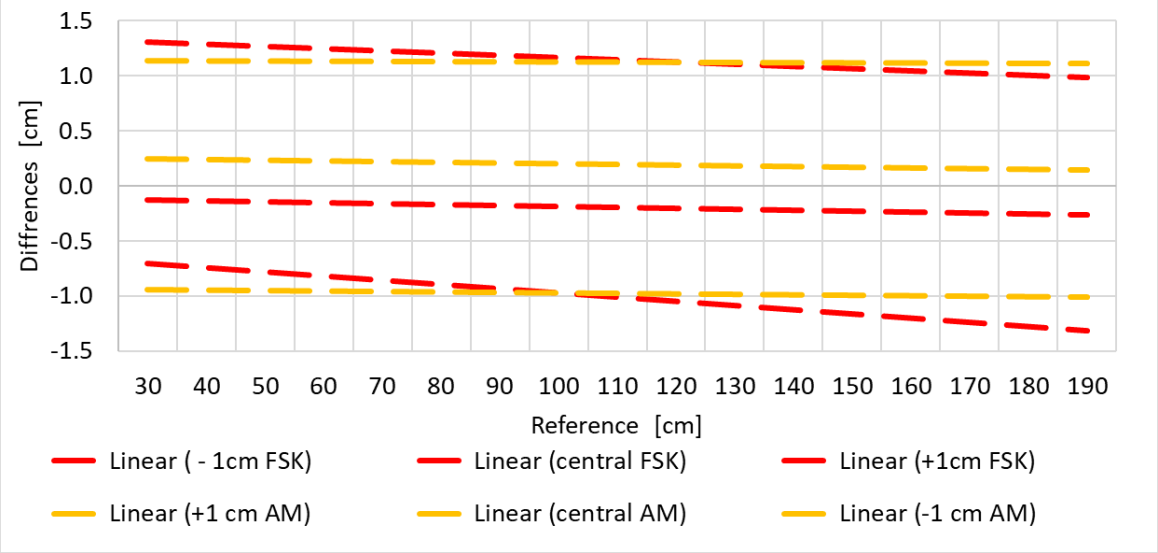

Figure 6.15 Matching the linear trend of data between the FSK signal and AM signal.

This graph shows in yellow the values referred to the method with amplitude modulation, whereas the red functions are associated with the method based on the FSK.
It is obvious that the results obtained by the iterative method, in this case, are more corresponding to an ideal state. Moreover, the yellow trends are constant and quite centered at -1, 0 and 1 cm. Contrarily, this is not true for the values relative to the method based on the FSK signal that has trends that deviate more from the ideal values.

6.4.3 Repeatability comparison

The last characteristic to compare between the two methods is the repeatability of the measure. The sections in the first part of Chapter 6 describe how the system was tested. These variance values for both techniques have been reported in the graph in Figure 6.16.

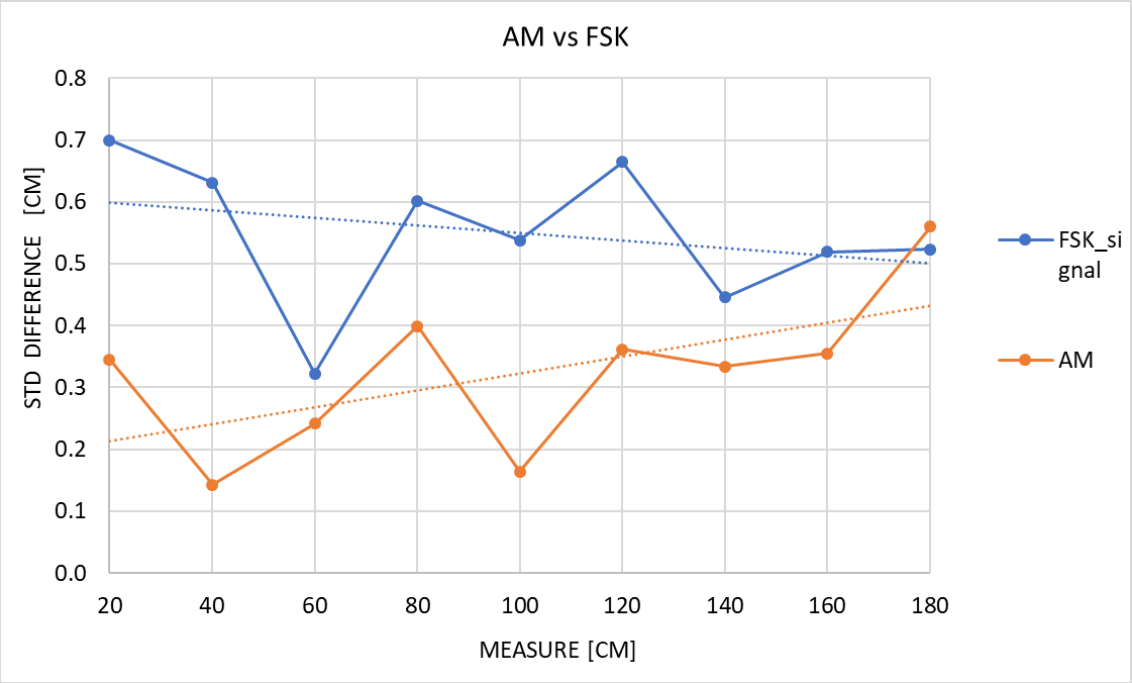

Figure 6.16 Standard deviation of differences between the reference value and the five-distance assessment for both algorithms.

It is possible to establish by analyzing this simple diagram that the AM method has a greater repeatability than the method based on the Frequency shift keying. In fact, with the amplitude modulation always lower standard deviations have been obtained, except for the reference distance 180cm, where the difference is quite neglectable.

6.4.4 Comparison conclusion.

From the three graphs seen in this comparison, it is possible to evaluate which of the two proposed modulations performed better for this work purpose.
For the accuracy, the best method results in the amplitude-modulated signal. Since it has not made errors in estimation greater than one centimeter contrary to the approach based on an FSK signal.

On the other hand, the frequency modulation method has greater precision. Even if its standard deviation increases with the distance it is always lower than the results obtained with the other AM algorithm.

For the resolution and repeatability of the measure, there is no doubt the results obtained with the parabolic iterative fitting are much better than the other. Moreover, another quality of the method is that it allows reaching distances below 30cm, it evaluates 6 cm with high accuracy.

It is possible to conclude, that for the data obtained, the most efficient was the iterative method.

Chapter 7 Conclusion

All the activities carried out during this thesis work aimed to develop a system able to measures the distance of the acquisition sites involved in the pulse wave velocity estimation. Specifically, the designed prototype allows a sound wave emission through a speaker linked to a MEMS microphone-based recording system. Immediately after the acquisition, the emitted and recorded signals are processed and thanks to the implemented algorithms, the distance between speaker and microphone is estimated.

To address this purpose, 5 different algorithms were tested, 4 of them exploiting amplitude modulated signals, and one that exploits the frequency shift keying modulation.
On the amplitude modulated waveforms, several delay evaluation methods have been considered and evaluated: the difference between maxima, simple threshold, parabolic fitting with two thresholds and parabolic iterative method.
All the identified approaches were implemented ad correspondent algorithms developed. Several trials have been conducted in order to make assessments in terms of accuracy, precision, repeatability of measurement and resolution of the various methods.
Analyzing the results collected on the performed tests, it can be said that the method with a greater accuracy, a better measurement repeatability, and a higher resolution is the parabolic iterative method. Only for the precision point of view, better results have been obtained by using the frequency variation technique.

In conclusion, the pulse wave velocity distance evaluation system using the iterative method achieved interesting results matching the defined prerequisites and reaching a resolution less than one centimeter with a good repeatability of the measurement.
Furthermore, another important achievement is the operating range of the final prototype that can operate from 6 to180 cm without impacting performance. With this working distance range, it is possible to cover all the practical requirements related to pulse wave velocity evaluation equipment.

However, there is still room for improvements both in terms of device usability and distance estimation reliability. Future works or the topic can address the following aspects:

- Evaluation of the estimation errors due to temperature and humidity effects. Those trials should be conducted in a temperature and climatic anechoic test chamber. This will allow to address environmental conditions by implementing dedicated compensation algorithms.

- Test the system using obstacles to address a more realistic application scenario. This will allow to evaluate the system behavior and usability on more critical circumstances.

- Evaluate other algorithms able to exploit other signal characteristics for the delay estimation, for example evaluating the phase variation of the emitted signal.

- Use low frequencies for the emitted signal and investigate possible advantages and limits.

- Addressing higher signal frequencies in the ultrasound field, adopting appropriate actuators and sensors.

- Using techniques based on Time Difference of Arrival (TDOA) such as trilateration or multilateration.

Bibliography

[1] **https://www.britannica.com/science/heart**

[2] **http://www.uniroma2.it/didattica/FISIOLOGIA-BIOLOGIA/deposito/Lezione14.pdf**

[3] **http://www.texasheart.org/HIC/Anatomy/anatomy2.cfm**

[4] **https://upload.wikimedia.org/wikipedia/commons/3/38/2027_Phases_of_the_Cardiac_Cycle.jpg**

[5] Tania Pereira, Carlos Correia, Joao Cardoso, **"Novel Methods for Pulse Wave Velocity Measurement"**, J.Med. Biol. Eng. (October 2015) 35:555–565

[6] Stephane Laurent, John Cockcroft, Luc Van Bortel, Pierre Boutouyrie, Cristina Giannattasio, Daniel Hayoz, Bruno Pannier, Charalambos Vlachopoulos, Ian Wilkinson, Harry Struijker-Boudier "**Expert consensus document on arterial stiffness: methodological issues and clinical applications",** behalf of the European Network for Non-invasive Investigation of Large Arteries.

[7] "**Prevention and epidemiology Determinants of pulse wave velocity in healthy people and in the presence of cardiovascular risk factors: 'establishing normal and reference values'**
The Reference Values for Arterial Stiffness' Collaboration", European Heart Journal, June 2010.

[8] T. Pereira, C. Correia, J. Cardoso **"Novel methods for Pulse Wave Velocity Measurements"**, In: J. Med. Biol. Eng. 2015,

[9] P. Salvi, G. Lio, C. Labat, E. Ricci, B. Pannier, A. Benetos. **Validation of a new non-invasive portable tonometer for determining arterial pressure wave and pulse wave velocity: The PulsePen device**. *Journal of Hypertension*, 2004;

[10] **http://Pulsepen.com/Pulsepen.html**

[11] F. Stea, E. Bozec, S. Millasseau. **Comparison of the Complior analyse device with sphygmocor and Complior SP for pulse wave velocity and central pressure assessment**. J Hypertens. 2014.

[12] **http://www.complior.com/products**

[13] **http://www.vasomeditech.com/overview.html**

[14] Jonathan R. Weir-McCall, Liam Brown, Jennifer Summersgill, Piotr Talarczyk, Michael Bonnici-Mallia, Sook C. Chin, Faisel Khan, Allan D. Struthers, Frank Sullivan, Helen M. Colhoun, Angela C. Shore, Kunihiko Aizawa, Leif Groop, Jan Nilsson, John R. Cockcroft, Carmel M. McEniery, Ian B. Wilkinson, Yoav Ben-Shlomo, J. Graeme Houston, **"Development and Validation of a Path Length Calculation for Carotid–Femoral Pulse Wave Velocity Measurement A TASCFORCE, SUMMIT, and Caerphilly Collaborative Venture"**, *J. Hypertension*.2018;

[15] Sofie A.M. Huybrechts, Daniel G. Devos, Sebastian J. Vermeerscha, Dries Mahieu, Eric Achtenb, Tine L.M. de Backer, Patrick Segers and Luc M. van Bortel, **"Carotid to femoral pulse wave velocity: a comparison of real travelled aortic path lengths determined by MRI and superficial measurements"**, *J. Hypertension*, August 2011.

[16] Zsófia K. Németh, Peter Studinger, István Kiss, Taha El Hadj Othmane, János Nemcsik, Bertalan C. Fekete, György Deák, József Egresits, Miklós Szathmári, and András Tislér, **"The Method of Distance Measurement and Torso Length Influences the Relationship of Pulse Wave Velocity to Cardiovascular Mortality",** *J. Hypertension*, February 2011.

[17] Weber T[1], Ammer M, Rammer M, Adji A, O'Rourke MF, Wassertheurer S, Rosenkranz S, Eber B, "**Noninvasive determination of carotid-femoral pulse wave velocity depends critically on assessment of travel distance: a comparison with invasive measurement"**, J Hypertens., August 2009

[18] Sugawara J, Hayashi K, Yokoi T, Tanaka H, "**Age-associated elongation of the ascending aorta in adults"**, *JACC Cardiovasc Imaging,* 2008; .

[19] Sebastian J. Vermeerscha,d, Ernst R. Rietzschelb, Marc L. De Buyzereb, Luc M. Van Bortelc, Thierry C. Gillebertb, Pascal R. Verdoncka, Stephane Laurentd, Patrick Segersa, and Pierre Boutouyried**, "Distance measurements for the assessment of carotid to femoral pulse wave velocity",** J Hypertens., December 2010.

[20] Alberto Avolio, Junli Zuo, Isabella Tan, Mark Butlin, **"Pathway for Elimination of Distance Measurement in Studies of Pulse Wave Velocity"**, J Hypertension, March 2018.

[21**] https://www.researchgate.net/figure/Carotid-femoral-pulse-wave-velocity-cfPWV-and-central-arterial- waveform-assessment_fig1_260994460**

[22] **https://www.britannica.com/science/sound-physics**

[23] C. H. Knapp and G. C. Carter, **"The generalized correlation method for estimation of time delay,"** *IEEE Transactions on acoustics, Speech, and Signal Processing*, August 1976.

[24] Jingdong Chen, Jacob Benesty, and Yiteng Arden Huang, **"Time Delay Estimation in Room AcousticEnvironments: An Overview",** EURASIP Journal on Applied Signal Processing, 2006.

[25] T. G. Manickam, R. J. Vaccaro, and D. W. Tufts, **"A leastsquares algorithm for multipath time-delay estimation,"** *IEEE Transactions on Signal Processing*, vol. 42, no. 11, pp. 3229– 3233, 1994.

[26] J.-J. Fuchs, **"Multipath time-delay detection and estimation,"** *IEEE Transactions on Signal Processing*, vol. 47, 1999.

[27] S. Doclo and M.Moonen, **"Robust adaptive time delay estimation for speaker localization in noisy and reverberant acoustic environments,"** *EURASIP Journal on Applied Signal Processing*, vol. 2003, 2003.

[28] Billur Barshan, "**Fast processing techniques for accurate ultrasonic range measurements",** Meas. Sci. Technol., 20000.

[29] C. H. Knapp and G. C. Carter, **"The generalized correlation method for estimation of time delay,"** IEEE Trans. Acoust., Speech, Signal Process., vol. 24, August 1976.

[30] Guowei Shen, Rudolf Zetik, and Reiner S. Thomä, **"Performance Comparison of TOA and TDOA Based Location Estimation Algorithms in LOS Environment "**, Proceedings of the 5th workshop on positioning, navigation and communication 2008

[31] **"MP33AB01H- MEMS audio surface-mount bottom-port silicon microphone with analog output."** Datasheet, STMicroelectronics, October 2013.

[32] **"Datasheet RS essentials speaker"**, RS PRO

[33] **"LM386 Low Voltage Audio Power Amplifier datasheet"**, Texas Instruments, 2017.

[34] **"Discovery kit with STM32F429ZI MCU - User Manual"**, STMicroelectronics, 2016.

[35] **"STM32F405/415, STM32F407/417, STM32F427/437 and STM32F429/439 advanced ARM®-based 32-bit MCUs - Reference Manual"**, STMicroelectronics, October 2015.

[36] **"Datasheet - LM217, LM317 - 1.2 V to 37 V adjustable voltage regulators",** STMicroelectronics, 2018.

[37] **"Rail-to-Rail Input/Output Operational Amplifiers w/ Shutdown datasheet (Rev. J"),** Texas Instrument, 2004.

[38] Billur Barshan and Roman Kuc **,"A Bat-Like Sonar System for Obstacle Localization",** IEEE *transactions on systems*, man, and cybernetics, vol. 22, July/August 1992 .

[39] W. G. McMullan, B. A. Delanghe, and J. **S.** Bird , "**A Simple Rising-Edge Detector for Time-of-Arrival Estimation",** , IEEE transactions on instrumentation and measurement, vol. 45, August 1996.

[40] Donald W. Marquardt, **"An Algorithm for Least-Squares Estimation of Nonlinear Parameters",** Journal of the Society for Industrial and Applied Mathematics, Vol. 11, June 1963.